An Integrated Building Method Based On Robotic Winding

Jansen, D.

Award date:
2021

Department of Built Environment
Master Architecture, Building and Planning
Specialization Structural Design

An Integrated Building Method Based On Robotic Winding

Master Thesis

Daniël Jansen

Supervisors:

prof. Dr. -ing. P.M. (Patrick) Teuffel
Chairman Innovative Structural Design
ir. A.P.H.W. (Arjan) Habraken
Assistant Professor Innovative Structural Design
ir. R. (Rijk) Blok
Assistant Professor Innovative Structural Design

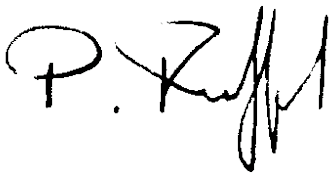

Eindhoven, July 2021

Preface

The fascination for finding structural applications for fibers has had its origin in several places. Firstly I have always been interested with nature where fibers are a frequent occurrence. Starting at the human body, where the collagen fibers in the bones align perfectly to create a strong and light application, perfectly adapted to its intended purpose. These bone fibers show their versatility by appearing in skeletons of the largest animals on earth and at the same time in birds of flight. The structural demands of both skeletons are vastly different but still they are made from the same material only with altered orientations and lay-up. I was captivated by the high specific strength that natural fibers possess, sometimes exceeding that of common building materials like steel. The human race has progressed in so many different ways since ancient times yet wood (based on cellulose fibers) is still considered a viable construction material. In some ways, like sustainability or reactivity to salts it can be seen as superior to steel. A drawback to the use of wood is its unidirectionality. The cause for this is that the tree grows the fibers in the direction where they are most needed when the wood is still in the tree. An interesting concept is to give the designer of the structure control over the fiber placements and with that control over the structural behaviour. I noticed that in several sectors these natural structures are already used to their advantage. The sector that has my interest is that of the bicycle sport. This sport cannot be imagined without the use of carbon fiber. This material is so versatile that basically all of the bike components, excluding the tires, could be manufactured from this material. This results in meeting the ever increasing demands of performance within the sport.

My desire for applying fibrous materials within the construction culminated in this thesis with the application into structural panels.

I would like to thank everyone who was involved. Thank you Arjan Habraken for the guidance. Additionally I would like to thank the staff from the Pieter van *Musschenbroek Laboratorium* for helping me realize the practical support for my theoretical framework. The robotic winding process was supported by Lizzy who is my peer in graduating on robotic winding. I appreciated her hands on mentality in times of doubt. I would also like to thank Franka for being additional support during the winding process.

And finally this thesis, and my entire education for that matter, would be impossible without both the mental as well as the financial support of my family.

Abstract

The goal of the research is to create an efficient, light weight building method, integrating design until assembly. In order to meet this goal a robotic resin infused fiber winding concept is elaborated. Modular panels will be wound using a robotic arm placing the material at the exact locations where its structurally most needed. The forces in the panel will be separated, the tension will be taken by a thinly wound tensional web with compression being present in a thicker edge. The concept is based on design with integrated, high precision manufacturing. The integration was met on different levels such as design, structural considerations and manufacturing. In order to reach a maximum amount of efficiency a proportional sizing optimization is included iteratively redistributing the material over the panel. This takes place after the boundary conditions and design considerations of a single panel or a panel assembly are specified. The optimized panel is translated into a windable path which can be directly fed into the robot. The building method is applied to a theoretical structure in the form of a bridge railing. In order to support the theoretic framework as presented an applied winding took place. For this the entire winding peripherals such as end effector and fiber conditioning are designed. Subsequent to this winding the panel is subject to testing in order to judge its structural behavior. The panel was resistant to higher forces than calculated most probably due to underestimation of material properties. Some additional structural effects were identified: pushing out of the threaded end and buckling most likely aggravated by bending.

Contents

1. Introduction

Nature has a high efficiency in structure which could be learnt from. She thickens areas of high stress and leaves areas of low stress thin. An instance where this phenomenon can be seen is the shell of the horseshoe crab. Ribs and ridges follow the highest stress (Stevens, 1974). All this without blueprint but as a direct effect of the forces that flow through the material. There is some intrinsic efficiency in the way nature does these things. Nature essentially ran an optimization process for millions of years. Small variations in genotype could cause variance in shell thickness. The result of using too much material could mean starvation, while on the other hand using too little material could mean getting crushed by a predator. Both of these effects causing a lesser chance of creating offspring and therefore cause upper and lower boundaries for the optimization. Every generation where genetic mutation occurs can be seen as an iteration.

To emulate this efficiency in a manmade structure there are some challenges to consider. The first challenge is that of design. How does the crab know where to place material in the most optimal way? Computer models could approach optimal design using their own mathematical methods. The way the optimization in this research works is similar to the way optimization works in nature. The design is iterative and adjusts to changing flow of force by placing the material at high stresses. The second challenge is that of material placement. Nature distributes material using complex biological systems. In prevailing building methods however the strategy is to make structures as generalised as possible. This in order to help with ease of manufacturing. However using computer aided design this high complexity can be achieved and directly fed into a robotic manufacturing process. For the robotic arm it doesn't matter what the manufactured panel looks like. It is open to high degrees of differentiation. If the link between design and manufacturing is seamlessly executed, efficiency in manufacturing can also be achieved using this method.

In this thesis a research will be presented into the robotically winding of structural panels that can be assembled into a wide array of structures. The winding will take place using a rope-like material and a resin in order to stiffen the material so that it will take compressional forces. The thesis presents a building method which integrates design, structural considerations and manufacturing into a single algorithm. These three main aspects also guide the structure of the written part of the research. Aside from this theoretic foundation a practical application is presented in order to support the validity of the theory. A wound panel is manufactured and subsequently tested in order to provide additional data on structural considerations. Finally a worked example is presented where the wound panels form an assembly in the shape of a bridge railing. This example shows just one of the possible applications of the building method.

2. Design concept

The goal of the research is to create an efficient, light weight building method, integrating design until assembly. The proposed method will be elaborated from initial shape to assembly. Some structural concepts that lie at the core of the method are explored in this chapter, afterwards the manufacturing and materialization will be discussed. All these aspects of the design concept are focussed on the efficiency of the building method. Efficiency can be seen as the ratio between either the strength or stiffness and the amount of material applied. Central to the efficiency is the way in which the material is distributed and used in structural terms. In terms of choosing an efficient material the question is mostly which material has the highest strength or stiffness to mass ratio.

Another interpretation of efficiency can be with regard to the subject of manufacturing. In terms of manufacturing efficiency means the easiest or cheapest (cost per unit) way to make something. This might be contradictory to the efficiency in structural concept, as specific placement of material is at the core of structural efficiency but detrimental to manufacturing efficiency where standardisation is the cheapest, most reliable and time efficient way. While this contradiction might feel like a fundament of the current building climate it is questioned in this design concept. With the help of modern methods like computational design and robotic manufacturing the efficiency with regard to manufacturing and structural behaviour might become aligned. And at the same time new structural concepts and materials can be explored.

2.1 Structural concept

Structural concepts where normal forces dominate are considered. Normal forces in a structure offer material efficiency and are essential for lightweight structures. Analogy can be made with truss structures, these constructions are able to span larger distances than solid beams. This could be explained by the way they are able to separate the bending forces into tensional and compressional elements. As bending moment can be described as force multiplied by its arm, the height of the truss can be increased without having to apply much more material.

In a externally post tensioned beam as schematized in figure 1 the separation of forces is taken even further. The tensile and compressional components are internally isolated into different materials. The compressional element is usually executed in a material like wood or steel while the tensional element is usually a cable like material. The tensile element can be executed with smaller dimensions because buckling is no concern, this way material is saved. From this it essentially can be concluded that tensional elements are the most efficient way of transferring forces. This concept of separating forces has been inspiration for the design as described in this thesis.

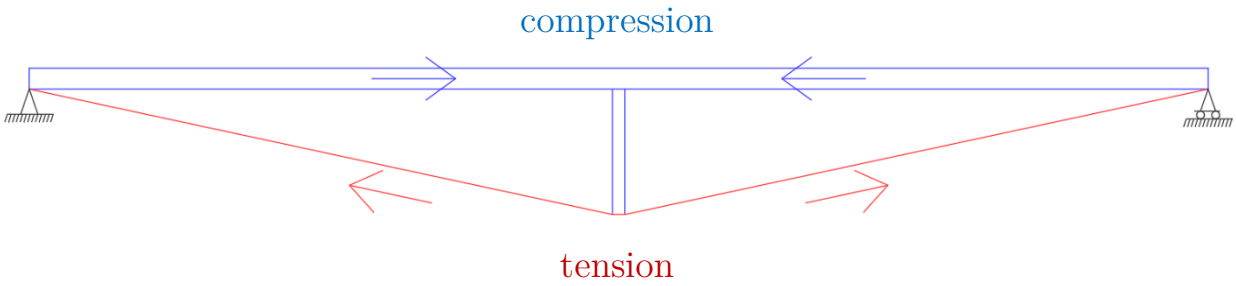

Figure 1: Externally post tensioned beam showing separation of forces

Another structural concept where forces are separated into different materials are cable net constructions. These light weight cable nets can span large distances and often form prestressed double curved surfaces to ensure tension in all situations. However a roof consisting of purely tensional elements cannot be constructed without peripheral components taking compression. These peripherals can consists of compressional rings and columns transferring the forces towards the foundation.

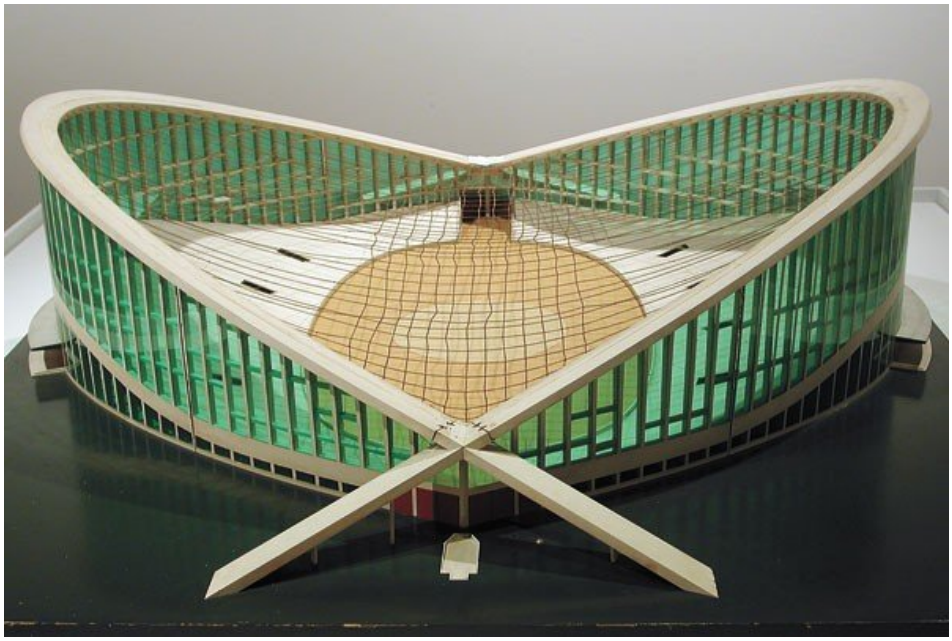

Figure 2: Model of cable net structure (Dorton arena), from Ariail, 2010

Combining these concepts creates the ambition to construct a building component where forces are separated to create efficiency. A component will be created where forces will be partitioned into a compressional edge and a tensional web. The tensional web could be realized using a cable-like material, in order to stiffen the edges in order to provide resistance to buckling resin could be used in combination with the material. Aside from considering the single panel as shown in figure 3 the panels could be combined into more complex structural assemblies. In these assemblies the individual panels have the function of resisting tensile as well as compressional forces. Even though a suitable structural concept is chosen this does not ensure the best efficiency. To maximize efficiency the material should be distributed in the optimal way. Therefor an optimization was included supplementing the structural concept.

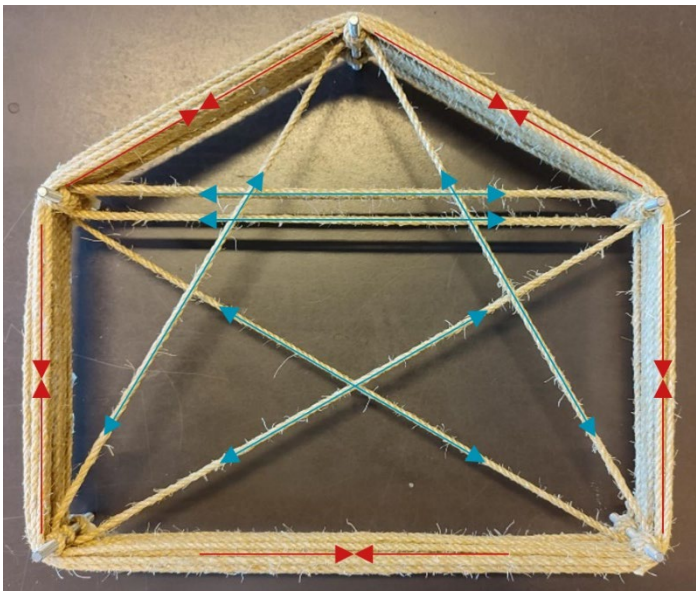

Figure 3: Separation of forces in wound panel

2.2 Manufacturing

Robotic manufacturing is well suited for the eyed application. A cable like material could be introduced by means of a spool and simply unwound by a robotic arm. The high plasticity of the material generates flexibility of application where the robot could effortlessly place material where it is needed. This placement will occur around threaded ends where the material will be fixated, this is shown schematically in figure 4.1. After placement the structure requires stiffness which could be realized by using a slowly hardening material. This combines structural and manufacturing demands in a single material. Another benefit of using robotic manufacturing is that complex actions can be executed without the need for standardization. When an assembly of panels is constructed the panels can all be different without changing the manufacturing process. The algorithm generating the robot code could be written in such a way to accommodate different panels. Which leads us to the final considered benefit which is the seamless integration between design and manufacturing. The robot receives instructions from a digital program. The same digital program could also be a tool for design and structural engineering of the structure. This creates a streamlined process where structures could be designed safely yet quickly

Robotic manufacturing should take place in a controlled environment. While this might change in the future, currently inside conditions are needed for reliable use of the robot. If a structure is planned outside, it will be made in parts in the controlled circumstances of a plant, transported and then assembled on site. In this way the definition of manufacturing is spread out over the terms ‘manufacturing and ‘assembly’. The structure receives a modular character which will be embraced by constructing each panel in a similar method. In this project this multifunctionality of the method is the central goal. The manufacturing will be closely connected to the design but not largely changed by it, and in that way whatever the design will be the manufacturing is automatically taken care of. An advantage of creating a modular building method is the possibility of reassembly. Finished structures can be disassembled on site in order to reassemble

somewhere else or to replace worn or obsolete modules. This can increase the life cycle of the structure and the materials used with obvious monetary and environmental benefit.

With the aims of manufacturing the structural panels a robotic arm will be used. The arm considered in this research is the IRB1200-5/0.9 manufactured by ABB. For exact documentation of this model of robotic arm it is referred to the website of ABB (ABB, 2021). The robot is a six axis robotic arm with a reach of around 900mm. The arm runs in collaboration with a controller unit where the RAPID code will be uploaded and processed. The IRB1200 that was considered for this research is not the only robot that could be used in conjunction with the presented process however. Only minor adjustments with regard to robot geometry have to be made when using alternative six axis robotic arms.

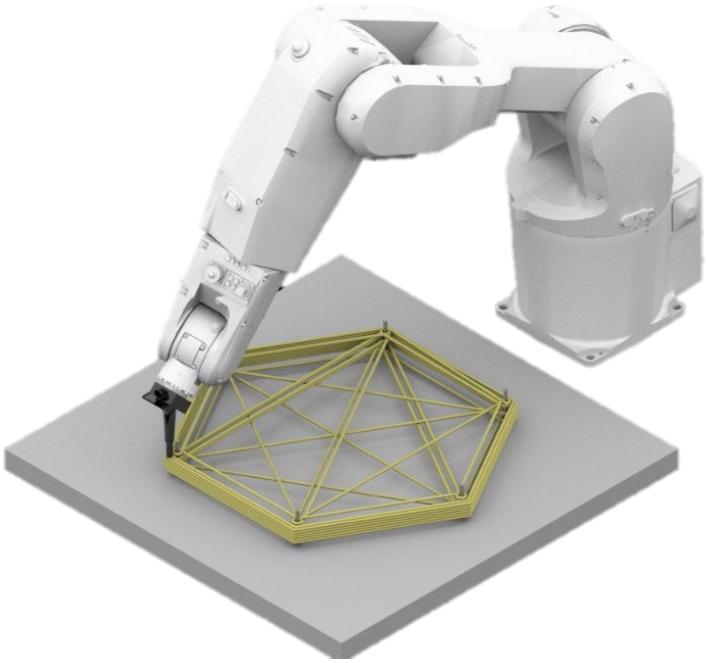

Figure 4.1: The envisioned manufacturing setup of the panel

2.3 Design phase

The first step in the design phase is to define a structure envelope. This envelope can be discretised into a single panel or into a panel assembly. The shape of the panels can be chosen with a large degree of freedom. Some restrictions do apply however. A condition on the panel shape is that it has to be a convex polygon. This is the case because reflex angles cause problems in the manufacturing process further down the line. In order to create a compressive panel edge the material will be wound around the entire panel. With reflex angles the winding would come away from the panel edge.

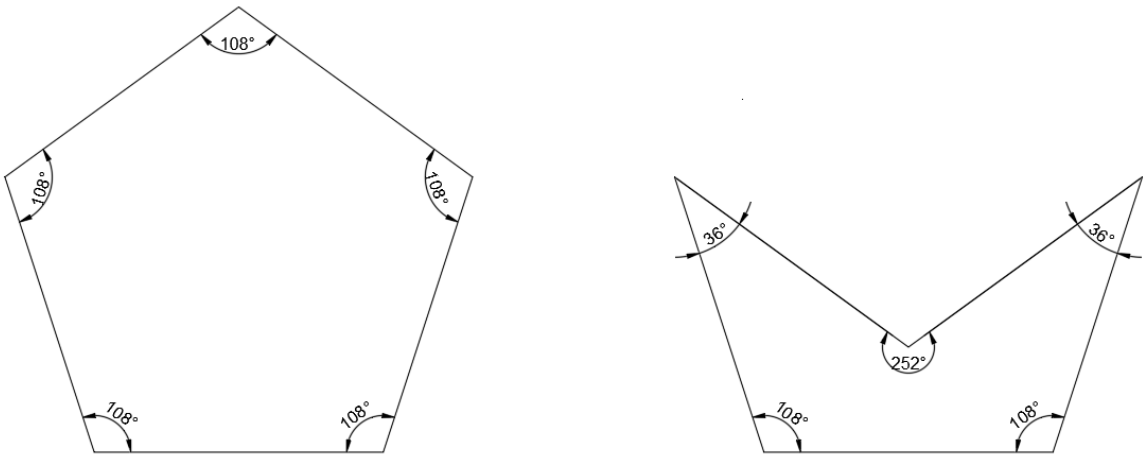

Figure 4: Left shows convex polygon, right shows concave polygon

In the image two pentagons are shown. The pentagon on the left is a convex polygon where all internal angles are smaller than 180°. The pentagon on the right has an internal angle larger than 180° which is called a reflex angle. This pentagon is categorised as a concave polygon.

All convex polygons are allowed in the design of a structure using the method described in this research. With the choice of polygons it is important to note that the higher order the polygon is the more complex the web is, as more vertices means more connections for the web. With a panel of higher geometric complexity the flow of forces is less restricted by the direction and amount of web elements. The optimized shape becomes a clear depiction of the flow of forces.

Some possible polygons are elaborated along with their limitations and benefits. The first planar polygon is the triangle. This shape is able to tesselate on a flat plane however it is not suitable for this research as there is no internal web formed after interconnecting all vertices. Therefor the concept of stabilizing a shape with internal webbings is not applicable. The same applies in a lesser degree to the square, despite its ability to tessellate it contains only two web elements which restricts the flow of forces. The pentagon and the hexagon are considered the minimum order of polygons to be used in the application that was explicated in this research. The pentagon has five internal elements while the hexagon has nine. It is evident that the amount of internal web elements grows exponentially with each increase of order of polygon. The equation for this effect in any, not only regular, polygon was found to be the following.

$$\frac{n^2 - 3n}{2} = W \tag{1}$$

With
n = amount of vertices
W = amount of web elements

This equation takes into account only the web elements, the edge elements are always of the same number as the amount of vertices. The algorithm presented automatically defines the web of the panels as designed. Every node and element in the structural assembly receives an index. The web and edge elements are processed in a different way in the rest of the algorithm and therefor it is imperative that these indexes are separated.

Both the pentagon and the hexagon are able to tile a flat plane. The hexagon is able to do this in its regular shape. The pentagon however needs some deformation. Tessellations using a variation of higher order polygons also exist. The tiling of a flat plane is a beneficial property for panels because of the ease of making assemblies. If tessellating panels are used the design envelope could simply be filled with repeating panels. If however the panel does not tesselate the assembly needs to be set up manually.

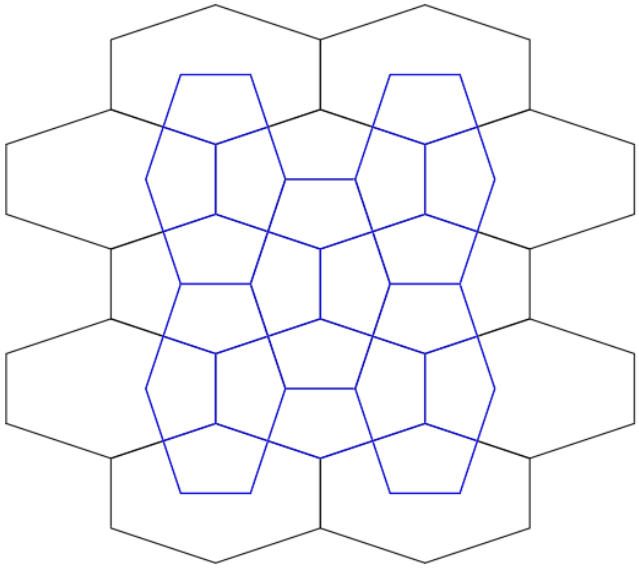

Figure 5.1: Hexagonal tiling with pentagonal tiling in blue

2.3.1 Design of assembly

In order to properly define the two dimensional assembly of panels care has to be put into its stability. Existence of a mechanism renders the subsequent FEM calculation impossible and in that effect causes the assembly not to be optimized. For the exact detailing of the connections reference can be made to chapter 7: assembly. The panels are exclusively connected by their vertices which solely consist of hinged interconnections.

For a deeper understanding of when an assembly is mechanically stable, the distinction between first order vertex connections and higher order vertex connections is made. First order connections join two vertices where higher order connections join more. When isolating a panel from the assembly into a free body diagram, first order connections can be viewed as roller connections. Higher order connections can be simplified as hinged connections relative to the individual panel.

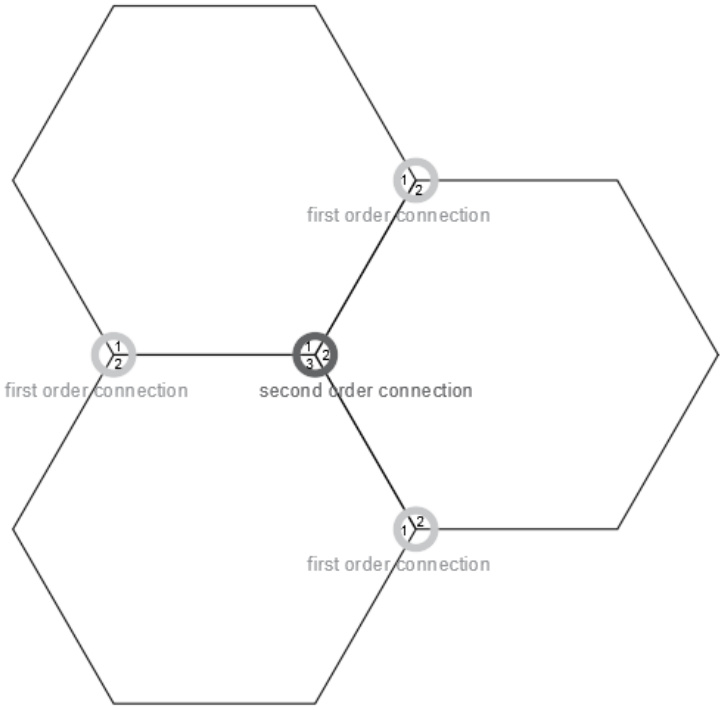

Figure 5: Connection elements in a hexagonal tessellation connect either two or three nodes

In order to be statically stable, the free body diagram of the panel requires at least three support reactions which are not in line with each other. This can be achieved with at least three first order connections or one first order connections and one second order connection. A first order connection signifying two nodes are to be connected while a second order connection means three nodes to connect as shown in figure 5. If every individual panel is statically stable and at the same time the assembly as a whole has three support reactions the system is stable. Same goes when considering the supports for the assembly. The assembly should be regarded as a single unit and then three support reactions are needed in order to avoid a mechanism.

The actual connections are automatically generated by the algorithm. The script lets the user define a connection length. Based on this connection length the individual panels are scaled down in size in order to accommodate the connection. Afterwards the connection elements are introduced between all vertices at a nodal location. This means first order connections receive a single connection element, second order connections receive three connection elements. The same pattern of interconnections occurs as seen in equation 1. Except in this case the edge is counted, leading to equation 2:

$$C = \frac{n(n-1)}{2} \tag{2}$$

n = amount of vertices at a node
C = amount of connection elements

An example is referenced in figure 6 where the grey hexagonal assembly is given as an input. The algorithm then adds the connections and webs for all of the panels which were provided. Additionally the algorithm numbers all elements for later processing by finite element method.

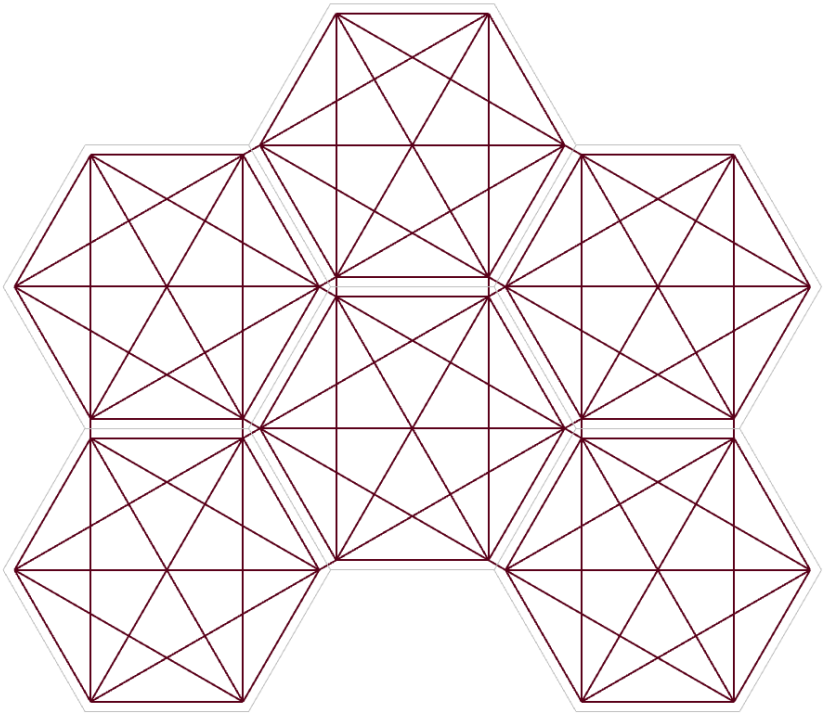

Figure 6: Assembly showing panels serving as input in grey, and generated web and connections in black

2.3.2 Size

Finalizing the design phase, the panels are isolated from the panel assembly and are moved to the working space of the robot. In order to ensure manufacturability it is important to check for robot limitations in an early stage of the design. Whether the design consists of a single panel or a panel assembly, every panel should be dimensioned in such a way that it fits within the robot reach. A check included in the script takes the panel and simply tries to encircle it with the robot.

This is done in order to test if the panel fits within the robots maximum working space. This working space is visualized in figure 7. The values given as the maximum and minimum radius of the robot range are extremes. In the placement algorithm the extreme radii are made more conservative in order to include some tolerance. For placement purposes the maximum radius is

considered to be 800mm and the minimum radius 275mm. This tolerance is introduced because the exact height of the panel is not yet known and the robot range is variable over the z-location of the robot tip. In the case of a regular polygon the maximum panel radius within this range is approximately 260mm. At this point the edge width is not yet known. There should be some estimation on the width of the edge defined by the user. This estimation is needed for the optimization as well and can be updated in a later phase.

Manually finding the optimal orientation for the panel can be troublesome and not suitable for the automated concept of this research. In order to fit the panel within the range of the robot automatically an algorithm was written. Importance of orientation is visualized in figure 7. The included algorithm is essentially a brute force procedure checking all reasonable panel orientations with robot reach. The area of possible locations is divided into points where the panel is copied to. Subsequently the panel is rotated into several different orientations. The amount of rotations and placements are user input and decide how precise, but also how heavy the algorithm is in terms of computing power. Finally each placement and rotation is checked for intersection with the outer bounds of the robot reach. The algorithm yields a list of possible orientations from which the user can pick one for further processing.

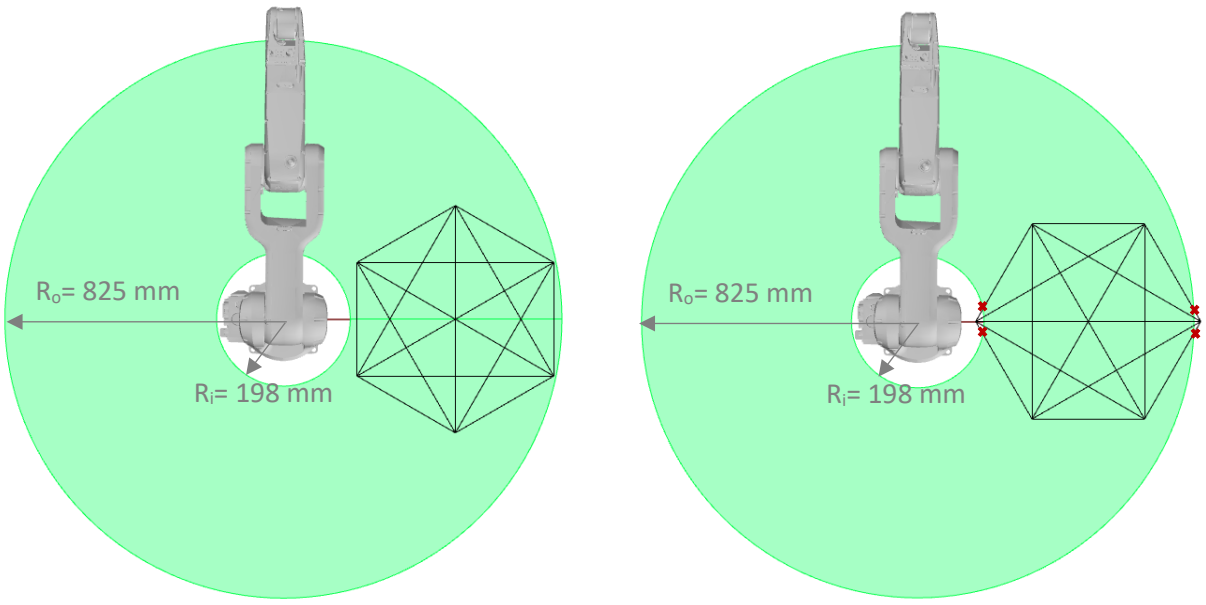

Figure 7: Robotic reach visualized, included algorithm checks for clashes with the extreme radii

The robotic working space is a stringent limiting factor on the panel dimensions. There are however methods of increasing the robots range. The most obvious solution is using a robot with a longer reach. This is however an inefficient option that only marginally improves the range. Using the same robot the range can be increased by using a rotational external axis. On this external axis a table could be mounted with the winding mold fixed on top of it. Instead of the robot tip moving from vertex to vertex, it will now be the external axis rotating the vertex in the direction of the robot tip. The robots function is reduced to rotating around the vertices in

order to establish fixation of the material. Since the vertices of the panel are on its edge the panels dimensions are increased without theoretical boundary. There are off course practical considerations, for instance the maximum size of the table in terms of weight. Additionally this concept only works in the case of regular polygons which vertices are all on a circular outline. Any variation from a circular shape has to fit within the robots reach. By definition the variation from the circle is not allowed to exceed 800-275mm = 525mm.

Another favorable aspect of using an external axis is the enabling of constant prestress during the winding. When the panel is stationary the robot intermittently moves in the direction of the material spool in order to reach the next vertex. Movement in the spools direction causes the material to lose tension as the spool is not unrolled. This tension is regained when the robot tip starts to move away from the spool during encircling of the vertex. Preferably tough the pretension remains constant. When properly using an external axis the only movement in the direction of the spool occurs during the encircling which is a much shorter phase than the movement between vertices.

There is however no external axis available for use at the university. For this reason the thesis is continued based on smaller panels that fit within the robotic reach.

2.4 Materialization

In terms of materialization the structural concept is viewed as directive. There are tensile elements present forming the web of the structural panels while the edge elements need to be able to take compression. The first consideration is to find a material that can fulfil both roles. Additionally forces vary in each of the elements which causes the need for differentiation of elemental area. The material which is to be used should be easy to place in order to achieve the intricate material distribution produced by these factors. Using a single material to fill all these requirements leads to the choice of cable materials. Cables are versatile in their placement as they can be moulded in any shape. They can be delivered on compact spools which is beneficial with regard to supply. The spools can be unrolled in order to get the material from the storage onto the panel without additional steps. Structurally cable materials are specialized in taking tensile loads as they instantly buckle under compression. With compressional edges required for the function of the panels an additional step is needed to stiffen the material. Compressional behaviour can be achieved by dousing the cable in resin. After hardening the material forms a fiber-resin matrix where the fibers are unable to move relative to each other. Before hardening however the material will still be malleable enough for placement with a robotic arm. The time before hardening, which is consequently the maximum application time, depends on the used resin material.

This research project is kept as inclusive as possible. Therefor the exact materialisation is open to be decided on. This material chapter is to be seen as a guideline in choosing possible materials. The entire project is based on simple material parameters which can be changed at any moment in the algorithm. With the algorithm changed to fit the material, the structural calculations as

well as the manufacturing will be automatically adjusted. The fitting of the algorithm is done by the following parameters:

Structural parameters: These structural parameters have an influence on the optimal material distribution as well as on the structural behaviour of the end result. The parameters are influenced by both the material properties of the cable material as well as the material properties of the hardened resin. The structural parameters are:

- Composite structural diameter [mm]

From which the structural area is decided. On this area the structural behaviour like strength checks, stiffness and optimization affairs are based.

- Composite tensile capacity [Mpa]
- Composite stiffness [Mpa]
- Connection capacity [Mpa]
- Connection stiffness [Mpa]

Manufacturing parameter: The manufacturing parameter has an effect on the manufacturing of the structure:

- Composite manufacturing diameter [mm]

This value is used in order to decide the actual diameter of the cable in order to ensure even placement and avoid clashes during manufacturing. The structural diameter can be seen as the minimum diameter and the manufacturing diameter as a maximum. The difference is especially visible in cables that consist of twisted strands.

The algorithm as presented in this thesis can be used in order to find if a certain material is suited for the envisioned application. This could be done by reviewing the structural behavior of the application. In order to fully do this the material parameters should be known in advance.

2.4.1 Material choice

When choosing a material for the structure several properties are to be researched. An important requirement is that of the materials sustainability. With this thesis presenting a future proof manufacturing method it would be paradoxical selecting an unsustainable material. For a material to be sustainable renewability is an important aspect. Renewable materials like biofibers essentially have unlimited supply possibilities. The plants which are the base of these fibers bind CO2 from the atmosphere and in that manner act as a buffer. With increasing demand the supply will increase and the CO2 buffer will grow as well.

Biofibers along with man-made fibers are plotted in an Ashby plot below. The horizontal axis denotes the stiffness while the vertical axis denotes the materials' strength expressed as the tensional yield strength. The plot shows there is a strength as well as a large stiffness difference

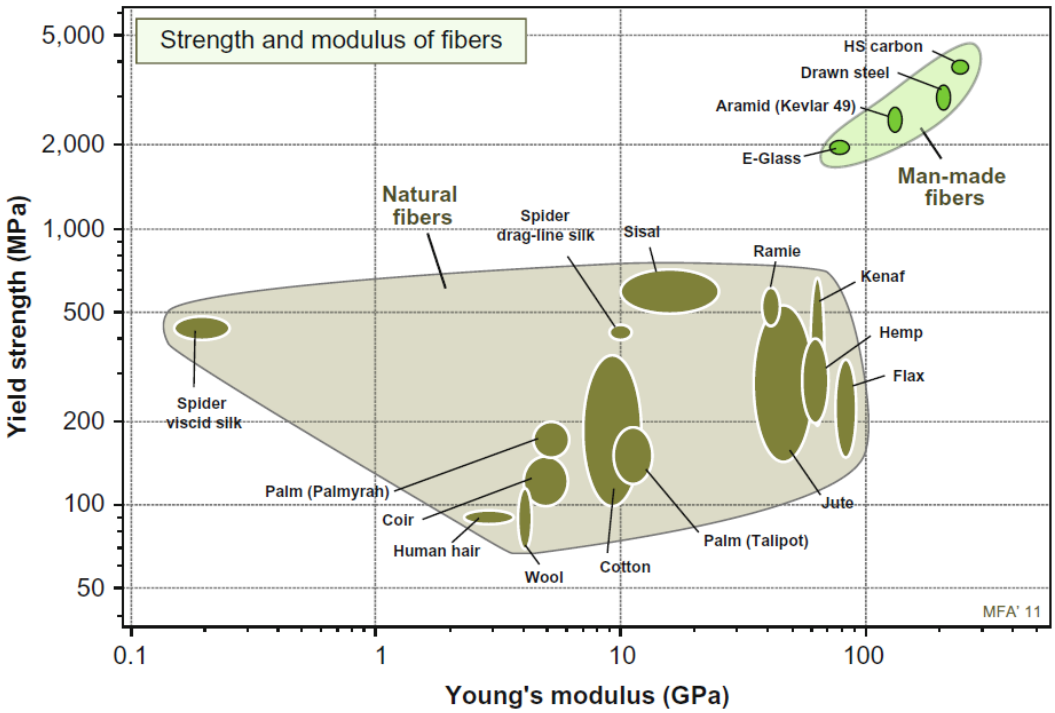

Figure 8: Ashby plot of biofibers and man-made fibers strength and stiffness, from Ashby, 2013

between the biofibers and the man-made fibers. Within the entire plot the high strength carbon fibers exceed in terms of material properties.

Carbon fiber has proven its versatility with numerous applications within high tech industries and is emerging in the construction field. An occurring application is in the stiffening of existing structures, for instance concrete bridges. Applications in the building industry are low volume, which is most likely due to its high cost. The notion of specialized usage is consistent with the concept presented in this thesis. The high material cost could be offset by efficient structural design and manufacturing.

There are material properties that shine a less positive light on the consideration of using carbon fiber. The carbon in carbon fiber is in prevailing fabrication sourced from crude oil. This sourcing is not sustainable because of its finite nature. Additionally high temperature processes are required in order to get to the final product which leads to emissions. There are however future prospects which will diminish both the cost of carbon fiber as well as some of the sustainability issues. Lignin obtained from renewable sources could replace the crude oil based carbon. This alternative manufacturing method could cut down costs by a factor two (Baker & Rials, 2013). These promising projections are however something to be reconsidered in the future as lignin based carbon fiber is not yet commercially available.

Conventional natural fibers should not be left out of consideration however. There is a property of biofibers which brings the category closer to that of synthetic fibers, and that is its low specific density [kg/m^3]. Correcting for this specific density gives the plot as shown below. It is

remarkable that between the two plots the relative positions of the natural fibers do not change a lot. The same can be said for the man-made fibers. There is however a large shift closing the gap between the two categories. Corrected for specific strength, flax fibers are stronger than steel and sisal fibers are stiffer. When looking for a truly efficient construction material this specific strength and stiffness is the information to base a decision on. In this regard the biofibers form a serious competition with the man-made fibers.

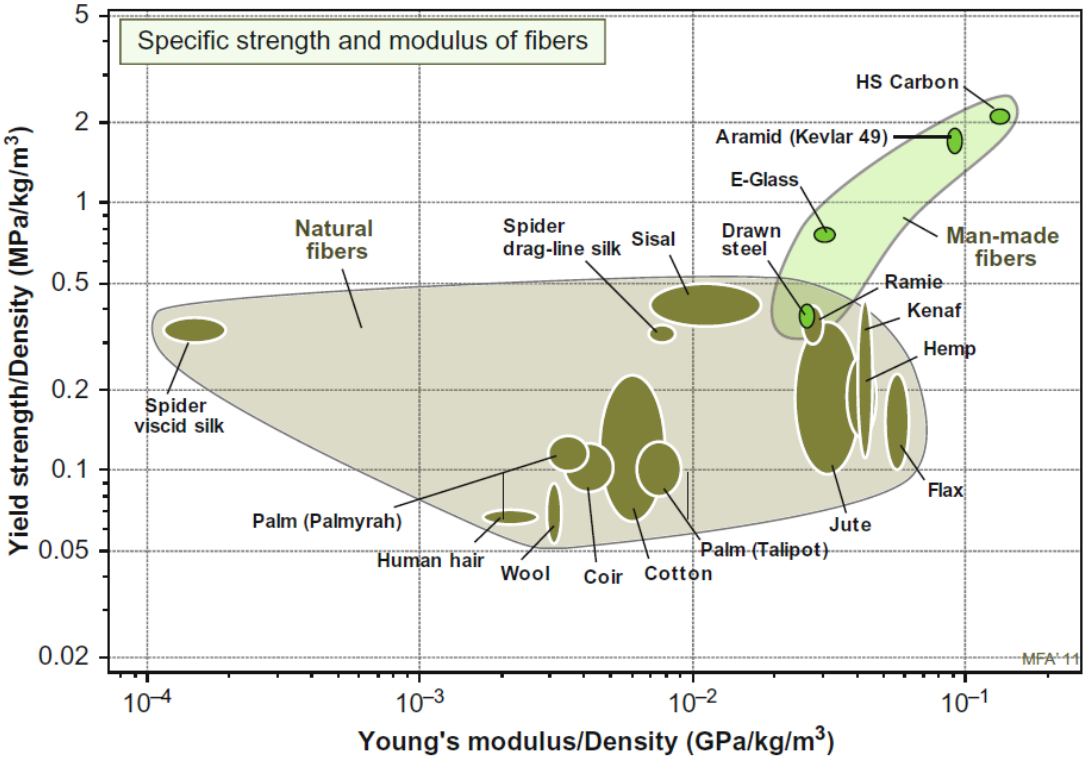

Figure 9: Ashby plot of biofibers and man-made fibers specific strength and stiffness, from Ashby, 2013

Chapter 9 will present a practical implementation using sisal fibers. The choice for this fiber was based on both its high stiffness as well as its commercial availability. This last factor allowed for ample experimenting and prototyping. The high stiffness was considered an important factor because the optimization presented in chapter 3 is based on the panel stiffness.

Until this point only the raw material has been considered. In order to actually apply the fibers they should be grouped together in ropes. Since ropes are essentially a composite of individual fibers their morphology can be varied.

Two general categories can be identified in rope structures:

The first one is laid or braided ropes which have high twist. This twist is introduced in order to keep the rope as one piece. This is especially necessary with biobased fibers where individual fibers are short, twisting presents with the framework to keep the rope as a whole. The twist also serves a structural purpose. The stresses in each individual strand are redistributed over the collection. This causes different material behavior than can be found in parallel fibers. From small scale to large scale the rope structure consists of individual fibers, then the yarn made up

from twisted fibers, followed by the strand made form twisted yarns and finally the rope made from twisted strands.

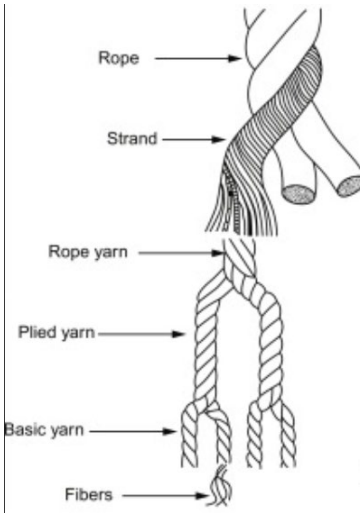

Figure 10: General rope construction of twisted ropes, from Elmogahzy, 2020

The second category is low twist ropes. These ropes are generally made from multiple parallel fibers or yarns. Since these are more geometrically straightforward, they perform better when high strength and stiffness are needed. Parallel strand ropes often have an external jacket in order to keep their parts together. Low twist ropes consisting of man-made fibers could be made directly from parallel fibers without any twist. Carbon fiber can be made continuously creating possibility of infinite fibers. Based on biofibers the possibilities depend on the fibers length. There will always be limits to this length and therefore using yarns as a component is more realistic. But even then, parallel strand ropes based on biofibers are not commercially available. This is theorized to be because they lack integrity and consequently have weak material properties. In this specific application where resin is used it might be viable to use low twist biofibers as the integrity is accomplished by the resin. Material research on this is needed.

2.4.2 Rope mechanics

Rope mechanics, while based on the same principles as the prevailing stress definition, can nevertheless be dissimilar to solid mechanics. Ropes have uncertainty in the available area. The area can have irregular boundaries and internal space. With stress being a relation of the force and the area of the material a different definition is needed. Linear density is a common metric used to replace area, it measures the mass per unit length in kg/m. The stress based on this metric is called the specific stress and is defined as follows

$$\sigma_s = \frac{F}{\lambda} \tag{3}$$

With

σ_s = specific stress [Nm/kg]

F = force [N]
λ = linear density [kg/m]

The linear density of a cable could be calculated by measuring the weight and length of a piece of cable. Dividing the weight by the length gives the linear density.

Together with the specific density of the material the specific stress and the stress are interchangeable quantities.

$$A = \frac{\lambda}{\rho} \tag{4}$$

With
A = area [m^2]
ρ = rope density [kg/m^3]

$$\lambda = \frac{m}{L} \tag{5}$$

With
m = rope mass [kg]
L = rope length [m]

With this detour the stresses of cables can still be defined in conventional ways, when the specific stress is known as well as the length and the ropes area. But even this definition of rope area can cause a wrong assumption of the total effective area as the fibers can be at angle with the rope direction. This is especially the case in cables with high twist.

Mechanical properties of ropes are both based on the raw material they were manufactured from as well as their geometric make up. Tensile properties of ropes are influenced by obliquity, slip at fiber ends, variability along with load sharing and weak places and finally changes in rope structures or bedding in (McKenna et al., 2004). These factors will be further elaborated on:

- Obliquity is a geometric property of the fiber layup within the rope. The fiber properties are translated to rope properties with consideration to their individual angle to the rope axis.
- Fiber end slip occurs when individual fibers slip relative to each other. In the rope this shows as a reduction in tensile elasticity. The amount of slip of the fiber ends is based on the transverse forces acting on the individual fibers, their length as well as their radius, tensile strength and coefficient of friction. There is an optimum twist where the slip is reduced as much as possible.
- Variability, load sharing and weak places are the third factor. If the strands or yarns making up the rope show high variability the sharing of loads between them will be uneven, causing possible overloading. Also weak places in strands or yarns can cause them to overload in an unexpected way. These effects can all be reduced with stress

transfer between fibers. An effective slip length will be present where components act independently. This slip length reduced with transverse forces in twisted ropes.

- Change in rope structure or bedding in is an effect due to the existence of spaces between strands forming the rope. These spaces occur during manufacturing process and are reduced with each loading cycle. There is a limit in this reduction as more and more strands or yarns settle. This means with each loading the rope structure and therefor the mechanical properties change. The settling of individual strands could also has an effect on their obliquity.

All these factors having an influence of the mechanical properties of ropes. When using natural fibers the ropes that are commercially available have a high variance in material properties. This is due to the factors as described in combination with variations in rope morphology. Additionally both the geometric as well as the material properties of the biofibers show high variety. With man-made fibers in the form of parallel strands all these factors diminish in intensity.

2.4.3 Epoxy considerations

In order to generate compressive resistance in the ropes epoxy resin is introduced. Coating the rope in epoxy will create the stiffness needed for compressional capacity. It will also cause adjacent ropes to stick together creating an assembly with a higher buckling area.

Epoxies are readily used within the construction industry, however it is mostly as an additive in a diverse range of finishing products. Epoxy consists of large polymer strings that under the influence of a second 'hardener' material undergo cross linking. The mixture of both materials goes from a liquid to a solid state. There are different epoxies that harden under different circumstances, aside from two component resins there are also thermosetting resins for instance. The carbon needed for the polymers is generally sourced from fossil resources. With the emphasis of this thesis being on a future-proof design concept this sourcing is viewed as unsuitable. There are however steps being taken in the development of biobased epoxy resins. The carbon can be sourced from a variety of renewable resources like vegetable oils, rosin, furan, lignin and itaconic acid (Kumar et al., 2016). Current commercially available biobased epoxy resins are not fully biobased, but merely contain biobased elements. For the practical application presented in chapter 9 Sicomin SR infugreen 810 / SD 882X, is used along with the sd8824 hardener component. The resin has carbon from plant origin with a percentage of 38%.

2.4.4 Composite mechanics

Combining the two materials will generate a new material, the composite. Depending on the choice of fiber material being either a strictly unidirectional composite or a generally unidirectional composite for parallel carbon fiber or biobased ropes respectively. In either situation the material is anisotropic in nature. The rope always has a certain defined direction

within the matrix. The best mechanical properties are achieved parallel to the rope, and therefore the fiber direction. In the case of twisted strand rope there is a component of the fiber working in the perpendicular direction depending on the twist. In prevailing fiber composites it is the additive that is giving the assembly its structural cohesion. The resin matrix fills the function of binding all together. In the case of a twisted rope material the fibers are already partially bound together structurally. This binding however only applies in tensional loading. In compressional loading the individual fibers have less binding and could fail in buckling individually. The epoxy matrix formed around the fibers avoids this effect, creating a structural assembly in all loading circumstances. The epoxy also complements the structural properties of the fiber.

When considering the mechanical properties of the composite the mechanical properties of both of the materials forming the composite should be known. As mentioned before the mechanical properties of rope materials are influenced by both the raw material as well as the geometric layup. For twisted ropes the factors to be considered are: obliquity, slip at fiber ends, variability along with load sharing and weak places and finally changes in rope structures or bedding in. A lot of these factors are reduced with the integration of the rope within a matrix. Instead of the structural integrity of the rope being based on the slip factor between individual fibers influenced by the transverse forces the matrix causes a comprehensive whole. The rate in which the factors are decreased is based on the interface between the fiber and the matrix. In the case the interface is sufficient the slip at fiber ends is basically eliminated, the load sharing is greatly increased therefore reducing the effect of weak places. Finally also the bedding in of the fibers is eliminated as all of the empty spaces are filled with resin.

The exact collaboration of ropes with small fiber lengths in the epoxy matrix is subject to research. Even when the mechanical properties of the individual materials that make up the composite are known, the properties of the assembly might be unexpected. An important reason for this is the effect of the fiber matrix adhesion. In a longitudinally loaded composite the tensile forces in the material are transferred from the matrix into the fiber by shear force. The shear capacity of the interface between the two materials has an effect on this internal force distribution. When a new combination of materials is used to form the composite, it is useful to perform pull-out tests in order to establish a value for this interface shear capacity. Total adhesion is achieved when the interface shear capacity is as high as the shear capacity within the fiber, or most likely, within the matrix itself.

In order to provide some guideline for mechanical behavior of the composite the rule of mixtures could be applied. This method can define the stiffness and strength capacities of the composite by combining the individual parts. It should be noted that the rule of mixtures as presented only applies to parallel fibers with their length being the same as the composite length. In practice this applies to for instance a carbon fiber parallel fiber rope. The concept is visualized in figure 11. When shorter fibers are used the shear interaction between the fiber and the resin matrix should be established. In the case of short fibers the interfacial shear stress over its length would have a certain distribution being high near the fiber ends and near-zero at mid-length. Consequently the normal force in the fiber is also non uniform, opposite to continuous fibers

(Mallick, 2018). If the shear interaction is sufficient the rule of mixtures could be applied. Sufficient shear capacity will cause the isostrain condition to still hold which is required for the rule of mixtures.

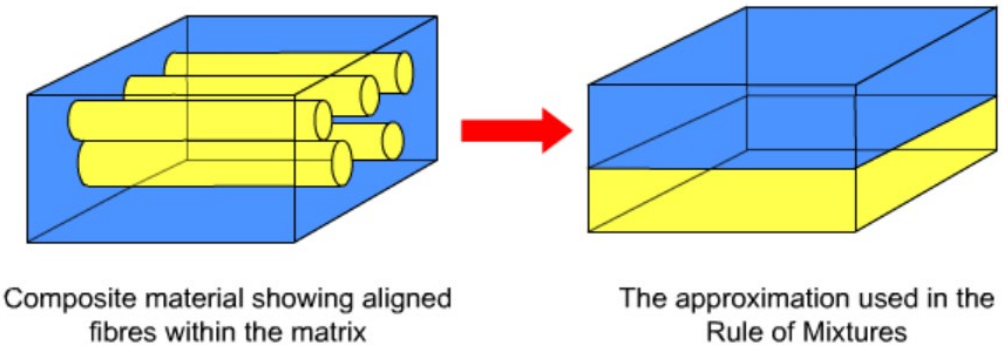

Figure 11: The concept of the rule of mixtures visualized, from University of Cambridge, n.d.

First the volume fraction of the parts of the composite are calculated as follows. In equation 6 the volume fraction of the fiber is calculated, in the same manner the volume fraction of the other constituents can be derived.

$$v_f = \frac{V_f}{V_c} \tag{6}$$

With
v_f = volume fraction of the fiber

Where composite volume is defined by:

$$V_c = V_f + V_m + V_v \tag{7}$$

With
V_v = void volume [mm^3]
V_m = matrix volume [mm^3]
V_f = fiber volume [mm^3]

The load on the composite is per definition equal to the loads on fiber and matrix summed:

$$P_c = P_f + P_m \tag{8}$$

With
P_c = force in composite [N]
P_f = force in fiber [N]
P_m = force in matrix [N]

In isostrain conditions:

$$\varepsilon_c = \varepsilon_f = \varepsilon_m \tag{9}$$

With the common equations for stress definition and Hooke's law are as follows:

$$F = \sigma * A \tag{10}$$

$$\varepsilon = \frac{\sigma}{E} \tag{11}$$

Combining equation 9, 10 and 11 will find the stress in each component of the composite to be:

$$\sigma_c * v_c = \sigma_f * v_f + \sigma_m * v_m \tag{12}$$

Combining equation 9 to equation 12 will define the stiffness of the composite.

$$Ec = Ef * vf + Em * vm \tag{13}$$

The calculated young's modulus is the maximum young's modulus where all the fibers are loaded longitudinally. in the case of perpendicular loading another definition is needed. When a twisted rope is used not all fibers are loaded longitudinally but instead under an angle. Depending on the angle of the fibers relative to the rope direction the actual young's modulus lies somewhere in between the values calculated in equation 13 and equation 16.

In perpendicular loading an equal stress assumption is made according to:

$$\sigma_{perp} \; = \; \sigma_f = E_f * \varepsilon_f = \sigma_m = E_m * \varepsilon_m \tag{14}$$

Overall perpendicular strain in composite is then:

$$\varepsilon_{perp} \; = v_f * \varepsilon_f + v_m * \varepsilon_m \tag{15}$$

Transverse modulus is calculated to be:

$$E_{trans} \; = \sigma_{trans} \, / \varepsilon_{trans} \tag{16}$$

With regard to structural failure the fiber orientation has a large effect on the mechanical properties. Fibers that are parallel to the loading direction are failing in tension. Alignment different than parallel will cause changes in failure mode from tensile to shear. Total shear failure is possible at very small angles depending on the interface between the fiber and matrix. For

this reason it is not advised to use ropes with high twist for structural purpose (Mittelman & Roman, 1990). It further underlines the need for research into the matrix-fiber interaction.

Other statements that should hold for the rule of mixtures are: Fibers and resin must be uniformly distributed. Especially in rope applications where the fibers are in contact to begin with, a proper surrounding of each fiber with resin is not self-evident. This reduces the efficiency of stress transfer and therefor reducing the samples strength. Additionally all materials in the composite are linear elastic materials or are in their linear elastic phase.

The combination of these factors make it very hard to theoretically estimate the mechanical behavior of any rope composite. It is important that before structural application plenty of research is done into the mechanical behavior of the material. As stated before this is not within the scope of this research.

3. Numerical calculation methods

In order to increase the efficiency of the panels as designed a finite element calculation was included in the building method. With this finite element method structural analysis is possible providing the option of finetuning elemental areas. Another numerical method is the implementation of tension only elements in the web of the panel. Using these algorithms the structural behaviour of the design can be estimated. The algorithms are also used in order to run an optimization on the structure as elaborated in 5.3.

The finite element program together with the optimization algorithms were written in python. This way full control over the calculations is possible. As opposed to using a FEM-program executing calculations as a black box, in this case integration of the optimization is achieved. This results in a more efficient and transparent workflow. In order to make the process streamlined it was chosen to write a FEM-calculation based on trusses with normal forces only. This was also done because the initial concept was to use hinges, in order to wind the panel as a whole this initial concept was relinquished. In reality there are bending forces present at the vertices. These bending moments generated by the material at the nodes is in de structural analysis considered to be negligible in calculating the normal forces in the elements. In the practical applications however these bending moments could have a significant effect as elaborated in chapter 9. Considering only the axial loads will save time, which is especially relevant with the large amount of iterations of FEM calculations needed with the optimization. The input for this FEM calculation is extracted from the design as made in grasshopper. Nodal locations, boundary conditions, introduced forces, material properties and so on are imported into the Python script. In this script the panels are optimized using an optimization process based around the finite element method as defined in this chapter. From the python script the optimized panel and mechanical behaviour statistics are exported back to the grasshopper script. The FEM calculation can also be used separately from the optimization, this can be done using an assigned toggle in grasshopper turning off the optimization algorithm.

3.1 FEM calculations

The FEM calculation is based on the axial stiffness relation of a single element loaded in tension or compression. The axial deformation of an element deforming elastically can be calculated using the axial stiffness (K).

$$K = \frac{AE}{L} \tag{17}$$

With
K = axial stiffness [N/mm]
A = area [mm^2]
E = modulus of elasticity [N/mm^2]
L = length [mm]

When the force and aforementioned axial stiffness are known the axial deformation follows from the general stiffness as presented in equation 18.

$$F = K * U \tag{18}$$

With
F = normal force [N]
K = axial stiffness [N/mm]
U = axial deformation [mm]

When considering the structural systems within the scope of this research multiple elements are used. These elements are interlinked and have different orientations. With these orientations different coordinate systems emerge, every element with a distinctive orientation has its own local coordinate system. To create a distinction between local and global coordinates the corresponding equation 18 will from now on be denoted with a lowercase and higher case letter respectively.

The initial step for the FEM calculation is to create a local element stiffness matrix for each element. This stiffness matrix is based on the local orientation of the element and is the same for every element in the system. The equations 19 are used in the local coordinate system.

$$f_1 = k * u_1 + -k * u_2 \tag{19a}$$

$$f_2 = -k * u_1 + k * u_2 \tag{19b}$$

Which can be assembled into the local stiffness equation which is a matrix notation of the equivalent stiffness equation 19 combined with equation 17.

$$\begin{bmatrix} f_1 \\ f_2 \end{bmatrix} = \frac{AE}{L} * \begin{bmatrix} 1 & -1 \\ -1 & 1 \end{bmatrix} * \begin{bmatrix} u_1 \\ u_2 \end{bmatrix} \tag{20}$$

To transform the element stiffness matrix (equation 20) from local into the global coordinate system a rotation matrix (equation 24) is used. This rotation matrix is built up using cosines of the elemental angles calculated using the length of the element. x and y denoting the coordinates of the points with subscript 1 and 2 for start and endpoint respectively.

$$L = \sqrt{(x_1 - x_2)^2 + (y_1 - y_2)^2} \tag{21}$$

$$cos(\tau_x) = \frac{x_2 - x_1}{L} = c_x \tag{22}$$

$$cos(\tau_y) = \frac{y_2 - y_1}{L} = c_y \tag{23}$$

In the local coordinate system two degrees of freedom exist, one for every node. In the global coordinate system on the other hand four degrees of freedom exist, two for every node. This is the case because the local coordinate system is a one dimensional system, whereas the global coordinate system is in this case two dimensional.

$$[\tau] = \begin{bmatrix} u_1 \\ u_2 \end{bmatrix} = \begin{bmatrix} c_x & c_y & 0 & 0 \\ 0 & 0 & c_x & c_y \end{bmatrix} * \begin{bmatrix} U_1 \\ V_1 \\ U_2 \\ V_2 \end{bmatrix} \tag{24}$$

This last formulation can be called the 'rotation matrix' or τ In order to rotate the local stiffness matrix it is multiplied as follows to form the rotated stiffness matrix K_r.

$$[K_r] = [\tau^T][k][\tau] \tag{25}$$

Now the stiffness matrix is rotated into the global coordinates, the goal is to assemble the rotated stiffness matrices of each elements into one global stiffness matrix. To achieve this the stiffness matrices of each element have to be scaled up to include all degrees of freedom, even of the nodes they do not connect to. For this intent a global placement matrix is constructed. This global placement matrix has the dimensions of four by the amount of degrees of freedom at the location where the element has influence on a degree of freedom a 1 is placed, on all the other locations a 0.

Subsequently the elemental stiffness matrix in the global dimensions is formed by the following formula.

$$[K_G] = [B^T][K_r][B] \tag{26}$$

Succeeding the formation of the elemental stiffness matrices for each element in the global dimensions, addition takes place. For each element in the system the K_G is summed to form matrix K. The general stiffness equation (equation 18) is then solved but first the restrained degrees of freedom should be removed from both the force matrix as well as the stiffness matrix. This implies that no nodal displacements can occur at the location of nodes that have restrained DOFS. After this preparation phase the matrix equation is solved leading to the nodal displacements expressed in every degree of freedom. The previously removed DOFs are reinstated with all zeroes after solving.

Consequently the global displacement matrix can be isolated to form the elemental displacement matrix where only the DOFs related to the element are left. From these DOFs the nodal displacements are derived. With one element and two nodal displacements the new length of the element can be calculated using equation 21. From this the strain can be obtained with the following equation.

$$\varepsilon = \frac{L_{new} - L_{old}}{L_{old}} = \frac{\delta L}{L_{old}} \tag{27}$$

From the elemental strain a few values can be derived which will be later used. The sign of the strain described the nature of the force, either compressional or tensional. The nature of the force can be used for identifying later described tension only elements. Additionally from the strain together with the elements Young's modulus the stress can be obtained using the following equation. From this stress the internal forces can be obtained. These elemental stresses can be used for strength analysis.

$$E = \frac{\sigma}{\varepsilon} \tag{10}$$

$$F = \sigma * A \tag{11}$$

A final use of the strain which is considered in this thesis is the calculation of strain energy. This strain energy will be used in the optimization phase and can be derived from the strain and the elemental force using the following equation.

$$U = \frac{1}{2} * F * \delta L \tag{28}$$

With:
U = strain energy [Nmm]

3.2 Tension only elements

In a general FEM calculation, all elements may be either tensional, compressional or zero force. However with the use of thin fibrous elements the high risk of buckling can cause problems with the existence of compressional capacity, this effect is only present in certain parts of the panel. The edge elements of the panels will be aggregated from several, by resin interconnected, strands which will cause resistance to buckling. The web elements however will be executed singular, there is no contact between individual web elements because of the height needed for winding. This effect will be elaborated further in the thesis. Even though there will be resin present in the material the strands will still be considered too thin to take any compressional loads. If these elements would be subjected to compressional forces immediate buckling would occur and the forces would redistribute over the other elements. As buckling is not considered in a general FEM calculation this lack of compressional resistance has to be simulated using some additional strategy which will be non-linear in nature. This method will be built up as follows.

The first step is to run the FEM calculation as usual in order to obtain the elemental forces. Subsequently all the fibrous elements present in the web that are subject to compressional forces will be identified and penalized. The elements in the edge will not be penalized when in compression, the resulting compressional elements do have to be checked for buckling in a later

stage. The penalisation is done by reduction of the element's young's modulus by a penalization factor (p) which is defined by the user.

$$E_{penalised} = p * E_{original} \tag{29}$$

With
E = modulus of elasticity [N/mm^2]
p = penalization factor [-]

By using the penalised Young's modulus the stiffness of the element in compression decreases with the next iteration of FEM calculation. For choosing a right penalisation factor it is important to realise that the factor is re-applied with each iteration. With decreased stiffness the forces are redistributed over elements which provide more stiffness. This redistribution of forces is best to occur in a gradual way in order to achieve a reliable convergence. Using a stringent factor will lead to faster but unreliable convergence. This unreliability is due to the existence of local and global optima in tension only force distribution. Stringent factors are quick to find an optimum but tend to get stuck in local optima. In general application the penalisation factor is chosen to be 0.9 for compressional elements. There is a minimum Young's modulus of 10Mpa after which the elements stiffness is not reduced further. This is a non-zero minimum which is negligible on the scale of the stiffness of the fiber material. This minimum was defined in order to prevent elements from having a zero stiffness which would lead to problems with the FEM definition.

In order to illustrate the workings of the tension only algorithm two panels were plotted in figure 12. On the regular pentagon a point load is introduced of 1000N, the internal forces are plotted for each panel. Red elements are denoting compression, blue elements are zero-force or tension. In the panel on the right the tension only algorithm was applied demonstrating the elimination of compressional elements.

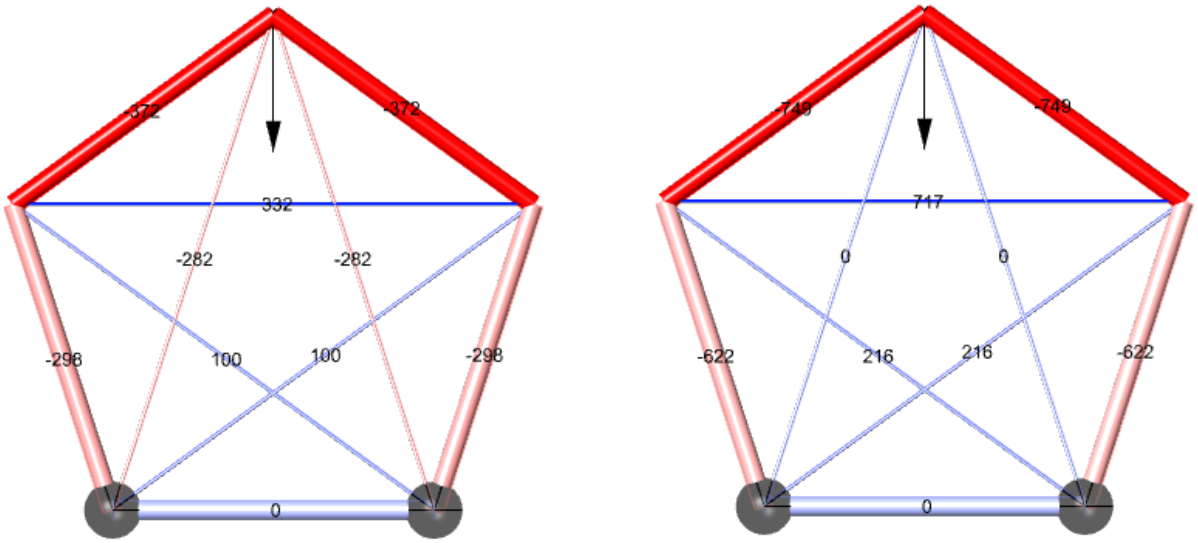

Figure 12: Tension only algorithm applied to a pentagon with a single point load, showing internal forces

In the following graph the convergence of the algorithm is plotted in terms of the change in strain energy of the total panel. Interpolations for three penalization factors are shown. Like stated before, choosing a higher penalization factor results in the need for more iterations before convergence is reached. Convergence is in this case defined as a state where the change in the total strain energy value is of zero magnitude.

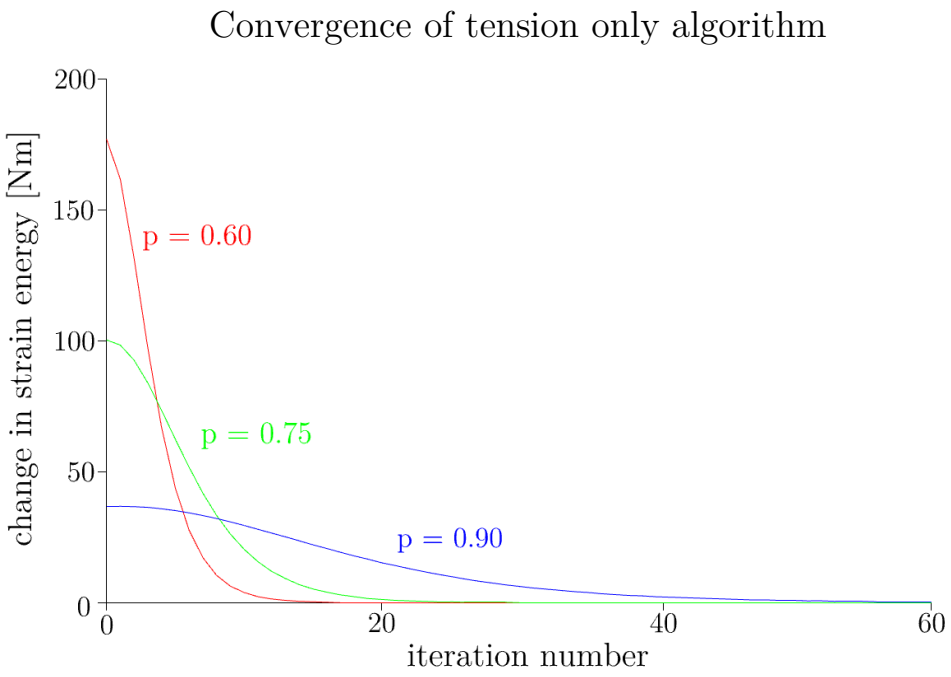

Figure 13: Convergence of tension only algorithm plotted against the number of iterations

The overall strain energy of the panel is observed to increase as the tensile elements are iteratively implemented. This seems to be the opposite of a design optimization, however it is merely including the relevant material properties (buckling) into the system. Should the strands in the web remain in compression the FEM calculations would seem fine but further in-depth calculations would recognise their high susceptibility to buckling.

3.3 Optimization

The project of fibrous winding is exceptionally suitable for optimization. As the panels will be wound using a robot, a high rate of control over the distribution of material can be achieved. The material will be introduced with a finite diameter and will be a modular part of the whole panel. Choosing where the material will be placed exactly is a logical consideration to be specified in order to increase efficiency. The panels will have a fixed geometry as decided by their initial design. This fixed geometry is constrained to the edges, the web can be freely formed within this boundary. The only constraint for the web strands is that they both start and end at a node. Starting in the middle of the edge elements would cause bending which is not included in the FEM-method as described. In order to include all possible elements a so called ground structure

approach is used. The optimization is free to change the sectional area of the web elements without ever making them zero. This essentially reduces the optimization from a topology optimization to a sizing optimization. All the nodes and elements present after the optimization were present as well before the optimization, only their size is adjusted.

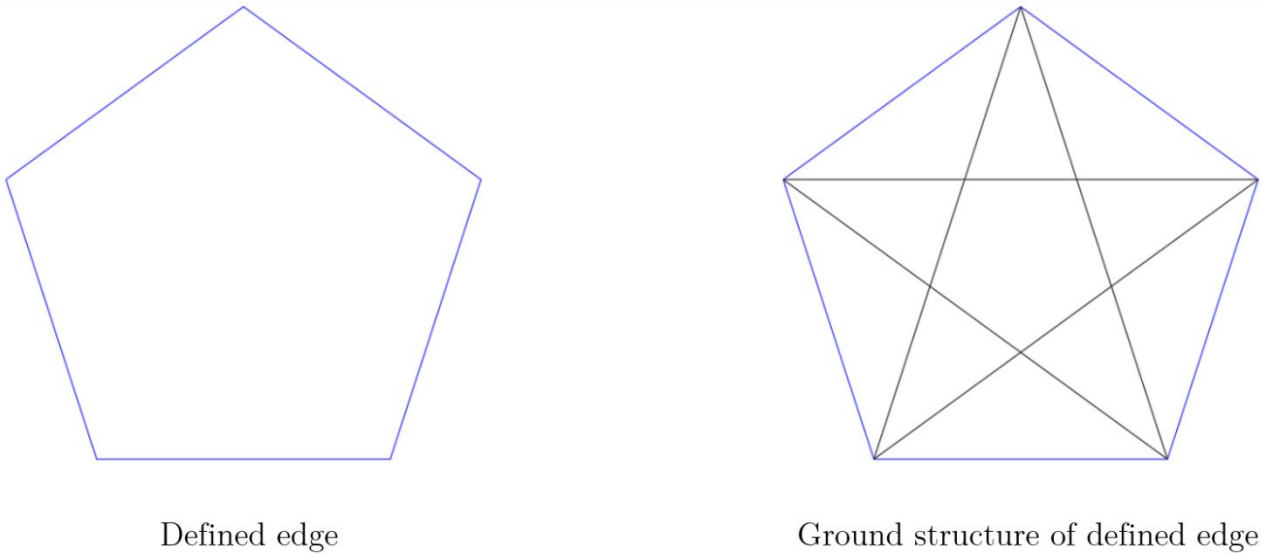

Figure 14: Definition of ground structure for optimization

3.3.1 Objective

Like with any optimization it is important to clearly state the objective. The objective of the optimization in this case is to create a panel where material is used as efficiently as possible. The main indicator of efficiency in a panel is chosen to be the total strain energy. This value is inversely proportionally linked to the stiffness of the panel. To increase the stiffness of the panel the objective value should be minimized.

$$min \sum U_j = \sum \frac{1}{2} * F_j * \delta L_j \tag{30}$$

3.3.2 Variable

The variable value in the optimization is the distribution of material over the elements. This is the only value which is allowed to change in the optimization. In this case the variable as used in the optimization is Vi-j which represents the volume of each element. This is however merely a derivate from the actual variable which is the area of the element. With each element adhering to equation 31 and the length being a constant. It is essential to note that the total volume of the panel is not allowed to change with a significant value at any moment of the optimization. With increasing total volume the objective value would be increased bypassing the need of the redistribution of this material.

$$V_j = L_j * x_j \tag{31}$$

With
V_j = elemental volume [mm^3]
L_j = elemental length [mm]
x_j = elemental area [mm^2]

3.3.3 Constraints

The constraints essentially provide for the realistic framework for the objective. Without well-defined constraints the objective function could never be satisfied. Below are the three constraints which the applied optimization adheres to.

1. General stiffness equation
2. Maximum total volume
3. Minimum elemental volume

The first constraint is that of the stiffness equation of the whole. This stiffness equation is solved in the FEM-algorithm. The displacements can only be found when the stiffness matrix has an inverse. The loads and boundary conditions have to be clearly defined and sufficient for a mechanically stable system. The optimization does not apply to mechanisms.

$$F * K = U \tag{18}$$

The second constraint is the total material volume. As mentioned before the total material volume has to be constrained in order to satisfy the objective in a realistic manner. The actual value of the total material volume is seen as a user variable and is to be decided based on the needed material.

Where there is a constraint on the total material volume of the system there is also a constraint of the elemental volume. As opposed to the total material volume constraint this is not a maximum but a minimum. The elements are permitted to be of any volume except zero. When a zero volume is detected in the algorithm it will force the element to take a volume of

$$V = 0.1 * L \tag{32}$$

This constraint was put in place in order to avoid elements being removed from the system. It could occur that a zero-force element seems irrelevant in one iteration but subsequently regains importance in the next. If it would be removed completely however there would be no way to reintroduce it into the system. Another reason why the minimum was introduced it the otherwise existing risk of creating a mechanism. When the system is no longer mechanically stable there is no way to adhere to the first constraint and no way of continuing the optimization.

3.3.4 The algorithm

The algorithm is based on the principle of proportional optimization. This method was chosen because of the relatively intuitive way of visualising the importance of each elements as a fraction of the strain energy density. The optimization can be ran without using complex mathematical definitions and is therefore easily customizable. The basis for the optimization is the following equation.

$$\frac{U_{density,j}}{\sum U_{density,j}} = \frac{V_j}{\sum V_j} \tag{33}$$

The ratio of the element's strain energy density to the summed total strain energy density is set to be equal to the ratio of the element's volume to the total area of the system. In order to find the volume, and logically area, of a certain element the formula is rearranged to form:

$$V_j = \frac{U_{density,j}}{\sum U_{density,j}} * \sum V_j \tag{33a}$$

Where the ratio of strain energy is called the optimization ratio:

$$\Phi_{optimization} = \frac{U_{density,j}}{\sum U_{density,j}} \tag{34}$$

The needed variables in the optimization ratio are simply obtained from the F and δL vectors from the previous FEM-calculation. Filling these in in formula 35 gives the $U_{density,j}$.

$$U_{density,j} = \frac{\left(\frac{1}{2} * \ F_j * \delta L_j\right)}{V_j} \tag{35}$$

The function that is being iteratively applied by the optimization algorithm is found by combining equations 33 and 34 into equation 36.

$$V_j, new = \Phi_{optimization} * \sum V_j \tag{36}$$

Finally the areas of each web elements are updated using the new volumes.

$$xj = \frac{Vj}{Lj} \tag{37}$$

Iterating this process of finding the strain energy and then redistributing the material is all there is to the core of the optimization process.

To get back to the optimization problem at hand only the webs of the panels are optimized. Therefore the equations as stated are used only on the web. In the coding there was however a window left open for the case where the edge would also be optimized. In practical terms however it is not possible to execute the edge with different areas for each element. This is the result from the way the edge is manufactured as will be discussed later in this thesis.

3.3.5 Multiple load cases

Regarding a real life application the structure would not endure just a single load case in its life time, instead multiple load cases are possible. Using the NEN norms these load cases can be described. With regard to their likeliness of occurrence each load case has its own safety factor incorporated. After correctly calculating the load cases as described in the norms they can be used to design the panels. No additional factors are needed as the load cases are already adjusted for importance with the included safety factors. In order to run the optimization for two load cases both load cases are run separately in the FEM-part of the code. Resulting from these calculations each element's strain energy density is identified based on each load case. The summation of the individual elemental strain energy densities is then divided by the summed total strain energy density to find the optimization ratio.

$$\Phi_{optimization} = \frac{U_{density,j,LCI} + U_{density,j,LCII}}{\sum U_{density,j,LCI} + \sum U_{density,j,LCII}} \tag{38}$$

It is important to note that with every added load case the optimization time increases. The biggest time consumer in the optimization is the FEM-calculation which has to be executed separately for every load case.

There is a significant difference between multiple load cases and different loads in the same load. Conceptualizing the idea of using multiple load cases is done with the figure underneath. The effect of two load cases is judged individually by calculating the strain energy of each element. Consequently the strain energies are added to calculate the optimum element areas.

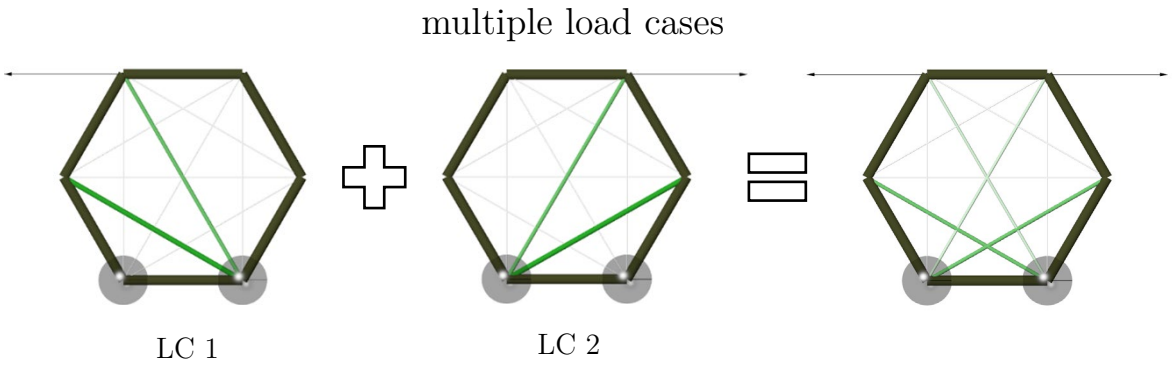

Figure 15: The effect of two load cases on the optimized panel visualized

If these two loads would be introduced on the panel in the same load case as shown below, no optimization of the web would occur. The applied forces cancel eachother within the upper edge beam and no forces are transferred to the supports.

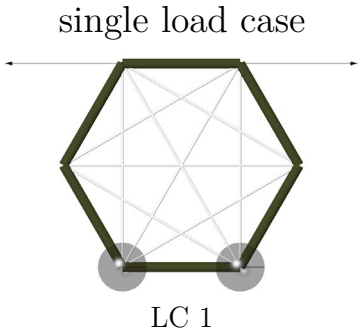

Figure 16: The effect on the optimized panel when a single load case is used

3.3.6 Optimization and manufacturability

Considering the manufacturability of the panel a specific addition was done to the optimization. This has to be done because the completed panel optimization is not the same as the actual structural design. The multiple load cases that were considered do not take into account incidental loads. These comprise of unexpected loads during transport or self-weight load during the assembly phase. In the case that the edge beam would be totally as modelled the hinges would cause instability by themselves. In reality there are no hinges at the vertex locations. The incidental loads would instead cause bending moments in the edge beams of the panel. The large deformations associated with this are problematic during assembly since the geometry could be changed in a way that is more drastic than the tolerance allows. In order to create additional stiffness in aforementioned situations, it was chosen to assign each web element with a minimum area. This minimum being the area of a single elemental winding. This creates a tensional solution for every incidental load. With tensional deformations generally being less large than deformations due to bending moment, the panel instability is reduced.

This minimum area is assigned when the elemental area dips below the threshold. This is done during the optimization. The optimization will still continue running with the initial total volume. This way no instability is created in the optimization but the minimum area is just added on top. The effect of this added material on the rate of optimization will be discussed in paragraph 3.3.9.

The minimum area is implemented in the same way as the elemental volume constraint. The previously discussed constraint limits the elemental minimum area to 0.1 in order to avoid said element to disappear from the FEM-calculation. This elemental volume constraint however is applied using a, depending on the total panel volume, negligible value.

3.3.7 Convergence of optimization

In order to retain control over the optimization process a damping coefficient was introduced. This damping coefficient is applied over the redistribution of material.

$$x_{j,new} = (x_j - x_{j,i-1}) * \eta + x_{j-1} \tag{39}$$

With

x_j = new areas (before damping) [mm^2]

$x_{j,new}$ = new areas (after damping) [mm^2]

$x_{j,\ i-1}$ = previous areas [mm^2]

η = area damping coefficient

In the specified equation it is evident that the damping is applied over the area instead of the volume. As the areas are simply a derivate of the volume this is essentially the same thing. With the implementation of a high damping factor the convergence is ensured to be more stable (Bendsoe & Sigmund, 2011). It avoids the optimization getting stuck in local optima and finding the global optimum instead. In order to elaborate on this statement figure 17 was included. In this graph three convergence developments are plotted for different damping coefficients. It is observed that using a more stringent damping coefficient less material is being displaced per iteration so it takes longer to approach zero change in strain energy. The highest dampening factor yields a result in the least amount of iterations.

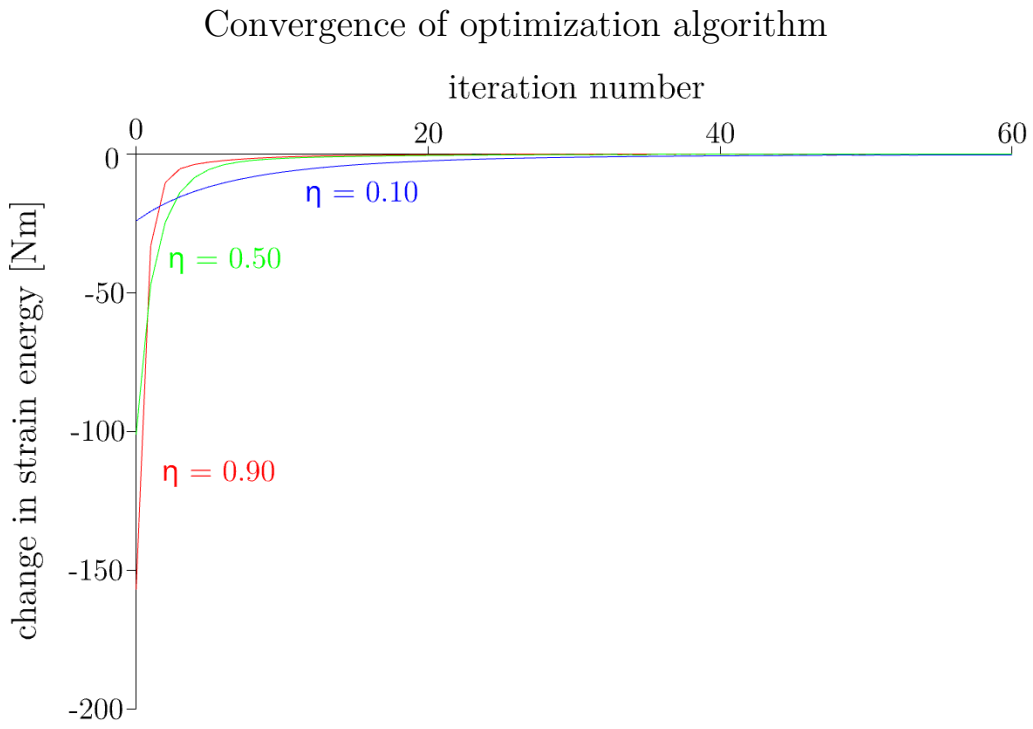

Figure 17: Convergence graphs for three dampening factors

Defining whether convergence is reached is an important part of any optimization. If convergence is not defined the optimization could essentially run forever. Absolute convergence would be reached when the parameters going into the algorithm are identical to the ones exiting it. At what point in time this state would be reached is a question of precision and the amount of significant figures that the algorithm framework handles. With increasing complexity of the optimization problem, reaching this state could take an unsatisfactory long time. For this purpose there were systems built into the algorithm in order to exercise control over the amount of iterations. The first way of control is simply defining the maximum amount of iterations, which is done as user input from the grasshopper script. The algorithm stops after reaching the defined number of iterations without regard to the result.

Another way of controlling the amount of iterations is defining cutoff values. The maximum amount of iterations is still being adhered to. However the actual amount of iterations might actually be lower due to the convergence being within the bounds for the cutoff values. For these cutoff values the convergence is defined in terms of the change of total strain energy in the system. After 3 iteration cycles the magnitude of change of strain energy is checked. When this value is smaller than the cutoff value defined by the user the algorithm is stopped. The following equation was used.

$$\frac{\left|U_{tot,i} - U_{tot,i-2}\right|}{U_{tot,i}} * 100\% < \zeta \tag{40}$$

With
$U_{tot,i}$ = total strain energy at iteration i [Nmm]
$U_{tot,i-2}$ = total strain energy at iteration i-2 [Nmm]
ζ = cutoff percentage [%]

For the previous value not Utot-1 was selected but instead Utot-2, this has to do with possible occurrence of state switching. This state switching can happen when the optimization changes between two material distributions. In this case the convergence might be sufficient but not showing that way due to a difference in strain energy between states. When state switching occurs the optimization continuous as otherwise. At the end of the optimization the state with the lowest strain energy is picked as the optimized distribution.

3.3.8 Convergence of compound algorithm

Both the tension-only algorithm as well as the optimization algorithm are implemented at the same time. As presented earlier the tension-only algorithm causes the structure to undergo an increase in strain energy while the optimization causes a decrease. In order to demonstrate the concurring convergence in several different scenarios the change of total strain energy was plotted in the graph in figure 18.

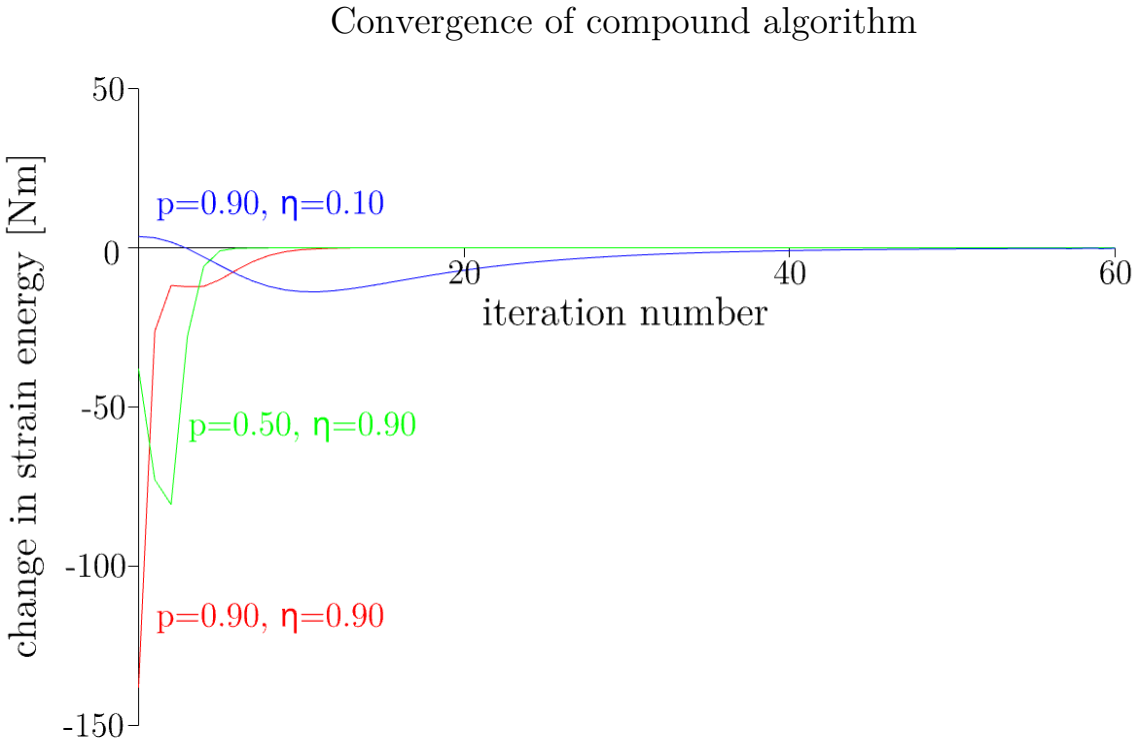

Figure 18: Convergence graphs for three combinations of dampening factors

From the graph some conclusions can be drawn. The optimization fluctuates around the actual optimized value which is reached when the change in strain energy becomes zero. From figure 13 It can be concluded the tension only algorithm enlarges the strain energy from the initial value. As explained before this does not mean the tension only algorithm is detrimental to the panel design. It merely imposes a more realistic scenario where compression is not possible. In figure 17 which plots the strain energy change for an optimization only it can be seen that with every step the strain energy increases. This is an expected result from the algorithm based on proportional optimization. Where these two situations are combined the fluctuation around the equilibrium is a result of the increasing and decreasing strain energies. Additionally the total amount of iterations for the combined convergence is observed to be smaller than that of both algorithms ran in sequence. This is hypothesized to be because of the summation of effects of both algorithms. The tension only algorithm reduces the stiffness of compressional elements, this causes the optimization algorithm to in turn reduce the area of the compressional elements. With both occurring at the same time in the iteration loop the tension only algorithm effect is amplified.

3.3.9 Effectivity of optimization

The effectivity of the optimization can be verified by considering the concept of volumetric strain energy. As opposed to the strain energy density that was introduced earlier this value is the strain energy multiplied with panel volume. The total volumetric strain energy of the panel is a marker inversely proportional to the panel stiffness. In the examples provided later in this paragraph the total material volume is varied using different minimum winding areas. Would

only the total strain energy be considered as a marker for panel stiffness the panels with more volume would have an unfair advantage.

$$W = U * V \tag{41}$$

With:
W = volumetric strain energy [Nmm^4]
U = strain energy [Nmm]
V = volume [mm^3]

The optimization rate is subsequently defined as the ratio of the volumetric strain energy before and after optimization occurred.

$$Optimization\ rate = \frac{W_i}{W_{optimized}} \tag{42}$$

With:
W_i= initial volumetric strain energy [Nmm^4]
$W_{i,\ optimized}$= optimized volumetric strain energy [Nmm^4]

In order to judge the optimization rate of the algorithm optimizations are conducted on three panels. Each panel is a regular polygon of radius 500mm. A pentagon, hexagon and octagon were considered. For all the shapes the initial web area is 25mm^2, corresponding to a diameter of 5.6mm and the edge area is 15mm^2. On all panels the bottom two points were horizontally aligned and simply supported. On the top point a point load of 1kN is introduced. In the case of two top points one of them is chosen. In table 1 the panels are considered in both an optimized as well as a pre-optimized state. For the full table it is referred to Appendix A. The optimization rates can be found for each situation after varying the minimum area. For the optimization a minimum area of 0.1 corresponding to a diameter of 0.36mm is always recommended as stated before. This minimum area keeps elements from being removed from the optimization. It also causes a small amount of material to be added during the optimization. In the table optimization rates are also noted for material diameters of 1mm and 4mm. It is noted that the optimization rates decrease with larger material radius. The optimization breaks if the initial web area is exceeded by the material area. The values in the table denoted with a 'd' are panels were discretization of area is assumed. This discretization will be further elaborated in chapter 4. As the discretization of an optimized area into a material area is always done by rounding up the d-values always add material. Since the material is always added on the location of an element that is not 1, the strain energy is increased. This could lead to minor changes in the optimization factor. In the table it can be seen that these changes can also be positive.

Table 1: Optimization rates for different polygons

		Volumetric strain energy initial [Nmm^3]	Volumetric strain energy opt. [Nmm^3]	Optimization Rate [x]
pentagon	∅0,36	2,10*10^8	5,06*10^7	4,15
	∅1	2,10*10^8	5,14*10^7	4,09
	d ∅1	2,10*10^8	5,13*10^7	4,09
	∅4	2,10*10^8	6,46*10^7	3,25
	d ∅4	2,10*10^8	5,94*10^7	3,53
hexagon	∅0,36	2,79*10^8	9,20*10^7	3,03
	∅1	2,79*10^8	9,33*10^7	2,99
	d ∅1	2,79*10^8	9,32*10^7	2,99
	∅4	2,79*10^8	1,17*10^8	2,39
	d ∅4	2,79*10^8	1,14*10^8	2,45
octagon	∅0,36	5,99*10^8	1,67*10^8	3,59
	∅1	5,99*10^8	1,70*10^8	3,53
	d ∅1	5,99*10^8	1,70*10^8	3,53
	∅4	5,99*10^8	2,18*10^8	2,74
	d ∅4	5,99*10^8	2,17*10^8	2,76

3.3.10 Optimization of panel assemblies

Up until this point only the optimization of single panels is discussed. The optimization as described however also works on assembled panels. The assembly should be optimized as a whole. This gives a different result than in the case of the panels being optimized individually and subsequently assembled. The reason for this is that the flow of forces changes with each iteration of the optimization. When the individual panels are being optimized isolated from the assembly, this change in flow of forces is not taken into account. The optimization of panel assemblies redistributes the material over the elements in the same way as within a single panel. This causes certain panels to have a higher amount of web windings than other panels.

When considering panel assemblies it is imperative that the inputs are processed correctly. Since only the web elements are optimized the corresponding element indices are transferred to the optimization algorithm. The web element indices are automatically identified by the algorithm when the assembly is properly defined. The volume of the edge elements is not considered a variable in the optimization. Their sections should be manually adjusted in order to satisfy the unity checks discussed in **5.6.2.** The edge elements will be formed by winding material around

the panel as a whole. Therefor the edge of each individual panel can be varied, but not the individual edge elements within a panel. Aside from just the unity checks the geometry of the edge beams is also based on the height of the web. With each panel having a varying amount of web elements also the height for each panel varies.

As discussed in the chapter design another consideration of panel assemblies is overall stability. When the stability requirements for the general stiffness equation (equation 18) do not hold, the FEM algorithm will return an error and the optimization will not run. The optimization is not able to run on mechanisms neither does optimizing the panels itself have an effect on the existence of a mechanism.

In figure 19 a six hexagon assembly is shown optimized for two vertical point loads. The minimum web winding area was defined to be 16. It shows the variance in web optimizations where some panels take most of the material. It also shows every edge element of a single panel having the same area.

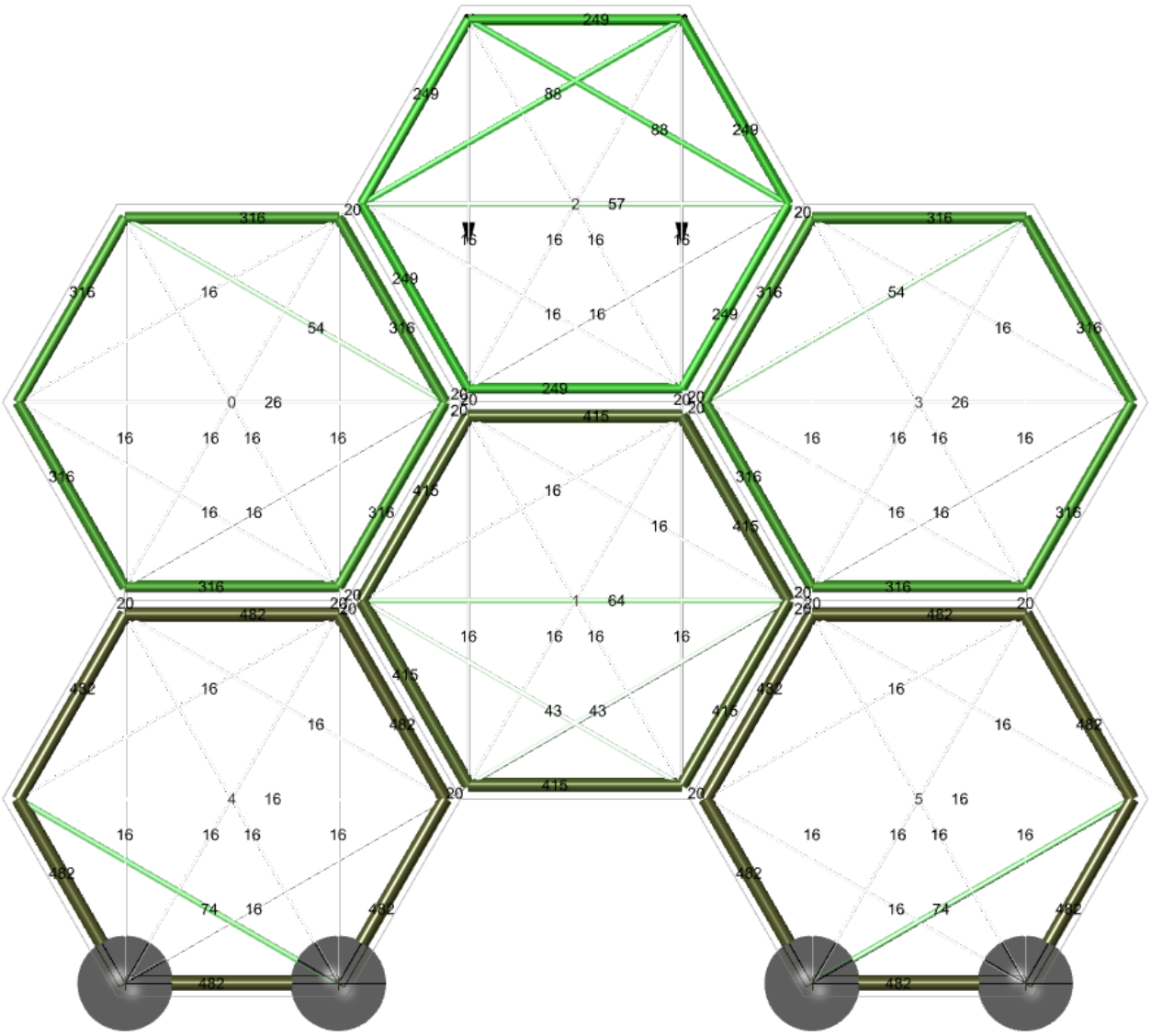

Figure 19: Six hexagon assembly with two point loads optimized

3.4 Visualisation tools

After the optimising of the panel has been completed, the area of each element is transferred to grasshopper. In order to gain insight in the optimization process additional data is transferred as well. This other data consists of the total strain energy per iteration and amount of iterations before the elemental areas were found. Beside optimization information also data about structural behaviour is transferred: forces and stresses for each element and the nodal displacements for each load case.

With the optimization data a visualisation was set up using a slider to scroll through the iterations. For each iteration the complete panel is visualised along with boundary conditions and each elements area. The areas are visualised as a scalable single pipe element that gets darker in color when the area increases relative to the other elemental areas. In the middle of each element the numerical area is showing. Along with this information the total strain energy is numerically shown on screen given in [Nmm]. This system makes the optimization visible and makes it clear how many iterations were needed to arrive at the optimized panel. The hexagonal panel is optimized for a horizontal point load as shown in figure 20. The elemental areas are visualized for 0, 1, 5 and 20 iterations respectively.

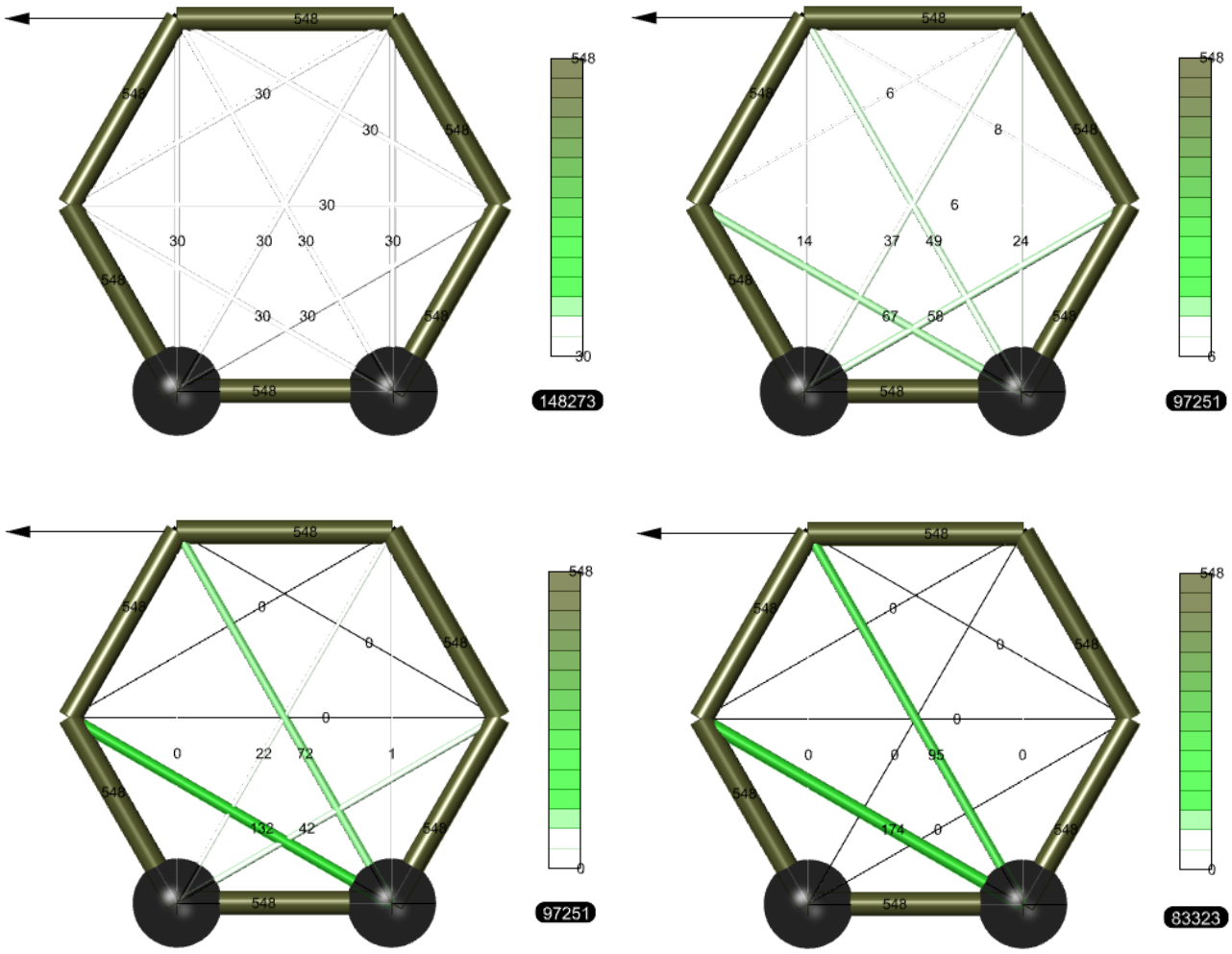

Figure 20: Hexagonal panel optimized for horizontal point load at 0, 1 (top) and 5, 20 (bottom) iterations

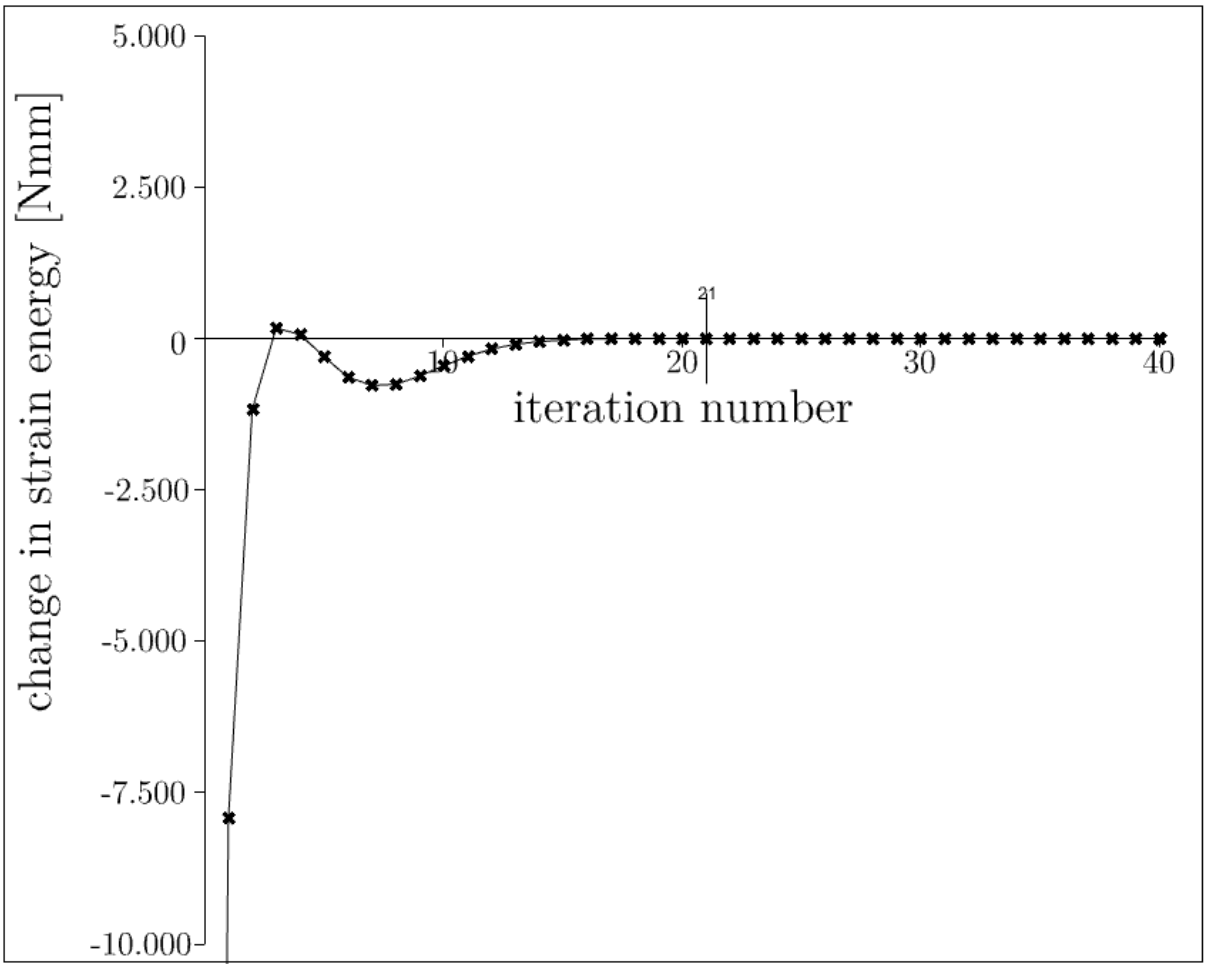

Figure 21: Convergence graph of the hexagonal panel as described

Another way of visualising the development of the optimization is by graphing the variation of strain energy for each iteration as shown in figure 21. Scaling can be adjusted with a slider, the same goes for a marker placed at the iteration number where the variation of strain energy is less than a user defined variable, in other words where convergence is reached. The graph plotted in figure 21 applies to the same hexagonal panel. The first iteration causes a change in strain energy of -50.000 Nmm and is not shown.

Aside from visualizing the optimization process the algorithm also functions as a more traditional FEM package. For the optimized situation the elemental forces can be plotted for each load case. Color gradient and on-element values show the magnitude of the force in each element in figure 22. Tensile elements are plotted blue and compressive elements are red. Supporting these visuals is a legend where the gradient is explained along with extreme values. The forces correspond to a point load of 10kN and are given in [N].

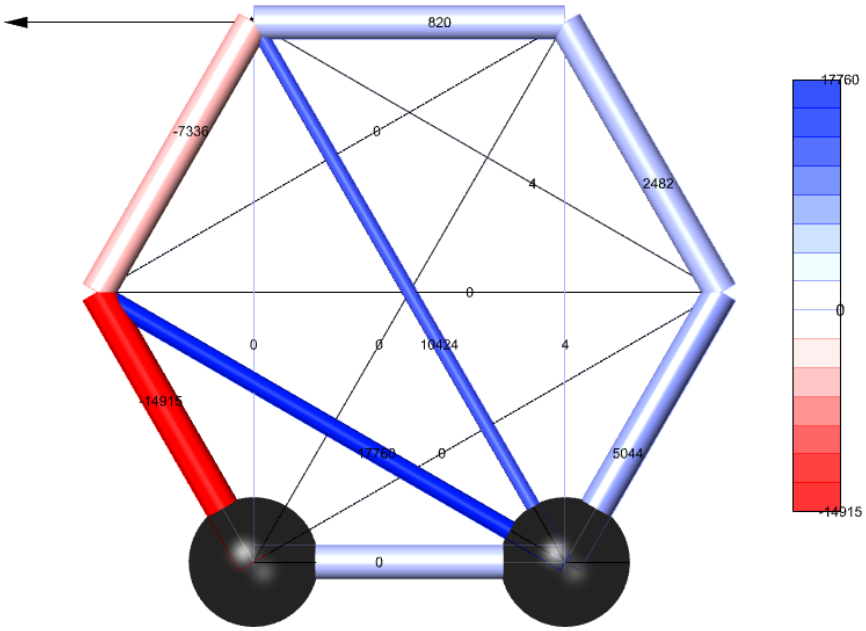

Figure 22: Visualization showing elemental forces in N

Additionally a visualization of the displacement is included in the algorithm and in figure 23. The nodal displacements are extracted from the calculation and translated into the deformed panel. Displacement is plotted for each load case separately, the load case is to be selected using a slider. Another variable is the scale of the displacement. As the true displacement is often too small to properly judge the visual is scalable. For quick analysis the maximum values of both the X and Y-displacements are shown at the location of the node where they occur. The displacements are given in [mm].

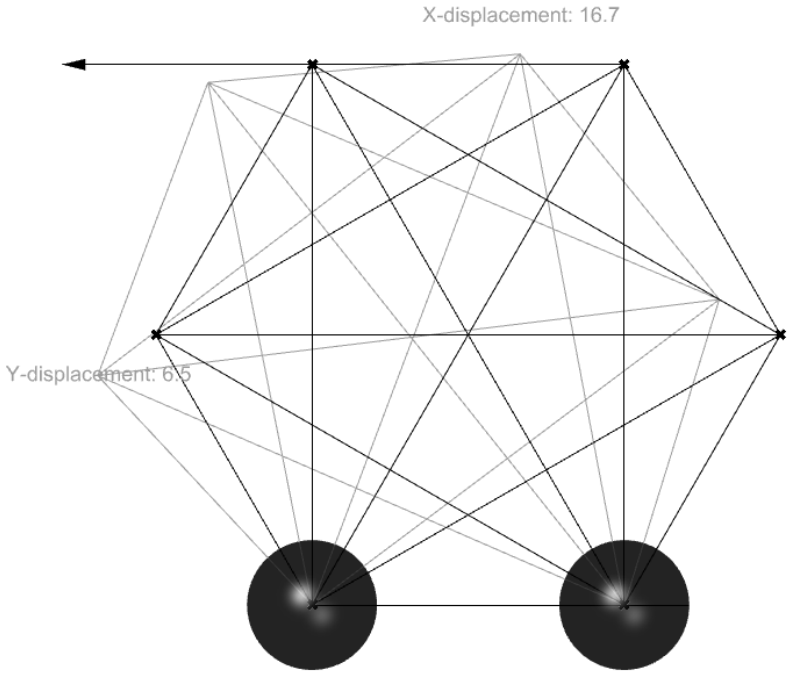

Figure 23: Visualization showing maximum deformation components in mm

3.5 Post processing structural analysis

As the Elemental forces are collected unity checks can be conducted. These checks take place after the optimization with the data belonging to the optimized panel.

Material properties are given as an input. The values of characteristic values should for UGT calculations be reduced according to EC.0 eq. 6.3 using a material factor. However with the character of the applied material in chapter 9 being experimental no material factor is known. Experimental values can be deduced but require large sample sizes.

Elemental loads are added from all load cases. This simulates the effect of load combinations as described in EC.0 6.4.3. When a combination of load cases is used it is important to establish the decisive load combination before the actual optimization is initialised. In that case the loads can be introduced into the algorithm with the proper partial load factors applied. If the decisive load combination is not known in advance this can be found out by trial and error.

The following Unity checks are conducted for each element that is subject to the corresponding failure mode. For each load case the unity checks are reviewed separately. The factors for each load case have to be manually adjusted depending on the nature of the load case. Afterwards the critical unity check for each element type is presented in a table. If the decisive unity check for every possible failure mode for every element in every load case is satisfied then the structure is considered safe.

3.5.1 Web elements

The web elements are tensile only. Checking the elemental load over its resistance is done as follows.

$$U.C. = \frac{\sigma_{Ed,t}}{\sigma_{Rd,t}} < 1 \tag{43}$$

Compression in web elements could theoretically occur since the minimum elemental area of one winding area is a small deviation of the true form as calculated by the algorithm. Additionally if different load cases are used it could be possible that some elements that would otherwise be in tension are in compression, this could be observed in figure 15. It is however theorised that buckling will occur elastically. The element subject to compression will lose stiffness really fast and subsequently cause the loads to be redistributed over other elements. Even if compressional forces would occur they would be small and therefor a unity check is not deemed necessary. It is important to note that the used material should have the capacity of large elastic deformations in this buckling failure mode. With the nature of the winding however the web elements do not have a connection between them, therefor buckling still occurs on an individual basis with relatively low forces. Returning to the previous load case the same element should show the same material behaviour under tension. The buckling that occurred during the compression phase should not degrade the tensional properties. More research should be done about the material

properties and the possibility of different load cases on the same material. If this research would show problems with the changes of force in the composite it is an option to leave the web windings free from resin.

3.5.2 Edge elements

Tension in the edge elements is not common but will still be checked with a unity check. This unity check is following the same principle as equation.

$$U.C. = \frac{\sigma_{Ed,t}}{\sigma_{Rd,t}} < 1 \tag{43}$$

Compression in edge elements will be checked using two methods. Simple compressional failure could occur in elements that have high area to length ratio. Elastic instability is a risk in slender elements.

Simple compressional failure is checked using the usual unity check.

$$U.C. = \frac{\sigma_{Ed,c}}{\sigma_{Rd,c}} < 1 \tag{44}$$

For elastic instability the geometric properties of the edge curve are considered. Euler's critical load is defined as the upper limit of the compressive load at which buckling will occur. This critical load can be defined by the following equation:

$$P_{cr} = \frac{\pi^2 EI}{(KL)^2} \tag{45}$$

With

P_{cr} = critical buckling load [N]
E = young's modulus [N/mm^2]
I = area moment of inertia [mm^4]
K = effective buckling length factor
L = elemental length [mm]

This effective buckling length factor is dependent on the boundary conditions of the individual element. It is a factor taking into account the actual buckling length that will occur. Since limited bending is able to accumulate within the elements relative to its normal force it was previously decided to assume the elements connections are hinged. For hinged connections the K-factor is decisive over the factor for fixed connections, being 1.0 and 0.5 respectively. For this reason the K-factor is assumed to be 1.0.

The area moment of inertia is a geometric property based on the section of the element. The actual section of the edge curve is established further in the algorithm. The build-up of the edge

is based on the height of the web, which is only known exactly when the winding path is complete. For this reason there is some manual iteration needed to run the algorithm with an initial assumption for the edge curve geometry needed. In chapter 4.4 elaboration on the edge curve geometry is given. In this section the method for calculating the area moment of inertia is described. The general equation for finding the area moment of inertia around axis y through the centroid of a composite section consisting of the same shapes is as follows.

$$I_y = \sum (I_{y,i\ +} A_i * d_i^2) \tag{46}$$

With
I_y = area moment of inertia of composite section [mm^4]
$I_{y,i}$ = area moment of inertia of element i [mm^4]
A_i = area of element i [mm^2]
d_i = perpendicular distance between centroid of element i and the axis y trough centroid of composite section [mm]

This general equation can be rewritten into the specific equation for a composite section consisting only of circular sections.

$$I_y = \sum (r^2 * \left(\frac{\pi r^2}{4} + {d_i}^2\right)) \tag{46a}$$

With:
I_y = area moment of inertia around axis y [mm^4]
r = radius of winding element [mm]
d_i= perpendicular distance between centroid of element i and the axis y trough centroid of composite section [mm]

The axis y is to be taken as the weakest axis because this will be the axis around which buckling will occur. When the critical buckling load is calculated a unity check is conducted according to **equation x.**

$$U.C. = \frac{F_{cr}}{F_{Rd}} < 1 \tag{47}$$

3.5.3 Connection elements

There are several possible connection elements depending on the amount of nodes they connect as shown in figure 5. The connection elements are modelled as longitudinal elements with hinged connections. In reality the small geometry might cause them to be executed as planar sheets

which will be further elaborated in chapter 7. Since the FEM will process these connections as longitudinal elements some translation should be made from longitudinal element to sheets. For first order connections the sheet element is essentially the same as the calculated longitudinal element. For second order connections the following preliminary design strategy was used. The longitudinal elements are drawn into the sheet elements. In figure 24 the longitudinal elements are shown to have a width of d without overlap. This d is considered to be the width of a single element within the FEM assumption. The extra material outside of this width is considered sufficient to resist additional structural effects occuring from the transformation from hinged elements to a single sheet.

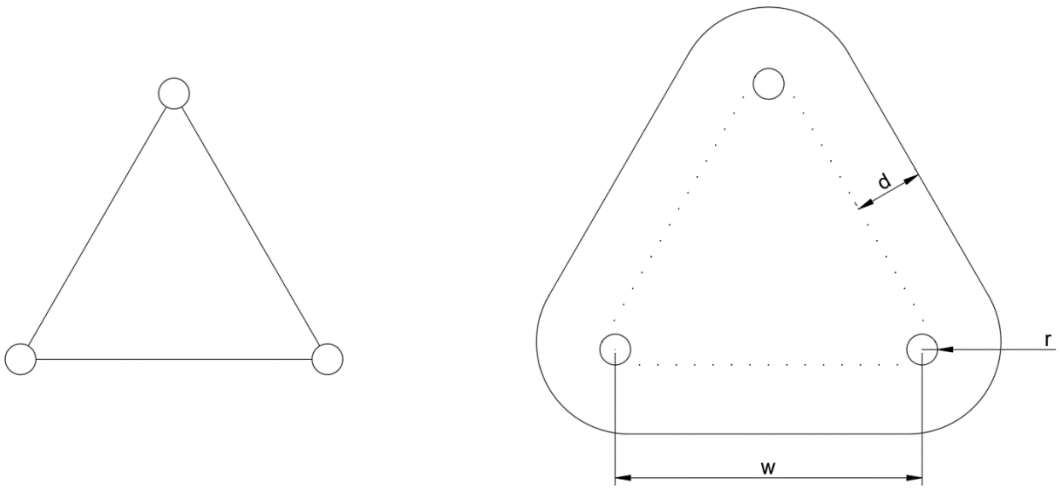

Figure 24: Hinged longitudinal elements as modelled on the left, proposed connection sheet on the right

In order to check the connection elements both a simple compressional and tensional unity check were conducted. Since the connection distance is small compared to the dimensions of the elements an elastic instability check seems to be unnecessary.

The unity checks are again as follows, equation 44 checks for simple compression.

$$U.C. = \frac{\sigma_{Ed,c}}{\sigma_{Rd,c}} < 1 \tag{44}$$

Equation 43 checks for tension.

$$U.C. = \frac{\sigma_{Ed,t}}{\sigma_{Rd,t}} < 1 \tag{43}$$

3.5.4 Stiffness

Checking a structure with regard to stiffness is loosely defined by EC.0. No strict conditions must be met, as instead the conditions are interpretable per situation. Since the algorithm was designed without specific application in mind these conditions are to be interpreted. When finding the extreme values for the displacement the visualisation can be used. Care should be put into properly defining the load combination with all partial load factors taken as 1.

4. Winding methods

After optimizing the ground structure the elemental areas should be translated into a discrete amount of windable strands. For this purpose the continuous areas of the elements are divided by the single strand area. The remaining number is rounded up to the next full integer in order to incorporate at least as many strands as the area implies. The discretising of the elements does cause the optimization to be diluted depending on the area of the strands. However this effect remains small especially with a small single winding area.

At this point in the algorithm the edge windings and the web windings are separated. They will be modelled in different ways by the program. There will also be differentiated between edge windings, which will be actually wound around the vertices, and the edge beam, which is a compound of elements that is wound around the panel as a whole. The edge windings are included in order to properly distribute the forces from the web into the edge. Without edge windings the threaded ends would only be connected to the edge beam by a resin interface with the web winding. While with the edge windings in place the forces could be redistributed along the entire length of the edge beam. This concept is further elaborated in paragraph 9.5.5. In order to keep the web in the middle of the edge beam the edge windings are executed in the same amount under as well as above the web. The amount of edge windings is an input in the script.

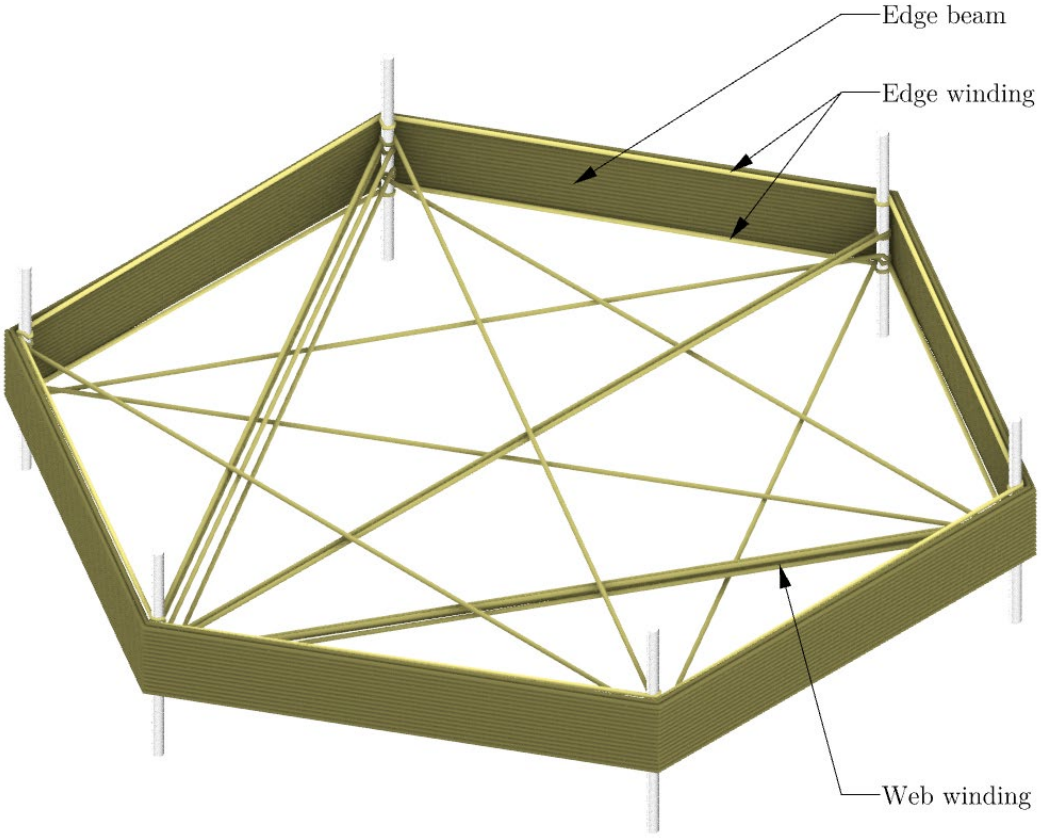

Figure 25: Wound panel showing the different approaches to the separate components

The winding process will start with the formation of the lowest set of edge windings. After this the web is wound followed by the upper set of edge windings. The panel is completed by winding

the edge beam around the panel. The formation of the web is the central part of the panel. Several actions are required to translate the web into a continuous material path. The edge beam is more straightforward in this aspect because only the amount of elements is defined and the path is already known. The path of the edge beam is always circular passing through the vertices one by one.

4.1 Web path

In order to find a path over all the strand elements of the web, aspects of graph theory are applied. Graph theory is a mathematical concept where the connectivity of a system is described with vertices and edges. In this case the optimized structure is translated into an undirected graph where the interconnections of all the nodes are finite edges and the direction of the edges does not matter. However the undirected graph will be translated to a directed graph at the end of this chapter. The directed graph will be the basis of the robot path that will connect the vertices in the established sequence.

Whether it is possible to wind a certain panel with a single strand is defined as the existence of a Eulerian path in the graph. A connected graph has a Eulerian path when there exists a closed trail containing every edge of the graph. The graph is considered semi-Eulerian when the trail is not closed but has a separate start and endpoint (Wilson, 1996).

After the graph is schematically deduced, the requirement to consider an Eulerian path is to analyse if the graph is connected. In the case the graph is not connected an Eulerian path cannot exist, and therefore it has to be connected first. Initial testing if the graph is connected is done with the following formula

A graph with n vertices and e edges is connected when the following equation holds:

$$e > \frac{(n-1)(n-2)}{2} \tag{49}$$

When this formula returns ‘true’ no edges are added. When ‘false’ is returned there are connectivity issues. In order to fix these issues an iterative algorithm was scripted in grasshopper.

The first step of this algorithm is to actually identify the existing groups. To do this the algorithm judges the branches representing all connecting edges. If the index of an edge is found in more than one branch this means that these nodes are a connected group. In order to combine the branches in such a way that sets of connected groups emerge, a python script was used which was retrieved from the grasshopper forum (Khaled, 2020). The connected groups are the output from the python script. When the output consists of a single branch the graph is connected, when the output however consists of more than one branch the graph is not connected and further action needs to be taken.

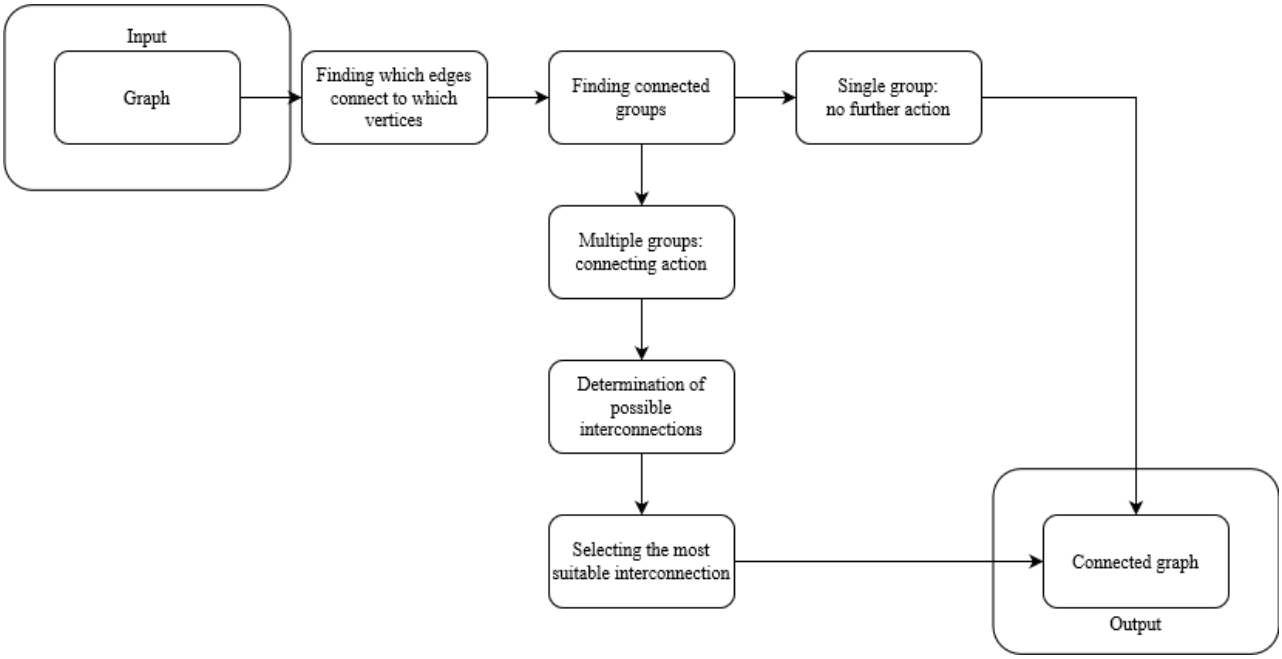

Figure 26: Process flowchart of checking and realizing graph connectivity

All separate groups are iteratively connected with their shortest possible connection, always forming an edge that did not previously exist. This new edge is not allowed to fall outside the boundary of the panel. The new edge is also not coinciding with an outline-element (later forming the edge of the panel) except when otherwise the connection of the graph is not possible. The end result of this algorithm is the first altered form of the graph where the edges are all connected. A flowchart of the aforementioned process is included in figure 26.

After the graph is defined and its connectivity is ensured, a test is performed in order to find whether or not the graph is Eulerian without further alterations. For this purpose the degree of each vertex is measured by counting the connected edges. This degree of connectivity is also called valence.

By definition a graph is Eulerian when the degree of each vertex is even.
THEOREM 1, (Wilson, 1996)

By definition a graph is semi-Eulerian when the degree of two vertices is odd while the rest being even.
THEOREM 2, (Wilson, 1996)

These theorems can be explained by the logic that if a path along the vertices would exist all vertices would have an incoming stream as well as an outgoing stream. Only the two vertices that form the begin and the end have an uneven amount of connected elements.

When the graph is known to be either semi-Eulerian or Eulerian the next step is to identify the path. However when the graph turns out to be non-Eulerian extra operations are necessary as shown in figure 27. These operations are based on the degrees of connectivity of the vertices in the graph. All odd degreed vertices are listed. By adding an edge to the odd degreed vertices

these can be made to have an even degree. In this process new edges are created. These new edges are preferred to run over existing edges in the graph if this is not possible a new edge is created. If the algorithm finds more than one possible edge the shortest one is applied, adding the least amount of material. This process will keep running until the graph is semi-Eulerian.

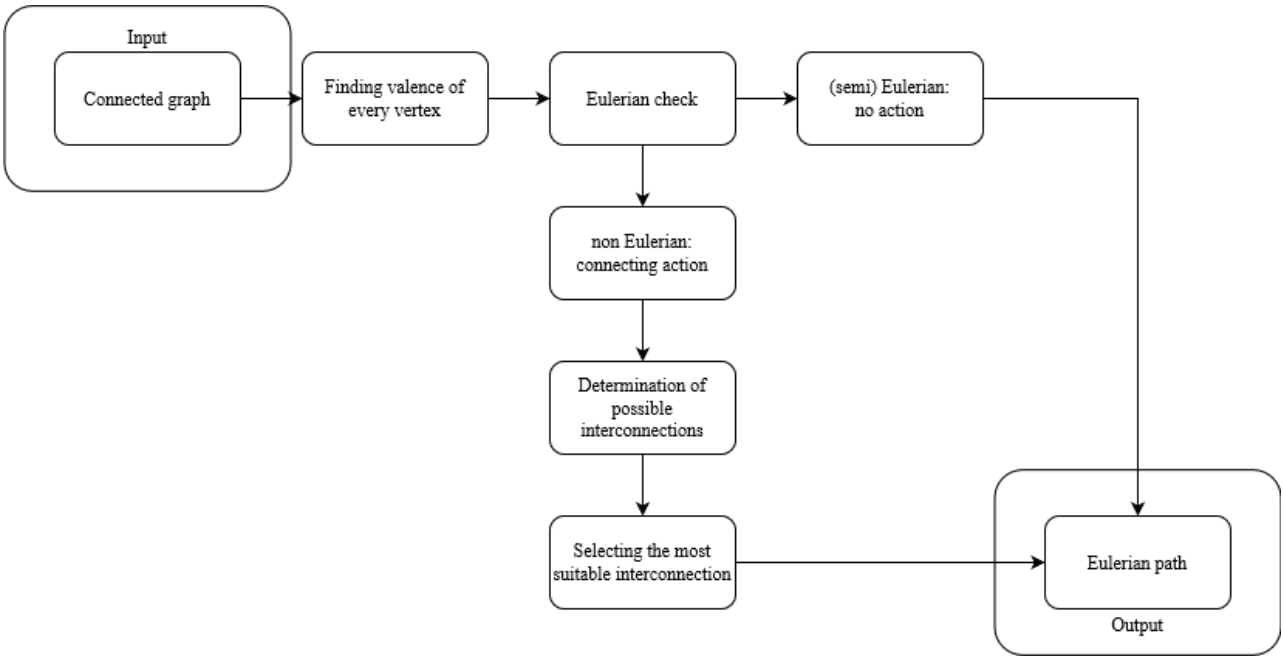

Figure 27: Process flowchart of checking and establishing existence of Eulerian path

The result so far is a panel that is known to be windable. If the graph is semi-Eulerian the start and endpoint are defined by the two vertices of uneven degree. If the graph is Eulerian the start and endpoint are irrelevant. During the process elements might be added to the panel after it was optimized. These elements are required for the manufacturability. It cannot be known in advanced how many elements will be added but the experience has been that the added elements are limited. This adding of web elements does have a negative effect on the optimization factor as described earlier. The exact effect is dependent on the total panel volume and the volume of the element. To keep the influence on the optimization factor as low as possible the added elements are of the smallest possible size. Adding of elements in the panels web is preferred over adding on the edge. This is the case because this is the location where the material usage is most stringent.

While the existence of a sequence is confirmed at this point, the sequence itself is not known. To find the Eulerian path a script was made, based on the Fleury's algorithm:

Let G be an Eulerian graph. Then the following construction is always possible, and produces an Eulerian trail of G. Start at any vertex u and traverse the edges in an arbitrary manner, subject only to the following rules: (I) erase the edges as they are traversed, and if any isolated vertices result, erase them too; (II) at each stage, use a bridge only if there is no alternative. THEOREM 3, (Wilson, 1996)

Fleury's algorithm is applied as shown in figure 28. The starting point of the sequence is one of the two vertices with uneven degree in a semi-Eulerian graph. In an Eulerian graph the start point is randomized. After the start point the next edge to form the sequence is picked, adhering to some restrictions. The edge is removed from the considered set but saved as the first edge forming the path. The first restriction is that the removal of the chosen edge is not allowed to result in two separate graphs. Grouping is checked with previously mentioned integrated python script, if more than one group exists after removal of the edge this move is not allowed. This restriction is defined as such because if the removal of the edge would cause separate graphs, there would be no possible way of finishing the panel with one continuous winding. Another requirement of the chosen subsequential edge is that it is not allowed to be a 'bridge' unless there is no alternative. In practice this means the vertex connected to the edge that is being removed cannot be of a valence smaller than one. This requirement can be bypassed when the possible edge connects to the end point and there are no other options left. In that case the last edge of the Eulerian path is reached and should be included in order to complete the graph. Iteratively implementing this algorithm until all edges are removed will lead to an Eulerian path. This algorithm essentially consists of a first iteration loop implemented within a second iteration loop. The first iteration looks for a suitable next step by testing all possibilities. In graphs where vertices have lots of connecting edges a same amount of iterations are needed to find the suitable next step in the path. The higher level iteration keeps track of the removed edges and the order of the points in the Eulerian path. A graph consisting of an x amount of edges needs an x amount of first order iterations to find a complete path, within these first order iterations the second order iterations keep track of all the possible edges connected to the considered point. The amount of these second order iterations is based on the amount of edges connecting to each point. Because of the second order iterations this part of the script is generally the heaviest and takes the most time to run.

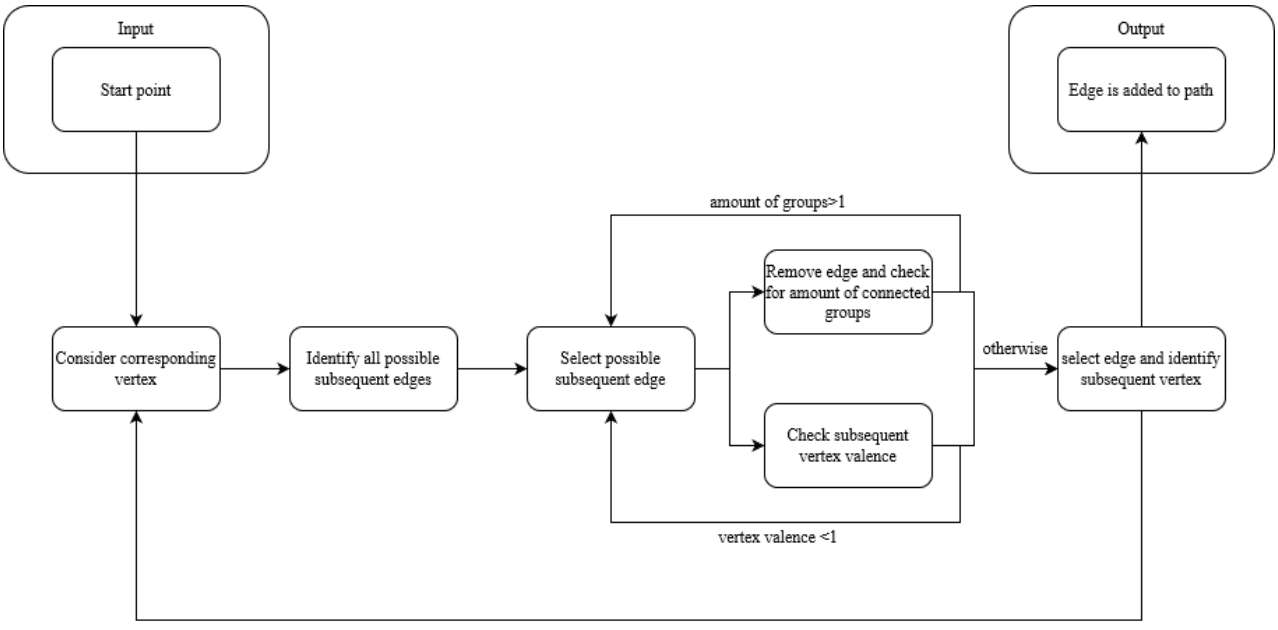

Figure 28: Process flowchart of Fleury's algorithm

4.1.1 Web height

The path as a list of vertices given by the Fleury algorithm is given as an start point from which the web path is formed. The web is created by forming an encirclement at each visited vertex. The way this encirclement is realized will be clarified in **section x**. Before this happens however the path needs to be expanded in height. The vertex path extracted earlier is two dimensional. This is cause for problems in the real life application. An important limitation is the fact that the winding around a vertex cannot take place in the same location where material is already present. If this fact would be ignored the end effector might damage existing material or it might cause unexpected and incorrect placement of the material. Another risk of damage or incorrect placement occurs when the material placement clashes with existing material within the web itself. To combat this effect the height of the windings should be varied when placing the material. These two clashing risks form the foundation of the following algorithm.

In order to create a reliable path a procedure for dividing the material over the height was developed. The vertex order is used as starting point. The algorithm (visualized in figure 29) iteratively considers all the points respectively. It keeps track of the points, and paths, formed in the previous iterations. When a clash is detected the height of the winding is increased in order to avoid it. After the height of the winding is increased the memory of the algorithm is cleared because clashes cannot occur over different height levels. By this method the algorithm essentially divides the vertices in layers checking for clashes at each layer. The height of each layer is assumed to be unity at this point. Depending on the amount of encircles and the diameter of the used material this height difference is adjusted after the algorithm is complete.

Figure 29: Process flowchart of inducing varying height

The height in the web is necessary for manufacturing purposes. In structural terms however this solution is not ideal. The web elements will connect to the edge in varying heights. Eccentricities are introduced for each element not connected to the middle of the edge beam. This causes torsion in the edge beam. Torsion in the edge beam can cause a complex failure mode based on shear failure. In the examined elements the torsion was considered negligible in comparison to the other failure modes. In further advancement of the presented building method it might be meaningful to include torsional calculations. These calculations would ideally include the summed individual effect on beam torsion of each web element adjusted for direction and magnitude of force. In order to translate the torsion into shear stress the edge beam section should be analyzed using a FEA deducing the torsional constant. The shear stress check is then dependent on the shear resistance of the composite material. This shear resistance takes into account shear within the material itself and also shear within the interfaces between elements. At this point no external control is exerted on the eccentricity of each web element. In the case that the material is sensitive to shear due to torsion it might be beneficial to optimize the web elements location. Optimizing in this case means positioning the web elements with the highest internal forces in the middle of the edge beam.

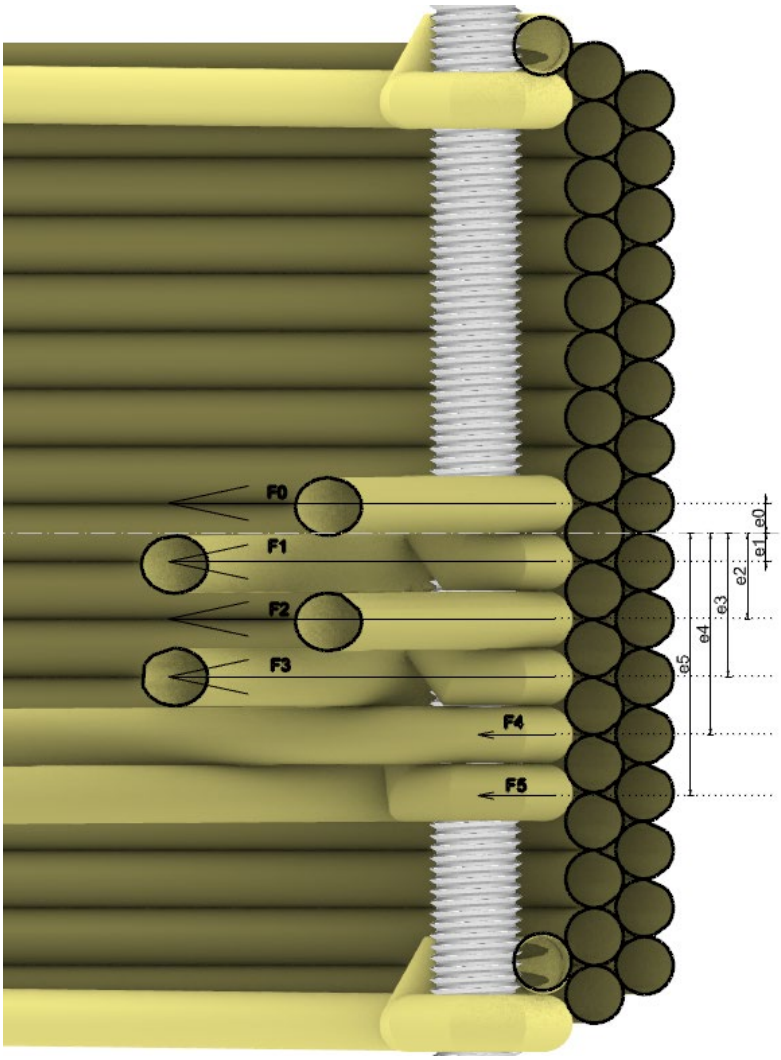

Figure 30: Web height introducing eccentricities into the edge beam

4.2 Edge windings

With the web path being expanded in three dimensions the vertex list corresponding to the edge windings are introduced above and below the web windings. The inclusion of the wound edge elements is done by simply creating a variable amount of extra levels both above and below the levels for the web winding. The exact amount of edge windings is user defined. Each edge winding is a full rotation sequencing all the vertices of the panel. The edge winding vertices order is adjusted to align with the vertex order of the web path. In practical terms this means if the web starts at vertex three the first edge winding sequence will stop at vertex three. When the web path finishes at vertex one this will be the first point of the edge winding.

4.3 Encircling vertices

To connect the weaving medium at every vertex these vertices are encircled as shown in figure 30 as a side view and figure 33 as a top view. The radius of this encirclement can be adjusted. In application the vertices are represented by threaded ends. A smaller radius decreases the distance between the end effector and the threaded end. In order to properly clear the threaded end a suitable radius is to be found. Besides this lower limit there also exists an upper limit. A radius that is large decreases the maximum size of the panel as the encirclement is to be taken into account when the robot reach is considered.

The amount of encirclements can also be adjusted. This value has an effect on how well the separate elements of the panel are interconnected. For instance if a force is introduced on the threaded end there is a risk of the threaded end simply being pushed out of the edge beam. If there are no encirclements this failure mode is dependent on the strength of the interface between the threaded end and the resin. If there is however encirclements present the failure mode depends on the strength of the composite and the interface between the composite and the resin. The more encirclements are present the larger both the composite area as well as the interface area are. Further clarification of this failure mode can be found in chapter 9.5.5.

Encirclements are also required to ensure all elements work individually without slip occurring at the vertices. Encircling the vertices creates more friction as a larger part of fiber is connecting with the vertex. In the case no slip would be prevented the forces occurring in the individual elements would redistribute over the consecutive elements. This is not desirable during the winding of the path because of the risk of temporary loss of pretension. If the tension on the system would even be temporarily lost it could cause problems in the whole previously wound panel. The redistribution of forces during the manufacturing phase can be calculated using the capstan equation. This equation is as follows:

$$T_{load} = T_{hold} * e^{\mu\varphi} \tag{50}$$

With:

T_{load} = maximum load [N]

T_{hold} = resulting force at other side [N]
μ = coefficient of friction [-]
φ = rotational angle of material in contact with vertex [rad]

The pre-tensioning force is approximately derived from the peripherals to be 20N. Assuming a single full encirclement of the fiber causes the minimum of encircling radius: 2π radians. The total force which is needed to keep the system in balance after the encirclement is 3.7N according to equation 50. This means that 80% of the pre-tensioning during manufacturing can be lost without losing pre-tensioning in the material that was placed before the last encirclement. These values are considered sufficient in order to use a single encirclement. In the case resin is used, after hardening no slip can occur due to the rigid circle geometry. In hardened elements no redistribution of forces is assumed to be present.

The encirclement algorithm is achieved with yet another iteration loop in grasshopper. For this loop the point order is an input. Around every point a circle of points with adjustable diameter and resolution is formed. In order to properly define the incoming location relative to the first point of the winding path an initial approach should be established. This input is expressed as the coordinates of the start point of the material. In less abstract terms this is where the material is attached to the mold in order to form a start point. The algorithm iterates over the point order. At each point it analyses the incoming and outgoing path, these paths being defined as lines which are tangent to the circles.

In order to cause a robot path that is as smooth as possible it is important to approach the actual shape that the material will assume. This will cause less variance in the pre tensioning force. The algorithm lets the path approach the actual material shape by not simply arriving at the node and starting the encirclement (shown in figure 31 left), but actually taking into account tangency of the arriving path (shown in figure 31 right).

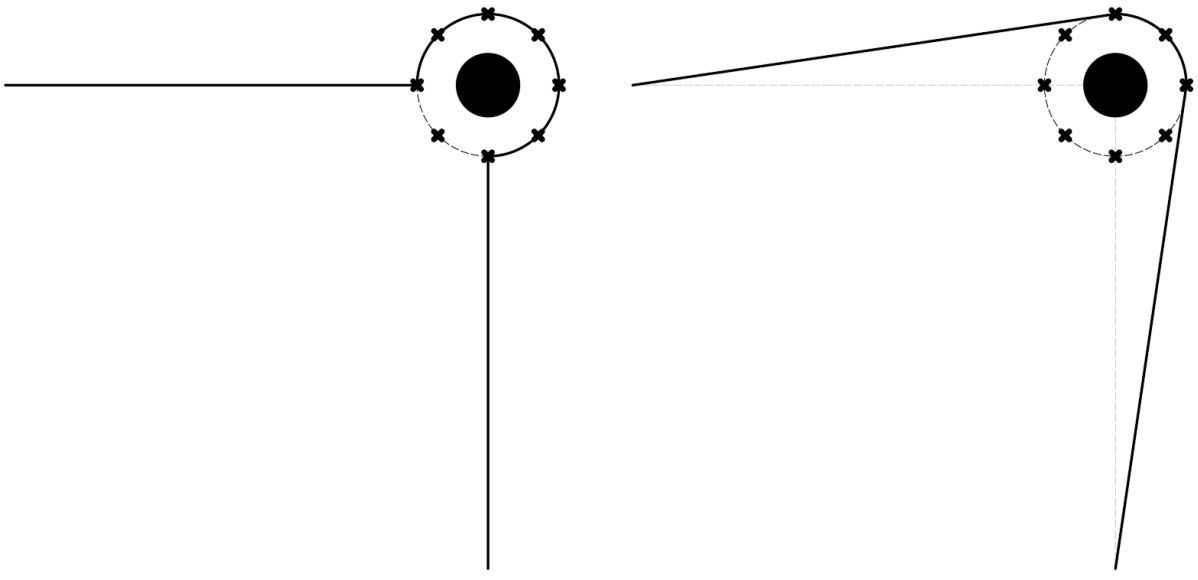

Figure 31: Simple path (left), using tangency (right)

The first point of the encirclement that is visited is decided by the point closest to the tangency of the incoming path. Subsequently the point circle is duplicated with the amount of encirclements plus one extra. This extra encirclement is then cut of at the location of the point closest to where the outgoing path is tangent to the point circle. This way the chosen amount of full encirclements is ensured at every point. Some extra encirclement might be present in order to bring the end effector to the outgoing path. In order to visualize this process figure 32 provides with a flowchart describing the encircling algorithm.

Finally the height increase is included. For every nth points of the encirclement the z coordinate is increased by one factor of diameter. The n value in this case is the resolution of encirclement.

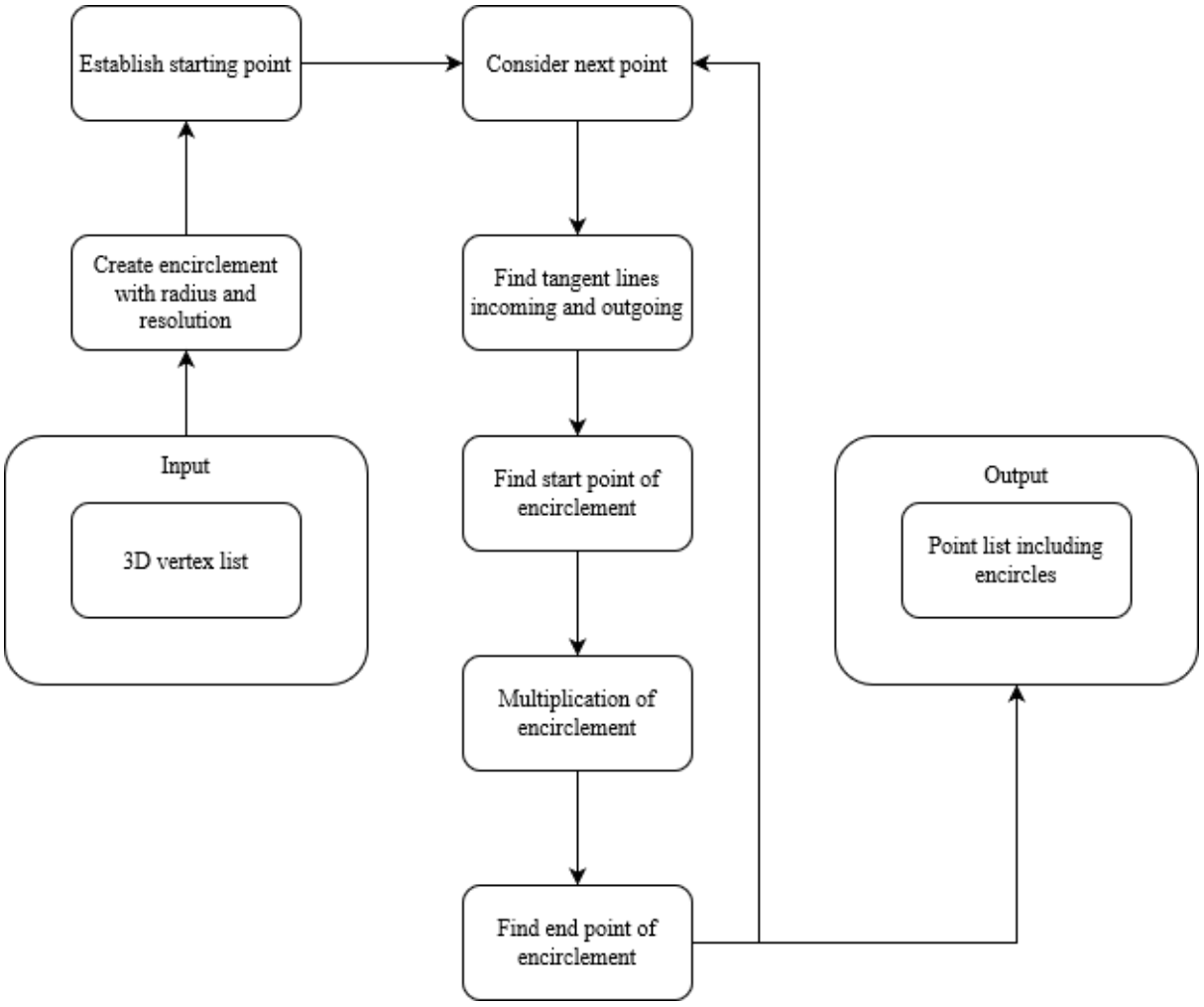

Figure 32: Process flowchart of generating encirclements around vertices

The encirclements being another essential manufacturing aspect that proves to be unfavorable in structural terms. At every vertex the encirclement starts at one side. This causes the forces to be introduced with some eccentricity into the edge beam. This eccentricity is defined by a combination of the winding material thickness, the edge beam thickness and the diameter of the threaded end as can be deduced from figure 33. The force in the web element together with its eccentricity causes bending moment in the edge beam. Most if not all of the vertices have an even number of incoming and outgoing winding in the case of an Eulerian circle. With the optimization inducing similar forces in all the web elements the effect of the eccentricities will be partly nullified. While even small amounts of bending could aggravate buckling, in the edge beam the bending caused by the eccentricities is minimal. Testing in chapter 9.4 partly confirmed this theory by showing buckling in the opposite direction than would be expected from the bending moments generated by this eccentricity. However in order to be completely certain more research is needed.

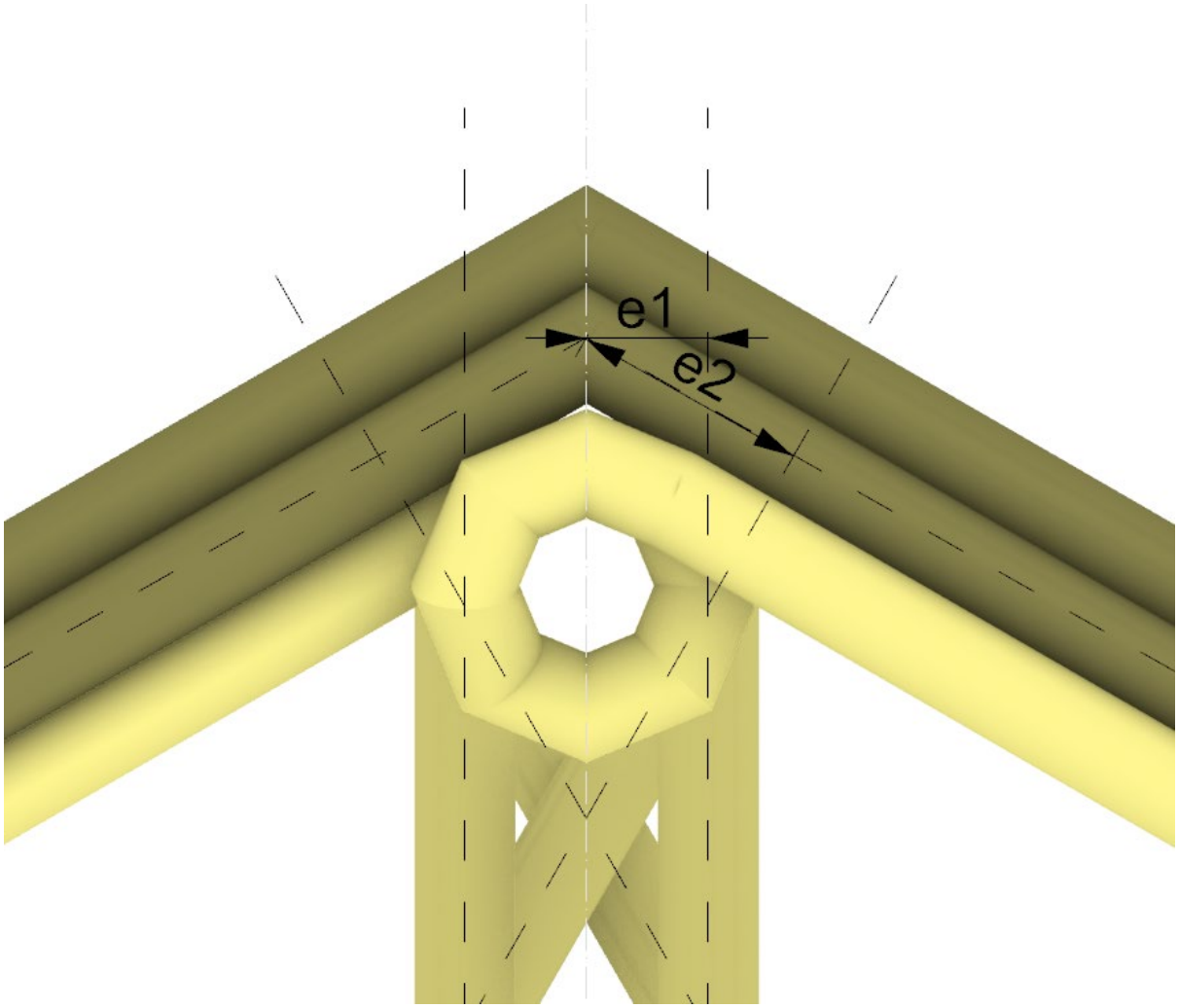

Figure 33: Eccentricities occurring as a result from winding the material around the vertices

4.4 Edge beam

Creating width in the edge curve is the last phase of manufacturing. Width cannot be created by simply winding more material around the vertices at the same location because a clash will occur. Width can however be created in a different way, namely winding around the entire panel. The height of the edge beam is influenced by the summation of the height needed to form the web and the height needed for the vertex wound edge elements. The width of the edge curve is user defined. In the figure 34 the winding order of all the elements is denoted. The edge beam winding direction is alternating with each layer. With each layer added on the edge beam the elements have an offset. A shift downward is applied with a value of Δy as defined by equation 51. The lowest element is removed from the path. This causes the edge beam to assume the shape of a truncated pyramid. With every next winding level having a winding less than the previous one. The narrowing of the geometry provides a stable base for every new winding. In order to assess the section, the elements are shifted in the x direction by equation 52. During winding however the elements are placed with an offset with the same magnitude as the user definition for winding radius.

$$\Delta y = r \tag{51}$$

$$\Delta x = r\left(2 - \frac{1}{2}\sqrt{3}\right) \tag{52}$$

With Δy being the offset in height and Δx being the offset in horizontal direction both in mm. The r is defined by the winding material radius in mm. The outermost level of the edge beam is not required to be fully wound. With a slider the outermost level can be reduced by a user defined value. The reduction takes place in a symmetric way, meaning the same amount of windings are removed from the top as well as from the bottom. With this finetuning the material used in the edge beam can be reduced as much as possible, following the course of an optimized design.

It is important for the structural integrity of the edge beam that the elements are connected. For this reason the edge beam should have a minimum of two layers. In this case the elements building up are always connected to at least three neighbors. This also reduces the change elements become completely disconnected because of possible placement inaccuracies.

As expressed before the edge beams are checked for buckling. For this the theoretical section of the edge beam is considered as defined using the equations 50 and 51. The edge beam is however not exactly as modelled. At the location of each threaded end the total height is only partially filled by web windings. As seen in figure 34 there is empty space between the threaded end and the edge elements as modelled. The amount and location of the empty spaces are different at each threaded end. During the winding phase the pretension present in the material causes the edge elements to fill these voids. This causes the edge beam to assume a different shape than assumed at the threaded ends. For calculation purposes however the

section is still considered following the theoretical definition. Because of the difference of voids at each vertex the edge beams are assumed to average out in midspan. Since buckling is critical at mid span the buckling check does not have to be changed. It however does reinforce the notion of using at least two edge layers in order to ensure the edge beam remains a single unit at all locations.

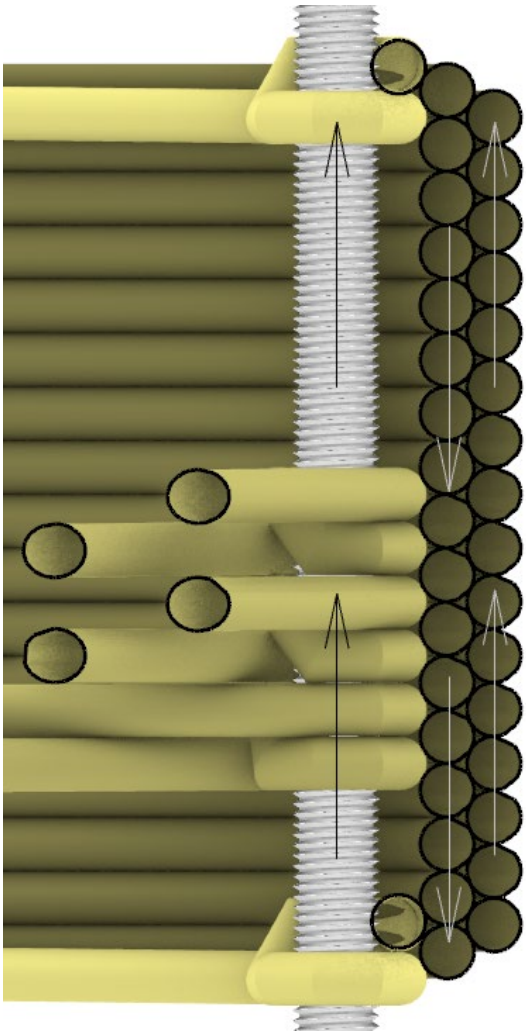

Figure 34: Winding order of separate components

During this chapter the definition of the winding path is construed. The winding path takes the form of a single polyline that does not show any self-intersection. This polyline will be baked into rhino and used as the basis of the robot path.

5. Robot path

The input for the robotic path is formed by the polyline defining the winding path. This polyline will be shattered into straight lines. Points will be placed on the polyline after a user defined distance and at each discontinuity. It is important for proper robot movement that the point distance is not to large. A point distance that is too small on the other hand could cause delays in the algorithm because of the large dataset needed. A maximum point distance of 30mm was generally found to work well.

The robot path is consequently formed by ABB plugin robot components. The input consists of frames based on cartesian (x,y,z) point coordinates formed by previously mentioned process. The output is rapid code generated by the grasshopper plugin 'robotcomponents'. Which includes axes velocities that can be read by the robot controller in the manufacturing phase. The way this works is considered a black box for this thesis' purposes as no control over it is possible. However a short explanation of a possible process is given in this chapter. It is deemed important to grasp what happens in the background of the plugin in order to interpret possible problems that arise by using it.

In order to generate robot path the first step is to analyze and understand the robots geometry. The process in robotics is called forward kinematics. This is essentially when the end effector location and orientation is calculated from axis rotation values. The robot used for this research project is an ABB IRB 1200-5 which is a six degrees of freedom, six revolute joint manipulator. The six joints are schematized according to the Denavit-Hartenberg convention in the following figure. Direction of rotation is found by applying the right hand rule to the blue z axes as shown. With θ_i denoting rotation of joint i.

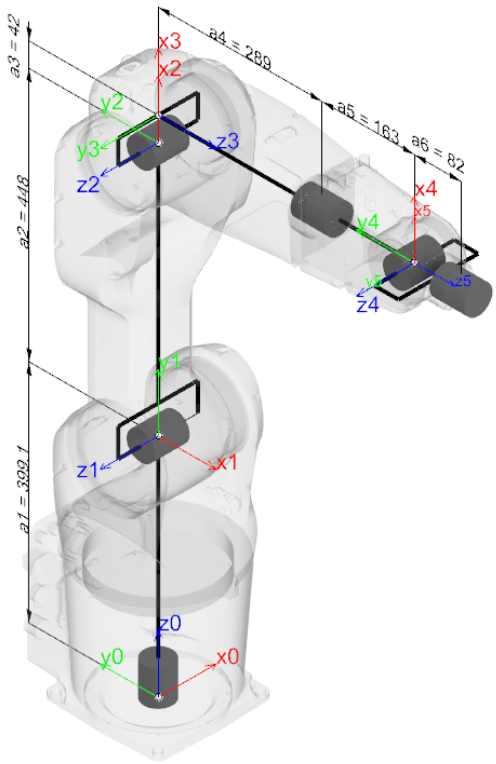

Figure 35: Denavit-Hartenberg schematization of the used ABB IRB 1200 robotic arm

From this geometry transformation and rotation matrices can be calculated using trigonometry. These matrices can be calculated for every joint i, relative to joint i-1 and then assembled to describe the geometry of the robot as a whole. Filling in the six axial rotations would lead to the orientation of the end effector relative to the base plane.

This is however not how a robot path can be calculated as it doesn't work the other way round. The robot movement is calculated from a list of cartesian frames defining the position of the tip of the end effector. From these tip coordinates the velocities of rotations of each internal axis can be calculated using a process called inverse kinematics. A numerical approach to this problem is the pseudoinverse Jacobian method. This is an iterative method which linearizes the movement of the robot. The first step to how this works is calculating the distance and rotation between the current end effector position and the goal position. This movement is then reduced by scaling it. When the movement is sufficiently small the joint rotations can be linearized. While rotational movement normally yields an arc at very small rotations this arc could be discretized into a line. The general kinematic equation is applied (equation 53).

$$[X] = [J][q] \tag{53}$$

$$\begin{bmatrix} x \\ y \\ z \\ a \\ b \\ c \end{bmatrix}_{6x1} = \begin{bmatrix} J_{11} & J_{12} & . & . & . & J_{1n} \\ J_{21} & J_{22} & . & . & . & J_{2n} \\ . & . & . & . & . & . \\ . & . & . & . & . & . \\ . & . & . & . & . & . \\ J_{61} & . & . & . & . & J_{6n} \end{bmatrix}_{6xn} * \begin{bmatrix} q_1 \\ q_2 \\ q_3 \\ . \\ . \\ q_n \end{bmatrix}_{nx1} \tag{54}$$

In this equation the inverse of the Jacobian matrix forms the relation between the end effector velocities (X) and the joint velocities (q). The end effector velocities are given by a 6x1 vector with three linear velocities (x,y,z) above three angular velocities (a,b,c). The joint velocities are found to be a 6x1 vector consisting of the axis velocity of each joint. The Jacobian matrix in the case of a 6 axis robot is a 6x6 matrix. The first three rows of the matrix are related to the linear velocities of the end effector due to the joint velocities. Using the process of forward kinematics the position functions can be extracted from the robot schematic. These position functions define x,y and z positions of the end effector with respect to the joint variables. The first three rows of the Jacobian are then formed by finding the first derivative of the position, which is defined as the velocity. This velocity matrix is defined in equation 55 as J_V.

$$J_v = \begin{bmatrix} \frac{\delta x}{\delta q_1} & \frac{\delta x}{\delta q_2} & \frac{\delta x}{\delta q_3} & . & . & \frac{\delta x}{\delta q_n} \\ \frac{\delta y}{\delta q_1} & \frac{\delta y}{\delta q_2} & \frac{\delta y}{\delta q_3} & . & . & \frac{\delta y}{\delta q_n} \\ \frac{\delta z}{\delta q_1} & \frac{\delta z}{\delta q_2} & \frac{\delta z}{\delta q_3} & . & . & \frac{\delta z}{\delta q_n} \end{bmatrix}_{3xn} \tag{55}$$

The last rows in the Jacobian matrix relate to the angular velocities of the end effector and consists of joint axes with respect to the base frame. These axes can be found by identifying them from the robotic scheme then multiplying with rotation matrices which are again deducted using forward kinematics. Now the Jacobian matrix is found by solving equation 56.

$$[q] = [J]^{-1} * [X] \tag{56}$$

In order to find the joint velocities the inverse of the Jacobian is needed. This is however not as straightforward as it seems. Like in most robots the ABB IRB1200 has some orientations were singularities occur. What this means is that certain joint axes align causing degrees of freedom to disappear from the Jacobian matrix. With a non-square matrix traditional inverting is not possible. For this reason pseudo inversion techniques are used in order to find the joint velocities. The used end effector velocity vector is a scaled down one in order to linearize the problem as described. However singularities can still occur. With the determinant of the Jacobian matrix approaching zero the robot approaches a singularity. This can cause high joint velocities and with that unexpected or inaccurate results. There is no way to realistically predict all singularities without calculations. For that reason it is imperative that every robot path that is programmed is first simulated digitally in a program like RobotStudio 2020.

The iteration is done by updating the current joint position with regard to the calculated joint velocities, bringing the end effector closer to its goal value. The described steps are repeated until the goal is reached.

6. Robot peripherals

6.1 End effector

The end effector of the robot has several functions. The main function is to distribute the fiber evenly and reliably. The fiber should always be distributed at the same point relative to the robots tip coordinates, which ensures the application is as modelled. Since the robot has a changing orientation the end effector should be able to accommodate fiber coming in from different angles. For rapid prototyping it was chosen to iterate end effector designs using 3D-print technology. The effector will be manufactured using Ultimaker 2 extended+ in combination with PLA filament. The workflow for this prototyping is as shown in figure 36. After several iterations the design was considered sufficient for the envisioned application. This design is presented in this chapter.

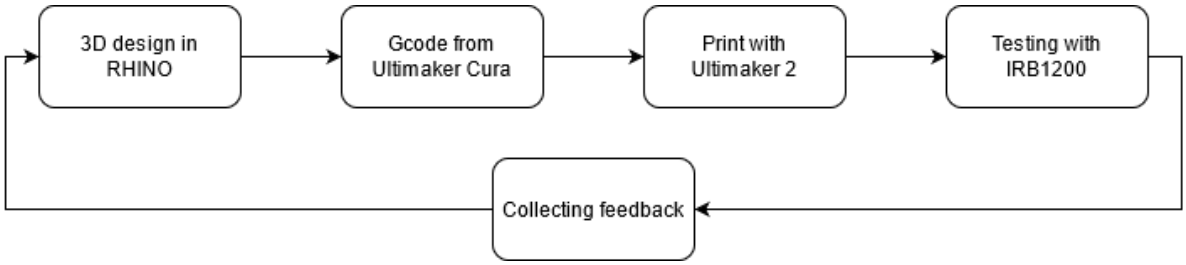

Figure 36: Iterative workflow of end effector design

The mounting point between the robot and the end effector consists of 4 M5 bolts with a depth of 6mm. The radius between the holes placed at a 45° angle is 31.5 mm. This information was deduced from figure 37.

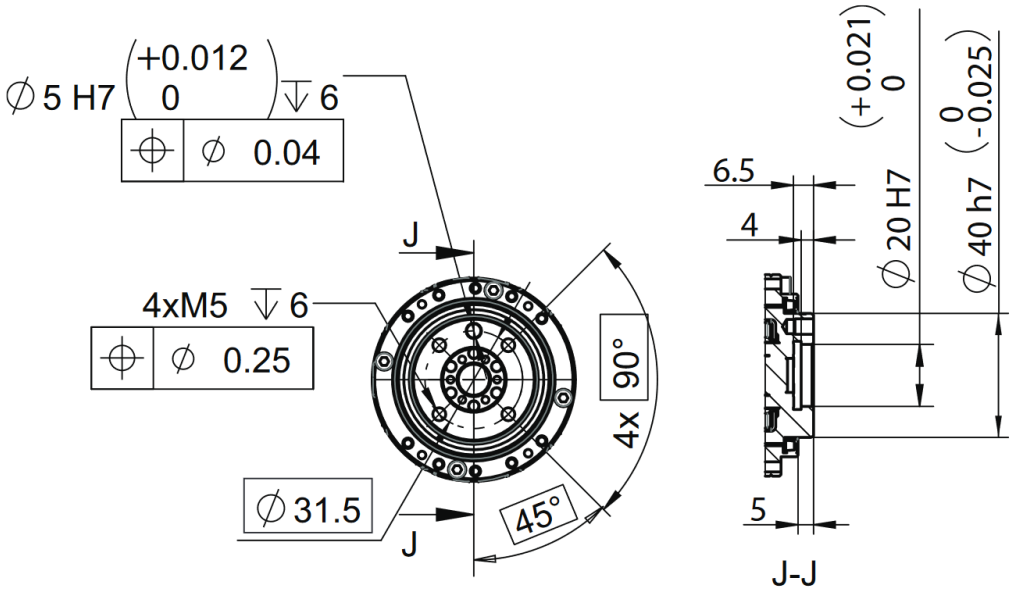

Figure 37: End effector mounting plane, from ABB 2021

The end effector to robot connection is shown in the 3D model in figure. Four M5 hex socket cap screws with a length of 15mm are used to fasten the end effector to the robot. The screws are embedded in the body of the end effector. The specific design of the end effector will be discussed. Technical drawings are provided in Appendix H.

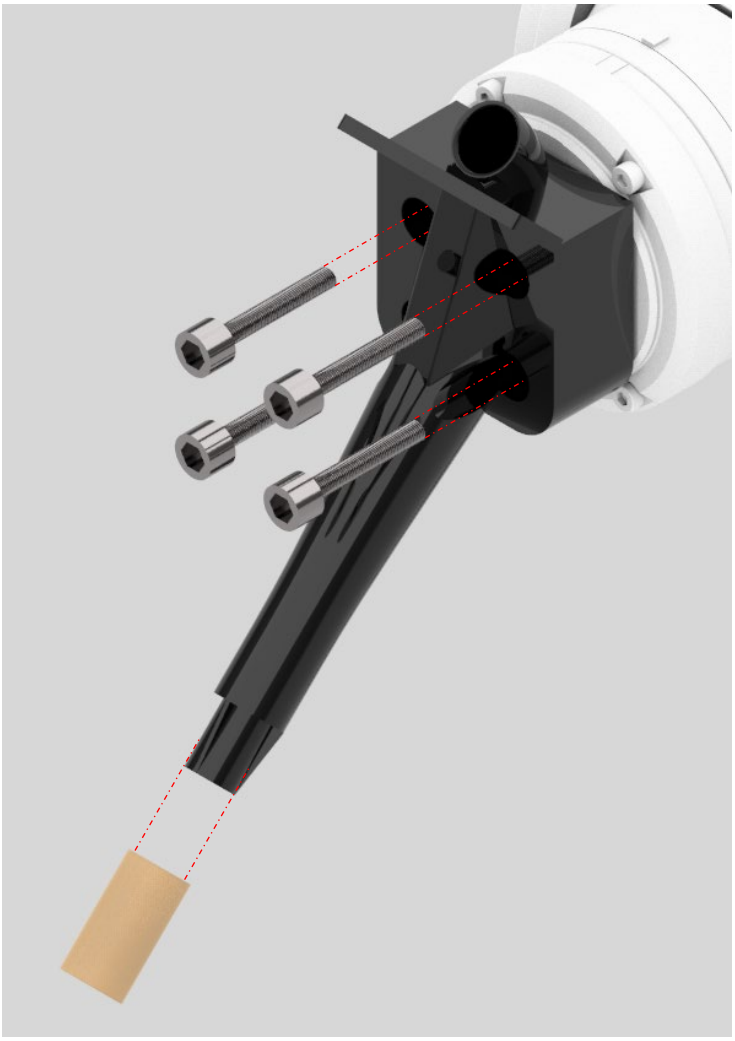

Figure 38: 3D model of end effector

It was chosen to put the end effector under a 45° angle with the connection plane in order to avoid wrist singularity. Wrist singularity occurs in the IRB1200 robot when joint 4 and 6 are aligned. If the effector would be placed under 90° angle this situation is more likely to occur when working on a flat plane. Under 45° however joint 5 is used to bring the effector in the 45° angle. By rotating joint 5, joint 4 and 6 are removed from the same plane.

The location of material inflow is modeled as a cone in order to be able to smoothly lead the incoming material in the direction of the application. As the material is not always incoming at the same relative angle to the end effector a large diameter was used along with rounded edges.

Under the inflow location a small platform is modelled for capturing excess resin. Instead of dripping on the workspace the resin is collected on the end effector itself allowing for easy

cleaning. The material inflow direction is changed 90° and led through a tube in order to clear the height of the threaded end. The tube is gradually thickened towards the base where it also has some additional stiffeners. This was done not only to increase stiffness but also to increase strength.

The end effector is applying the rope material at the mold. The exiting point of the end effector has a diameter of 8mm with an effective rope diameter of 5mm in mind. The material application is at an angle of 90° with the incoming material. This leads to a problematic radius at the end effector tip which the material has to assume. Whether or not the end effector will reliably apply the material becomes a question of the materials minimum bending radius and the friction between the material and the end effector. With a twisted rope material this friction can change and cause differing friction and bending behavior at different orientations of the twist. It should be noted that the minimum bending radius is not a true material property it is just a result of the materials bending resistance. In order to get the material to bend a force needs to be exerted on it. This force will in its turn be exerted on the end effector edge causing more friction.

In figure 39, left it is shown that the end effector without adjustments relies on the minimum bending radius of the material. This minimum bending radius is an approximated to be 2.5mm. Figure 39, right shows the inclusion of a rubber effector tip. This tip reduces the bending radius by deforming with the material. This is however just an approximation as the exact deformation of the rubber tip is not known. In reality the material specific for this end effector will have a smaller diameter of 5mm, with this smaller diameter also a smaller minimum radius is in effect because the material is free to place itself in the end effector tip. The rubber tip as applied is approximately 30mm long with halve of it being placed over the end effector tip. Like stated before it is important to reliably place the material. In this case the exact placement height is not known, it is however a fairly constant value. The placement height can be known by trial and error but an approximation is also sufficient. Since the material placement height is always the same the panel itself will be wound without issues, the height placement of the panel as a whole is the unknown in this case.

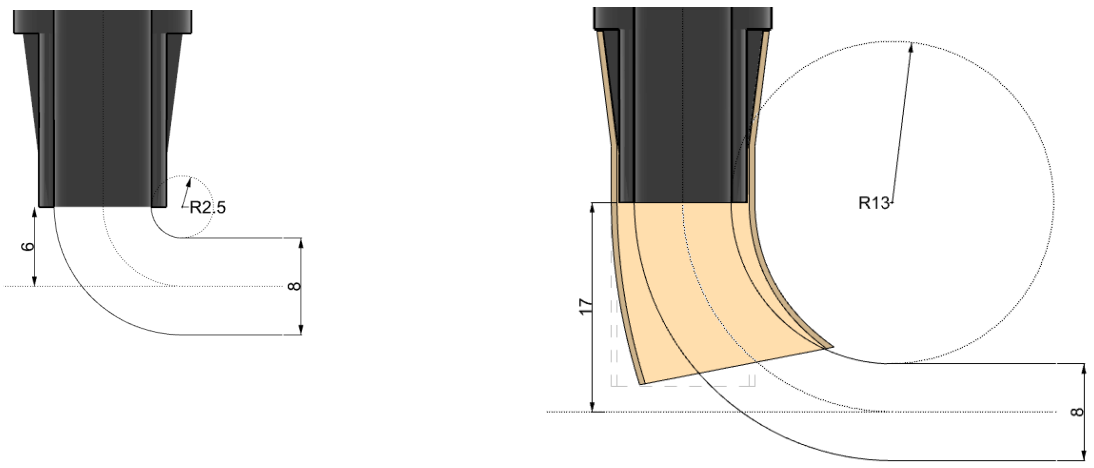

Figure 39: End effector tip section with material output radius

At the location on the end effector where the rubber tip is applied the PLA is indented in order to ease the rubber tips application. Three fins were designed on the effector tip. These fins cause the rubber tip not to suck vacuum when pulled. This way when the rubber tip gets stuck it will release instead of breaking the end effector with it. The rubber tip could get stuck when the encircling radius around a vertex is too small in comparison to the rubbers length.

For technical drawings of the end effector reference can be found in Appendix H. The current end effector nozzle length is 80mm, this is consequently the maximum height of a threaded end that the end effector is able to encircle. No experiments were done with nozzle lengths exceeding 80mm. It is theorized that more strength and stiffness are needed for reliable material placement if the nozzle length is extended as is. These properties could be achieved by increasing material thickness in the nozzle or choosing a different filament material for the 3D printer.

6.2 Mold

To provide with the vertices the robot will be winding around, M6 threaded rods are inserted in a stable base plate. The lowest windings will be vertically 'rested' on a bolt. In order to find the correct location for each of the vertices the outline of the panels will be drawn onto the mold. A printed 1:1 guide will be used for this. Holes for inserting the threaded rods can be drilled at the right location to accommodate each panel separately. The mold will be placed within the robots reach and screwed to the bottom plate.

After winding the panel will be removed from the mold together with the threaded rods. The threaded rods are now a part of the panel and will be used in the assembly phase. For winding the subsequent panel new rods are inserted at the necessary locations. In order to be able to remove the threaded rods after the hardening of the panel its important no resin seeped between the threaded ends and the holes in the MDF. Resin can be stopped by electrical tape or silicon sealant.

An isometric drawing of the complete mold setup is supplied in figure 40.

In combined use with the end effector as previously designed the panel cannot exceed a thickness of 60mm. The end effector nozzle has a length of 80mm which is the maximum height which the end effector is able to wind. Leaving 20mm at each side of the threaded end in order to accommodate later assembly the threaded end length will be 100mm. With the MDF board having a thickness of 18mm, after inserting the threaded ends there would not be enough space left over to attach the bolts. For this purpose the holes in the MDF where enlarged partially from the bottom with a hole saw. This way the lower bolt can be countersunk in such a way that the space on the threaded end above the upper bolt is exactly 80mm.

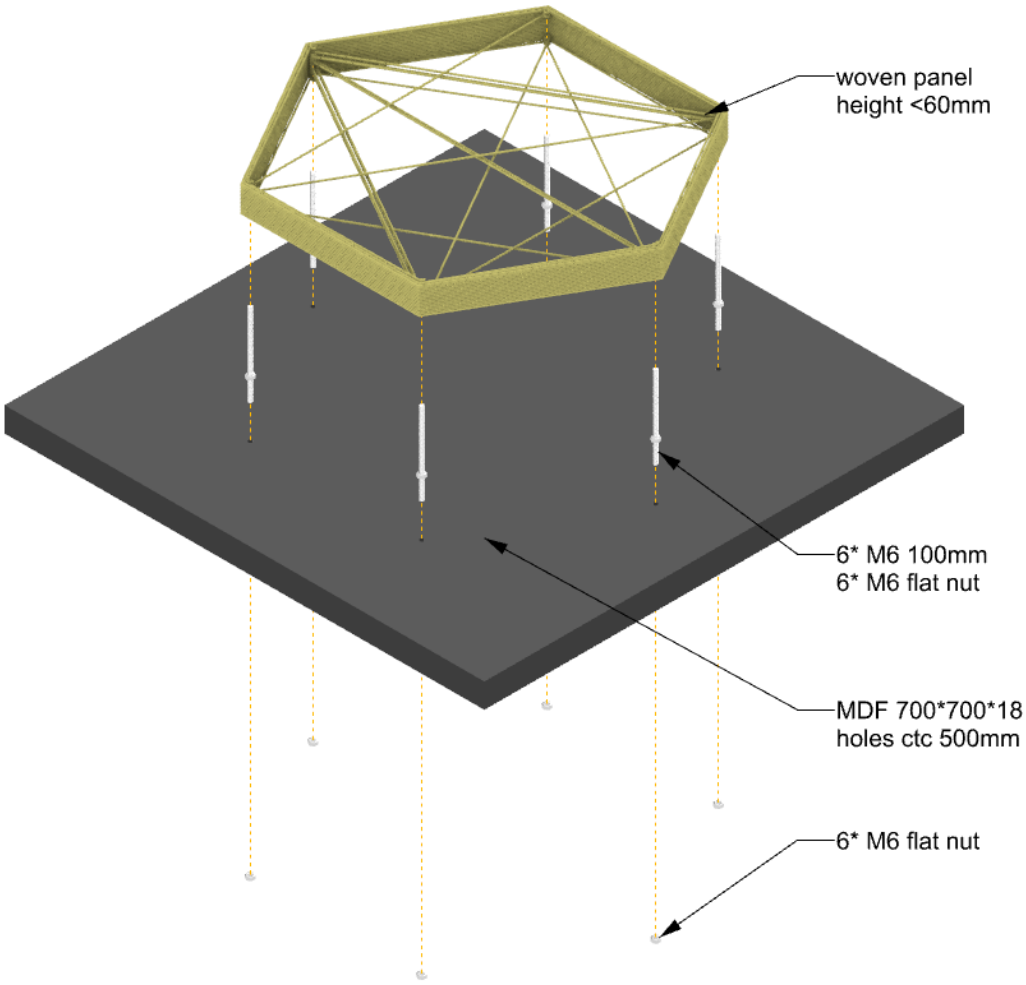

Figure 40: Isometric drawing of the mold arrangement for a hexagonal panel

In more general terms the length of the threaded end should be based on the panel thickness, leaving room on each side for connection purposes. The maximum length of the threaded ends is based on the reach of the end effector. With a flexible end effector design, longer threaded ends could be used. When considering a panel assembly the length of the threaded ends should be based on the neighboring panels. Since panels within an assembly could have different thicknesses the panel with the largest thickness should be viewed as governing.

6.3 Material conditioning

The condition peripherals are visualized in the 3D drawing in figure 41. It was designed from the starting point that most of wire conditioning should be removed from the robot in order to decrease load on the robot. This in turn increases the maximum size of the resin bath which leads to less refills while at the same time making these refills possible without pausing the winding process. Attention was paid in order to decrease leaking in the process. The process of wire conditioning consists of spool unwinding, resin impregnation and pre-tensioning.

The spool unwinding is actualized in the first step. The spool is installed onto a standard ensuring the right approximate height for the rest of the project. While unwinding the spool is able to

spin freely due to bearings installed in the middle of it. The fiber is led from the spool into a first metal eye which ensures the fiber are always arriving at the next step in the same location despite the spools winding pattern. This next step is the impregnation of the fiber. The impregnation bath is shown in detail in figure 42. The strand is led through a resin bath by a set of two cranks forming a controlling mechanism. The resin bath can be replaced without cutting the strand by simply raising the cranks. The cranks could also be raised during the winding process. This might be required if parts of the panel would be implemented without resin. In any crank orientation a bolt can be used in order to lock them in position. Simply refilling the resin bath does not require removal of the container. The pre-mixed resin can be poured into the resin bath using a funnel. Considering a consistent robot speed of 40 mm/s the time the fiber is soaked in the resin can be calculated from the length of the resin bath using the following formula. This is the minimum soaking time because when the robot moves toward the peripherals the pulling speed decreases.

$$s = t * v \tag{57}$$

With
v = robot speed [mm/s]
s = length of resin bath [mm]
t = minimum time soaked [s]

With the width of the soaking bath being approximately 180mm the minimum soaking time for the fiber is 4.5 seconds. From the experiment in Appendix C the conclusion can be drawn that after one second. The wire is considered fully soaked. This soaking bath width ensures proper material soaking.

After the fiber passed through the resin bath it will get squeezed by a perforated rubber sheet. This will keep the amount of spillage in later processing to a minimum. It also keeps the strand tensioned by causing some friction. This tensioning function of the peripheral has an effect on how tightly wound the end product will be. Finally the strand will pass through another metal eye in order to reliably keep the material approaching the robot from the same direction.

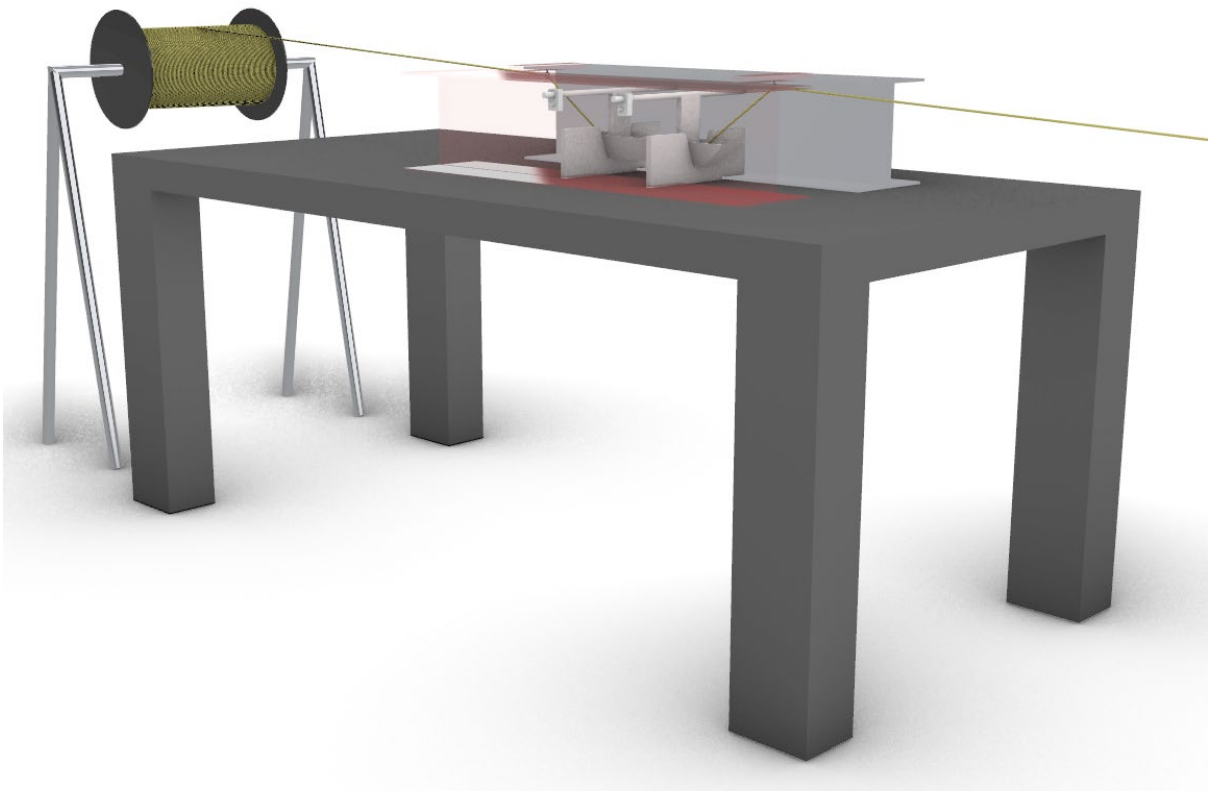

Figure 41: Visualization of winding peripherals overview

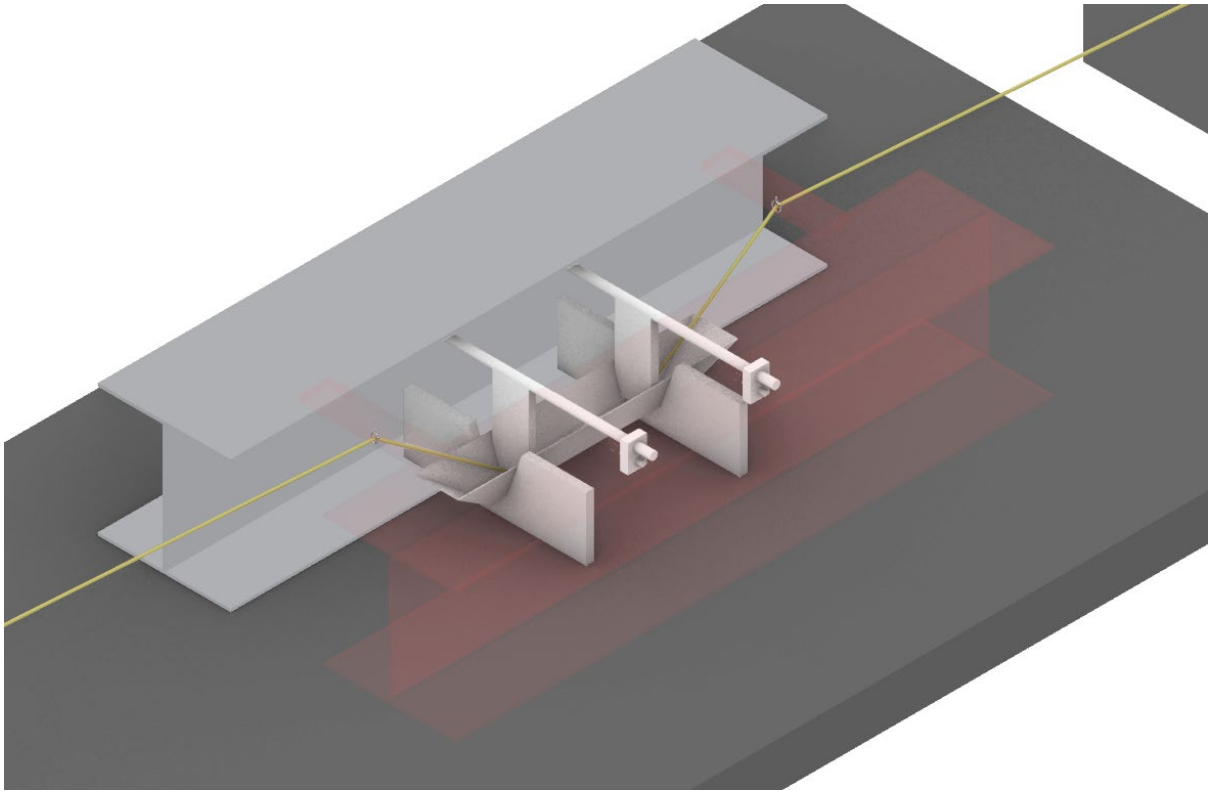

Figure 42: The material is being led through the impregnation bath

7. Assembly

After the manufacturing of the individual panels they will be removed from the mold. In the case of a panel assembly attention needs to be paid to the connection method. For connections several options are considered in this thesis. The first option is included in the design and the calculations and is shown in figure 43. The panels are wound around threaded end which will be considered lost in the panel. The threaded ends can be used to interconnect the elements using sheet-like connection elements. In order to facilitate the connections the panels should be scaled down in the design phase already. The connection elements are already included in the assembly during the FEM calculation and optimization. In practical terms these elements are bolted on either side of the panel assembly. In order to avoid slip at the threaded end the windings are also constraint by a washer and a bolt. The calculation for the sheet like connection elements is included in chapter 3.6. Possible materialization could be multidirectional composite sheets.

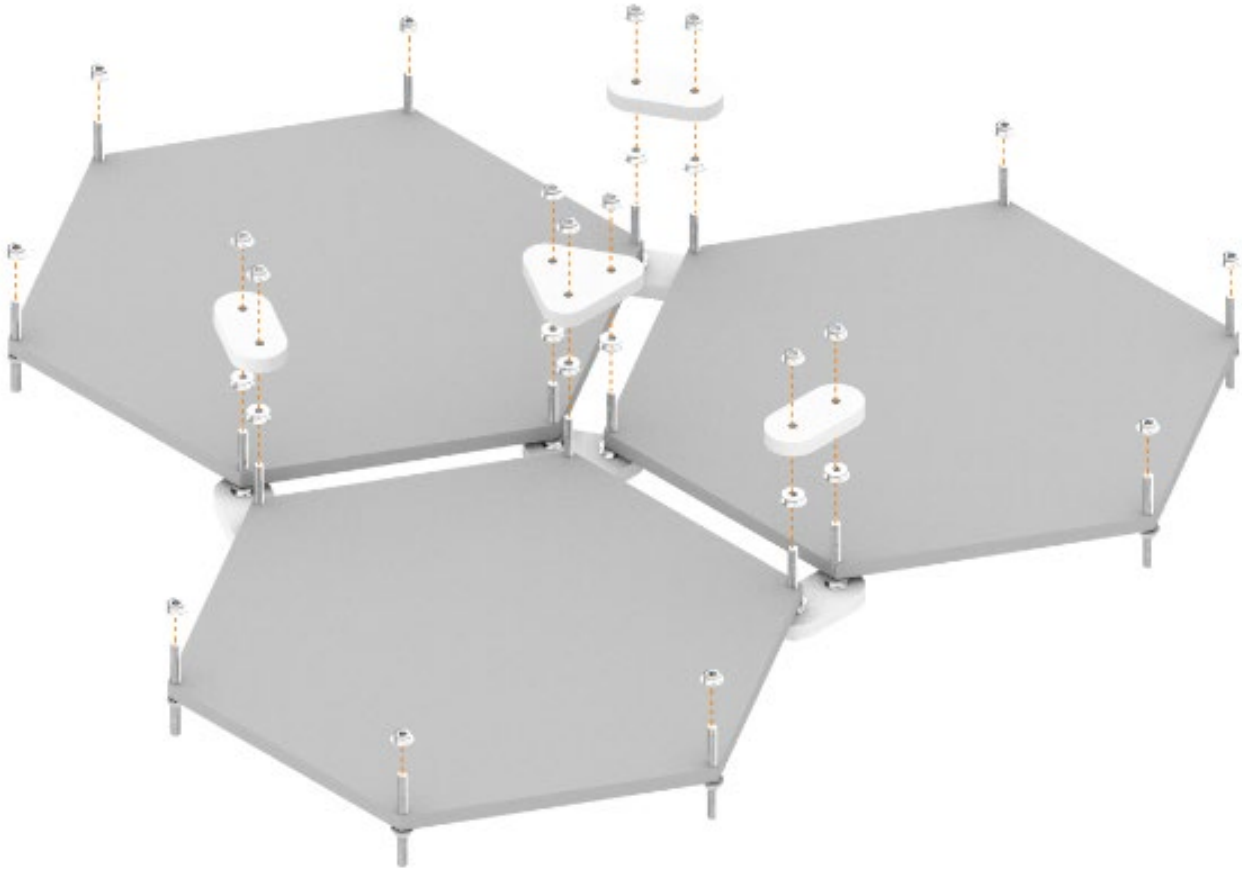

Figure 43: Panel connection method using dedicated connecting elements

A second option is simply stacking panels and in that effect creating an assembly that consists of only wound panels. This causes a relatively uniform way of manufacturing where only one type of material is used and even the connections are wound. The way this method is applied is by implementing the connection elements in the panel assembly from the start. Since it is not possible to interconnect panels without causing eccentricity, a panel can be split in two pieces and assembled on either side. This splitting of the panel will be done after the optimization by simply dividing the resulting line model in two. The weaving path will be made separately for

the two panels. The panel that was split in two will be made by winding the material around tubes. The tubes will be placed over the threaded ends that form the mold. This principle was tested when making samples for material testing as described in Appendix D. After winding only the tubes are removed and the panel will be slid onto the panels that were made by winding around threaded ends. The assembly will be fastened using bolts. A visualisation of this method is given in the following image:

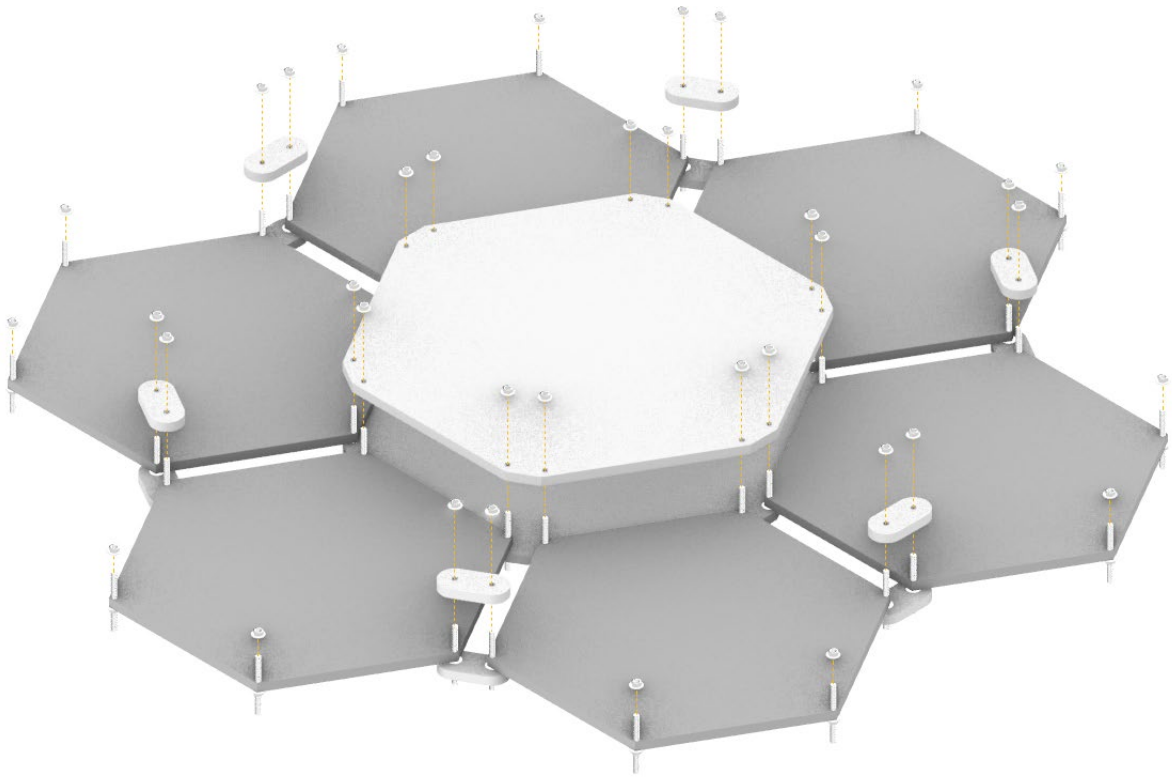

Figure 44: Assembly showing an alternative connection method using intermediate panels

The image shows a hexagonal grid with as a connecting element a dodecagon. At the edges of the hexagonal tiling the panels are connected with longitudinal elements. These elements could be the same as discussed at the first assembly option. It is also possible to use stacking panels at the edge as well. In order to wind the connection it has to connect at least four vertices.

8. Applications

Applications for this building method are divergent. The panels could be assembled in two dimensions to form walls or beams. With a possibility of expanding into three dimensions to include structures like domes which are easily constructed from regular polygons. In order to provide with a possible example a calculation for a bridge railing is included in Appendix F. While the bridge railing is not an integral part of the bridge itself it is structural to some degree. As described the loads on bridge railings are not unsubstantial.

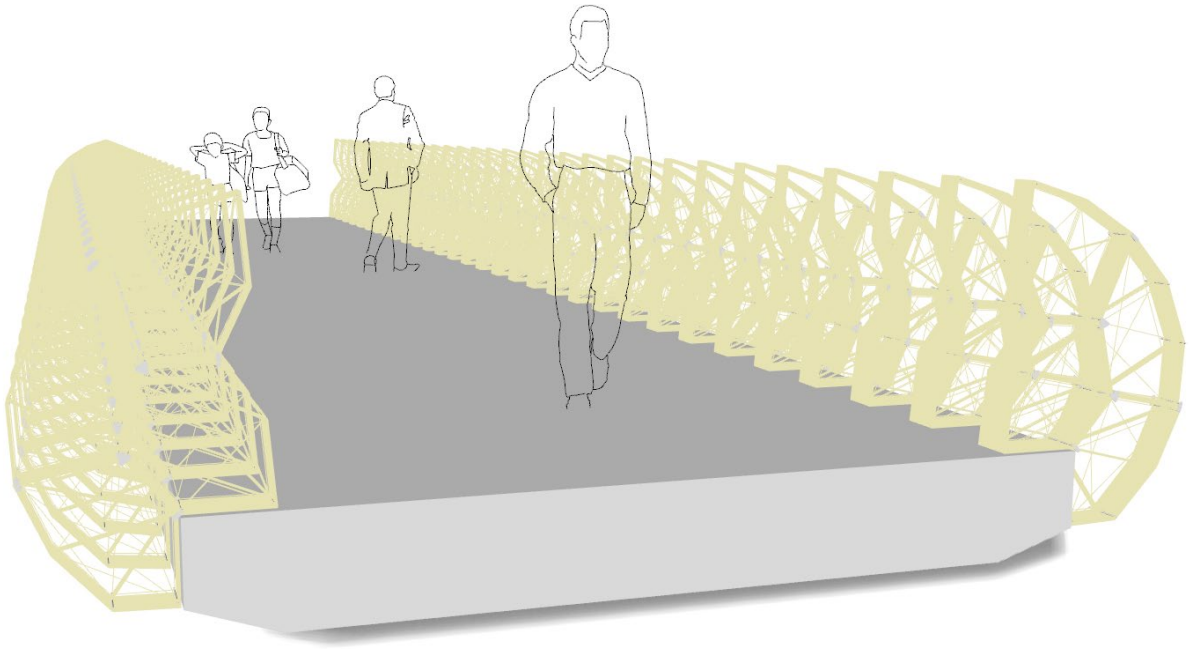

Figure 45: Render of a bridge using wound panel assemblies as a railing

For this bridge railing the entire building method was used. The design was done by simply defining the assembly built up from four similarly sized polygons. The program defined the web elements and the connections. From there the algorithm applied structural considerations consisting of an optimization of the web, manual optimization of the edge and unity checks for all elements. As a material the same sisal composite was used as will be described in the next section. Subsequently the winding paths were generated along with the robot paths which could be extracted from the script in the form of RAPID code.

9. Weaving panel sample

In order to test the theoretical context provided in this thesis in practical terms a test was set up. In this test the mechanical properties of a panel will be researched. The research question is formulated as follows:

Will a wound fiber panel which was designed, calculated and manufactured according to the context as stated in this thesis, give the expected result in terms of failure mode and its magnitude?

9.1 Material

The first step is to pick a material. When selecting a suitable material looking at strength and stiffness alone is not enough to make a comprehensive decision. Especially in this stage of the research. The practical research is mostly a means to underline the possibility of weaving panels. Since no direct structural application is planned the mechanical properties of the material are not that critical. At this phase availability of material is seen as a priority as its needed at short notice and exact quantities are still unknown.

9.1.1 Fiber

From the Ashby plot in figure 9 it can be concluded that sisal is among the stiffest biofibers. Higher strength can be found in biofibers like hemp or flax. However cross referencing other literature finds large variance in strength and elasticity properties of biofibers. Regarding pricing and availability it was concluded that it is easier and cheaper to obtain sisal. On these grounds the choice of sisal as a part of the composite was made.

With the fiber chosen the next step is to find a suitable morphology. Fiber can be supplied in different forms: raw material, short cut fiber, mats or different types of ropes. In the chapter 2.4 materialization it was stated that parallel strand ropes would give the most predictable results when assembled into a composite material. This theory was deviated from as parallel strand ropes are hard to obtain. The only parallel strand ropes that were found on the internet were based on man-made fibers. For this reason a twisted rope was selected. Three strand twisted rope gives the lowest twist compared to ropes with more strands.

In the algorithm the diameter of the rope can be adjusted with a single slider. In the real life application however there are some consequences to the choice of rope diameter. With a high diameter comes possible difficulty in processing. High diameter rope has higher resistance to bending which can be a problem when applying with the end effector but also while twisting the rope around the vertices. Small diameter rope is easier in application. There is also some added efficiency in using small diameters. With the optimized panel containing at least one rope per element in order to ensure overall stiffness. Making this one rope per element as small as possible gets the element closer to a truly optimized state. Using very small diameters however causes the manufacturing process to take longer with more windings to be made. For this practical research fast prototyping is important. For this reason a rope with an intermediate diameter of 4mm is chosen.

9.1.2 Resin

The bio composite to be tested consists of a biofiber material and an epoxy resin material. Following the same philosophy of sustainability a sustainable epoxy for this application was selected. The epoxy to be used is Sicomin SR infugreen 810 / SD 882X, full datasheet can be retrieved from their website. Partial datasheet is attached in Appendix B.

The resin is a two component epoxy system which consists of 38% carbon from plant origin. Therefor it has a lower environmental impact. The resin is used in combination with the SD 8824 hardener which has an intermediate reactivity level. After mixing 100/22 resin to hardener weight ratio the resin is hardened. Proper hardening occurs for 16hours on room temperature followed by 24 hours at 40 °C. The rated material properties are given in Appendix B.

9.2 Panel design

The next step in this research is to choose a design of panel and its boundary conditions. For the geometry of the panel a basic shape with a straightforward element distribution was chosen. The pentagon was chosen because of its limited number of web elements. The current setup of end effector leaves room for a limited panel height of 60mm to be wound. This setup was respected because it was successfully tested before. It is theoretically possible to make thicker elements with the same end effector when the radius around the vertices is increased. This however decreases the total panel size. The panel with numbered elements and nodes is schematized in figure 46.

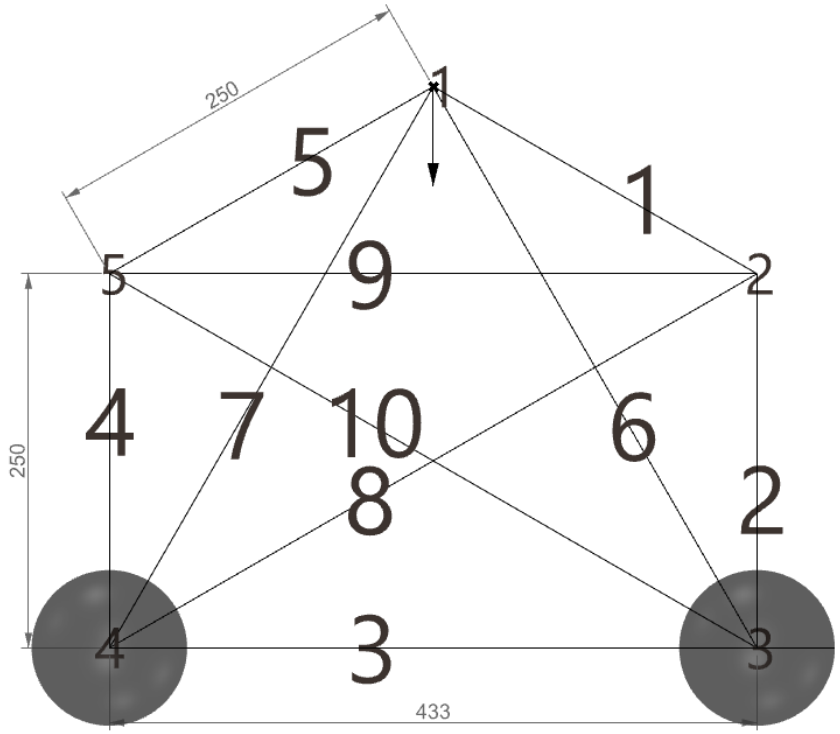

Figure 46: Schematized panel to be wound

The panel has a radius of 500 millimeters and is based on a hexagonal shape with one corner cut off. Elements 1-5 form the edge with elements 6-10 forming the web. The panel is simply supported by two nodes 3 and 4. A downward vertical force is introduced on node number 1. The magnitude of the force is designed to be 1kN. The panel fits well into the robot reach with room to spare for encircling the vertices and forming the edge elements.

Material properties that were assumed:

- Stiffness 9000 N/mm^2
- Maximum stress 10 N/mm^2

No safety factors were used on either the material properties or the applied force. It is important to note that at this point these material properties are an approximation. Also the sectional area of the strands is estimated at 15.9 mm2 for a round section with a diameter of 4.5mm. This diameter is based on the data received from the manufacturer. There might be a discrepancy between the assumed sectional area and the true sectional area. In a real life application the material properties should be established beforehand.

The optimization was ran as described in paragraph 3.3. A total of 25 iterations were done. The optimization converged after 11 iterations as shown with the marker in figure 47. Convergence was defined as the change of strain energy being smaller than 0.5Nm. The values for both the p and the η-factor were taken as 0.80. No cutoff was defined.

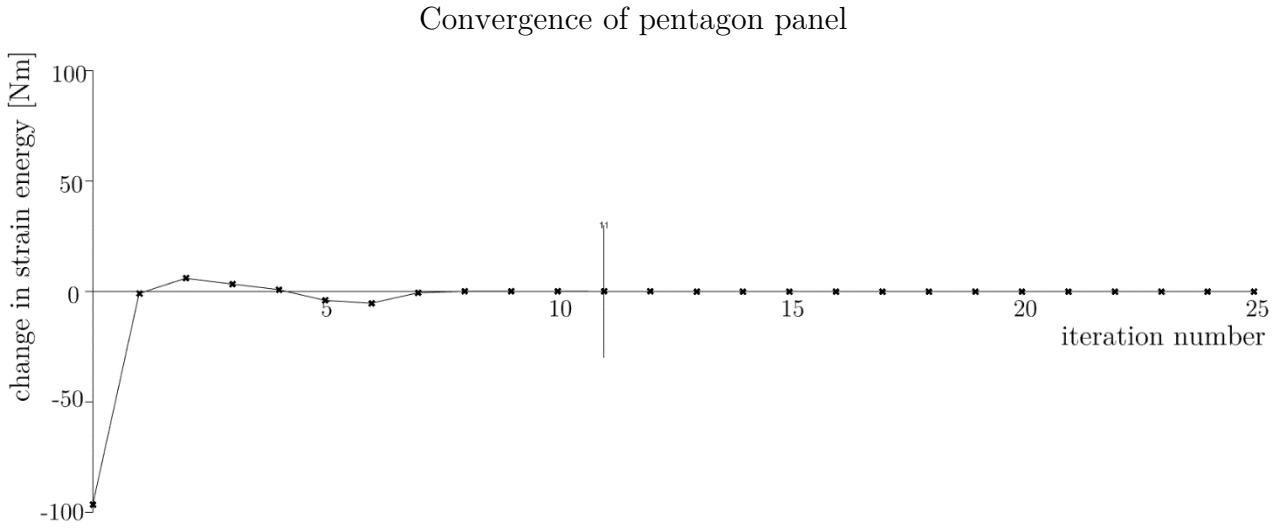

Figure 47: Convergence graph of the considered panel

The resulting optimized panel is as shown in figure 48. There are 21 strands forming the edge and 9 strands forming the web. After optimization one web element (element #9) seemed to be dominant containing 5 windings. The other web elements consist of only the minimum winding area which is 15.9mm^2.

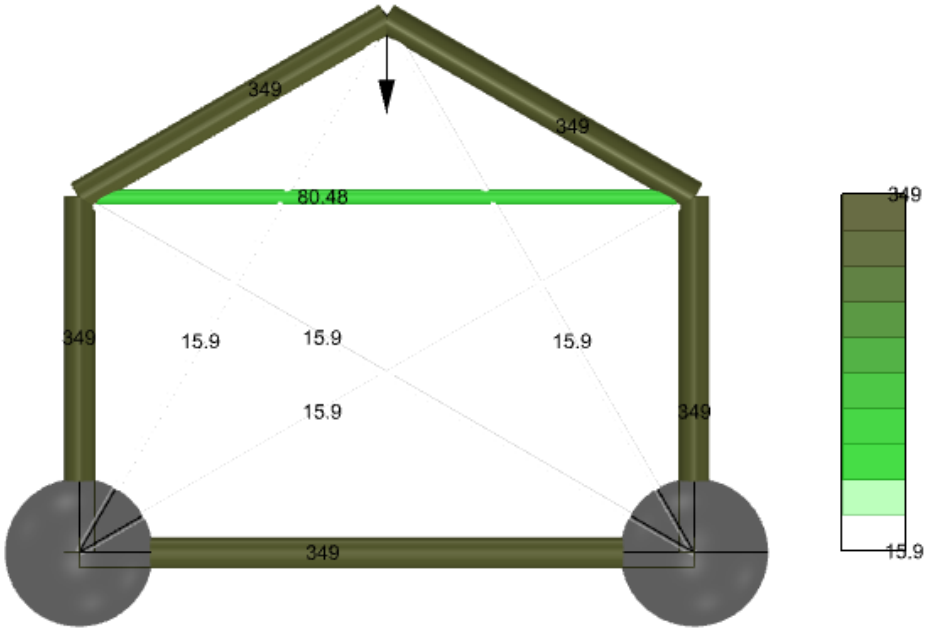

Figure 48: Material distribution on the optimized panel

Now considering the stresses and displacements as shown in figure 49. The vertical displacement of the element under a load of 1kN is expected to be 0.602mm. Looking at the stress levels at each of the elements none of them exceed the stated maximum value of 10 N/mm^2. In compression however there is another check that needs to be done in order to correct for buckling. Buckling is only checked in the edge elements.

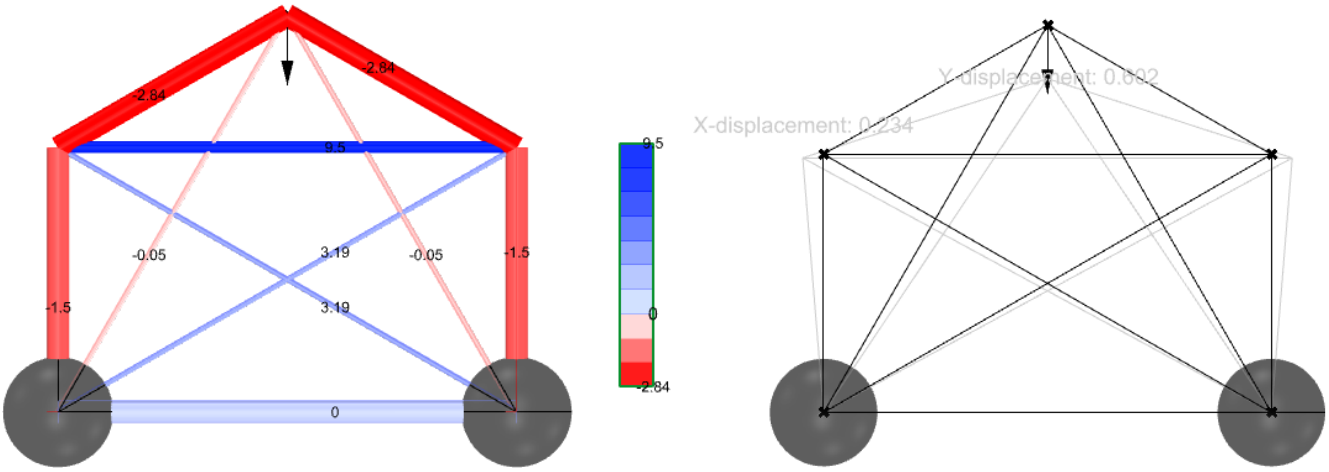

Figure 49: Left: stresses in each element [N/mm2]. Right: displacements with maximum x and y displacements at occurring node [mm]

For buckling the edge elements geometry is assumed to be as shown in figure 50. As stated before this is just a geometrical estimation. In this case a single web winding is executed above and below the web. The height of the edge curve was based on the necessary height of the web summed with the height needed for two edge windings.

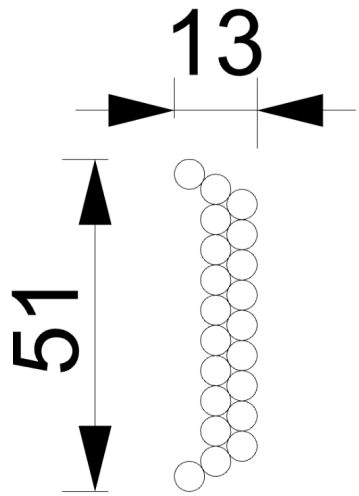

Figure 50: Geometry of edge curve

Using the theory for calculating the second moment of area for composite shapes (equation 46a) the Euler buckling force can be derived with equation 45. For each edge element under load this force is found to be 3.9kN. With the maximum compressional force of 967N in elements 1 and 5 this buckling criterium is amply met. It would be possible to reduce the outer row of the edge element. The Euler buckling force would still exceed the occurring element force with 1.0kN > 967N. It was however a design choice to stick with the two layers. This because of concerns about the precision of the rope placement. The chance of gaps occurring in a single layer is much larger. Additionally this was done because the Euler buckling load poses an upper limit so the actual force at buckling might be lower.

The Unity checks conducted are as follows.

Edge beam:
pure compression

$$U.C. = \frac{\sigma_{Ed,c}}{\sigma_{Rd,c}} = \frac{2.84\ N/mm^2}{10\ N/mm^2} = 0.284 < 1\ OK$$

compressional buckling

$$U.C. = \frac{N_{Ed}}{N_{Rd}} = \frac{967\ N}{3905\ N} = 0.247 < 1\ OK$$

tension

$$U.C. = \frac{\sigma_{Ed,t}}{\sigma_{Rd,t}} = \frac{0\ N/mm^2}{10\ N/mm^2} = 0 < 1\ OK$$

Web:
tension

$$U.C. = \frac{\sigma_{Ed,t}}{\sigma_{Rd,t}} = \frac{9.50\ N/mm^2}{10\ N/mm^2} = 0.950 < 1\ OK$$

All the unity checks were confirmed at the introduced load of 1kN. The most governing unity check is web tension. If the assumed material properties are correct the failure mode during testing will be failure in tension of the web. From the script it can be deduced that the most critical section will be at element 9. Possible compressional failure would occur at higher forces in either element 1 or 5. In the case that the tensional material properties are underestimated pure compressional failure would occur at a point load of 3.8kN. In the case the compressional resistance is underestimated the compressional buckling failure would occur at 4.2kN.

Table 2: Possible failure modes with corresponding point loads

Failure mode	Corresponding point load [kN]
Web tension	1.1
Pure compression	3.8
Compressional buckling	4.2

9.2.1 Winding path

The winding path was derived as previously described in this thesis. The variables for the path were set as follows: the encircles were realized with a radius of 25mm and a resolution of 8. Every connection to the threaded end is accomplished by a full encirclement. The material diameter of the windings is set to be 5.1mm. This is the measured diameter which is 13.3% larger than the 4.5mm which was assumed from the manufacturers data.

The panel thickness is 61mm which will be overshooting the previously tested height with regard to the end effector. The margin however is sufficiently small that the panel can be manufactured with confidence.

The polyline representing the winding path resulting from the algorithm is shown in figure 51. After calibrated placement of the polyline, which will be explained in the next paragraph, it is divided into points at a maximum distance of 30mm apart or at locations of discontinuities. This terminates the design phase of the panel.

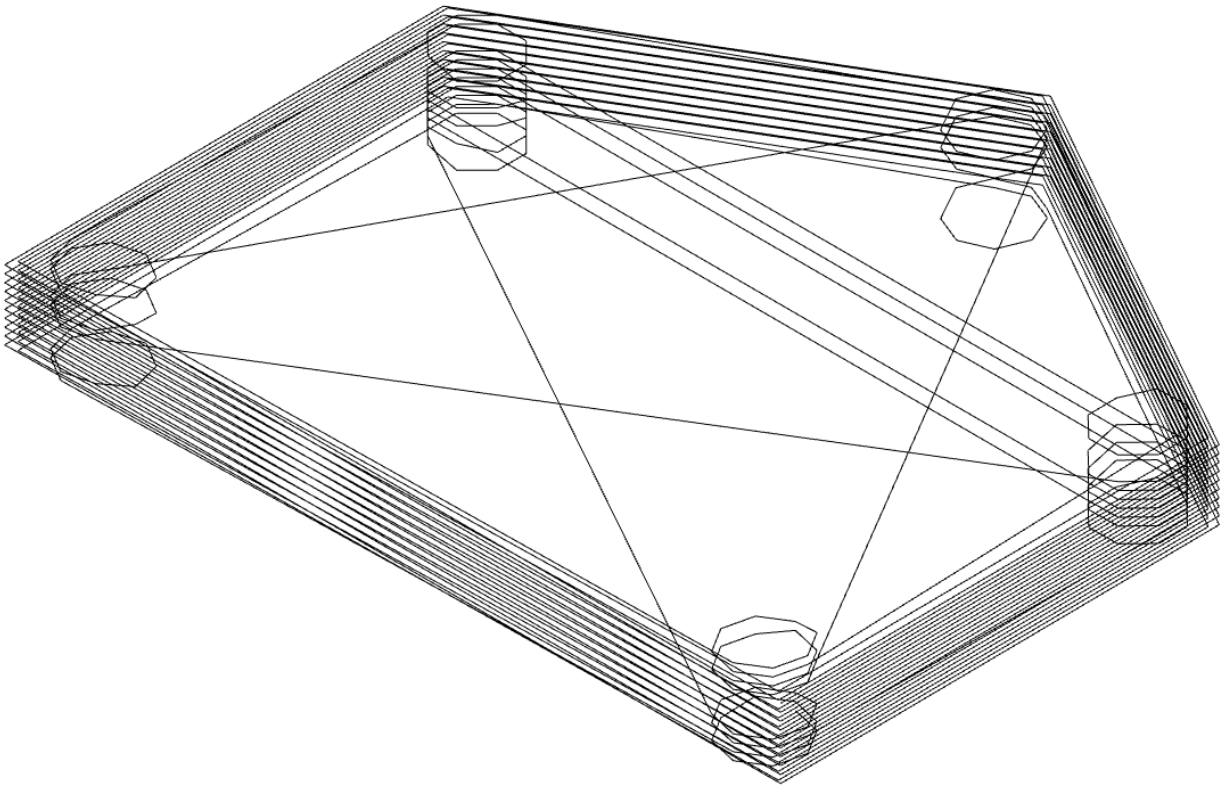

Figure 51: The polyline describing the winding path

9.3 The winding process

Robot path, mold and peripherals were set up in advance. With the mold at 67mm from the base of the robot the robot path was checked in Robotstudio 2020. During this simulation no errors were found.

9.3.1 Setup

The mold was used as earlier described in chapter 6.2. Five threaded rods form the vertices for the panel instead of six. The mold is placed 67mm from the base parallel to the robots edge. It is screwed in place on each corner to avoid any movement. In order to form the start of the robot path the used rope was knotted and clamped to the mold. The path will be completed by tying the rope around the sixth threaded rod. In order to avoid resin from seeping between the holes and the threaded ends tape was applied.

The placement of the mold is never precise enough, the vertices need to be calibrated with the robot path. This is done by first getting the end effector in the right orientation. The end effector is manually jogged to hover exactly over two opposing threaded ends. Coordinates are extracted from the robots user interface. The x and y coordinates are used to position and rotate the polyline that forms the basis for the RAPID-code in such a way to fit the two points. The height is decided by averaging the measurements and manually adjusting the z location of the polyline to fit the threaded ends.

The rapid code is uploaded to the robot controller. In order to be sure the winding will go as planned it was decided to run the entire robot path with dry material. When dry running the path the rope placement can be checked. No material is wasted in case of improper placement since the dry rope can be simply retrieved. Material placement was found to be acceptable so the process was to continue.

9.3.2 Winding

With the RAPID-code checked the next step is to prepare the resin. The infugreen 810 is mixed with hardener SD8824 in a ratio of 100/22, creating 200ml of mixed resin. The biofiber is led trough the peripherals and the end effector, knotted and clamped to the mold. The winding of the material took place by letting the robot cycle trough the RAPID code again.

When all the material was placed the rope was cut and attached to the final threaded end. The mold was removed from the robot reach. Observing the wound panel it was found that the edge elements slightly touched the mold. In order to prevent the edge elements from attaching themselves to the mold Teflon foil was cut and placed between the edges and the mold.

The Sicomin specification sheet (Sicomin, 2019) states that in order to reach the best material properties the resin should be hardened at room temperature for 16 hours. After room temperature hardening is complete the resin should be heated to 40° for 24 hours. The actual hardening times of the panel were kept as close to this specification as possible. The room temperature hardening was done overnight for 17.5 hours. Afterwards the panel was brought in a controlled environment of 40° for exactly 24 hours. Testing and demolding took place twelve days after the heated hardening.

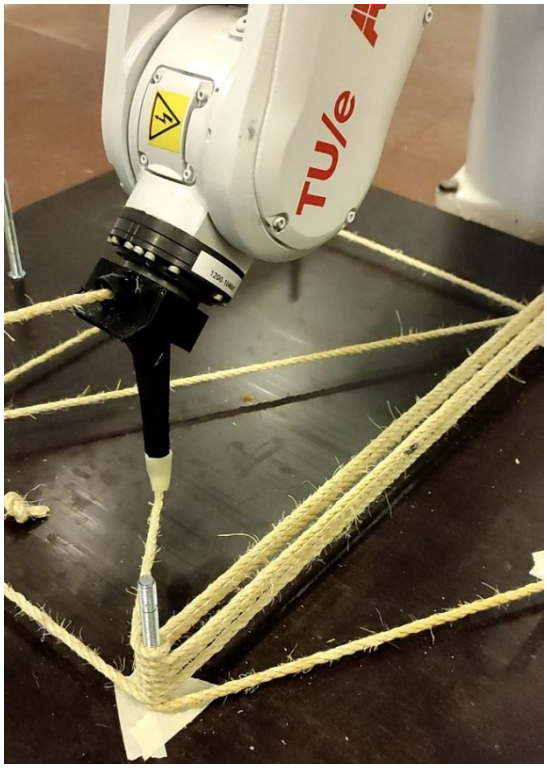

Figure 52: Robotic winding of the panel

9.4 Testing the panel

After curing the panel a test was done. The point load was introduced on the panel as designed. Two hinged supports were set up. The testing was done by displacement control with a speed of testing of 1mm/minute. The deformation of the graph was measured by directly taking the displacement of the tip of the jack of the testing machine. With the point load introduced onto the threaded end this measured displacement represents the displacement of the threaded end. It should be noted that the displacement of the threaded end is not necessarily the same as the displacement of the top point of the panel as there could be flexibility in the fixation of the threaded end.

The same panel was tested several times. The first test was conducted with a force measuring box of maximum 500N installed. The second test was done with a measuring box until 2000N. For both the tests the panel still remained in its elastic stage and no plastic deformation was identified either visually or in the graphs generated. The third test was done with the internal force measuring box of the testing machine itself. The limit of this internal measuring box was never reached. During this test the panel showed two failure mechanisms which will be elaborated later in this chapter. After the testing the panel returned to a state very similar to the beginning state. This arose the question how much of the deformation was elastic and which influence the plastic deformations had on the panel. A last test was done on the panel. In this final test the force introduction was changed from a hinge to a rigid setup.

Table 3: Overview of test results

Test #	Force measuring box	Test speed (mm/min)	Peak force (N)	Elasticity (N/mm)	Failure mechanism
1	<500N	1	504	493	None/ Elastic only
2	<2000N	1	1996	521	None/ Elastic only
3	Internal	1	2026 & 4373	552& 571	Tension resin & buckling of composite
4	Internal	2	1987	386	Buckling / tension in composite

9.5 Results

The results of the test will be plotted on force-displacement graphs. From these graphs the peak force, panel elasticity and other structural properties can be derived. In order to further analyze the panel behavior videos were taken of all the tests. Combining these videos with the force/ deformation graphs gives insight in the failure mechanisms that occur.

9.5.1 Test 1 and 2

As mentioned the first two tests were conducted without the panel showing significant plastic behavior. This was supported by the video not showing plastic deformation. The deformation graphs are analyzed for elasticity as follows.

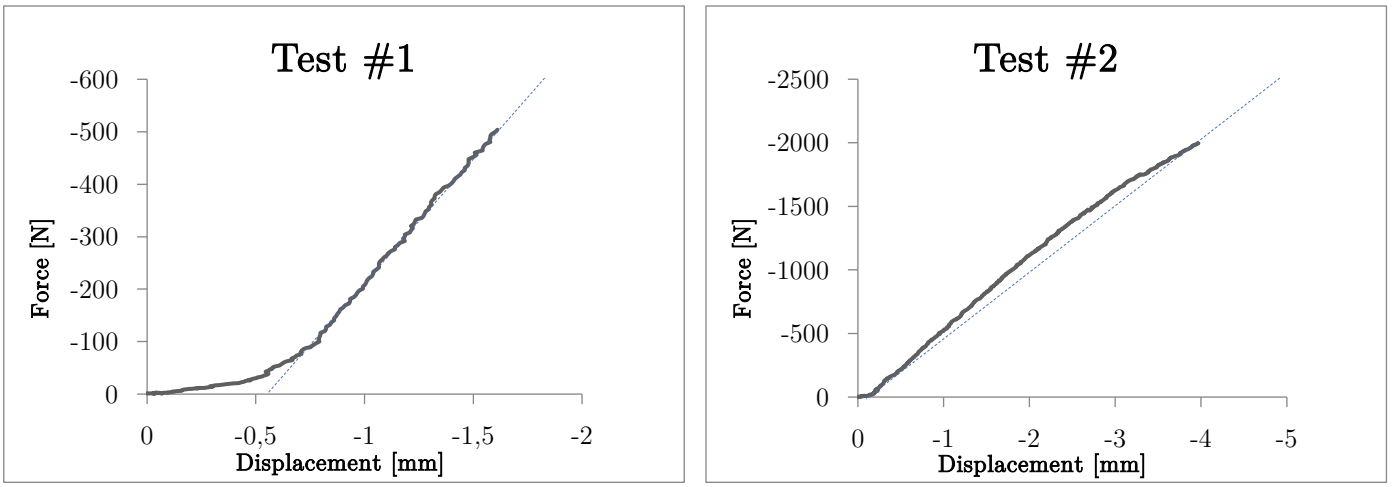

Figure 53: Force/displacement diagrams of test 1 left, and test 2 right

In test 1 a clear run-up phase is identified until 0.79mm of displacement, the force is then 100N. In this phase the elasticity of the panel is changing. This can be interpreted as an initial settling. After this run up the elasticity of the panel can be calculated since the elasticity is very linear in the domain of 0.79mm up to 1.61mm.

$$k_1 = \frac{\Delta F}{\delta} = \frac{504 - 100}{1.61 - 0.79} = 493 \ N/mm$$

The peak force of test 1 is reached at 1.61mm and is limited by the use of the force measuring box at 504N.

In test 2 the run up is also present but much smaller stopping at 0.18mm of displacement at just 25N. This could be explained by the fact that the run up consists of effects of the panel and effects of the setup itself. Since the panel was already tested the internal effects were likely reduced. After the 0.18mm the deformation graph is relatively linear so a stiffness could be calculated. It is however noted there are some minor plastic effects already present since the graph is not exactly straight.

$$k_2 = \frac{\Delta F}{\delta} = \frac{1996 - 25.0}{3.96 \ - \ 0.18} = 521 \ N/mm$$

The peak force of test 2 is reached at 3.96mm and is limited by the use of the force measuring box at 1996N.

The elastic stiffness of the panel in these two tests only differs by 5.7%. This change in elasticity could be explained by some plastic behavior in the panel. It is however a minor effect as demonstrated by the small percentual difference.

9.5.2 Test 3

After the previous test the load on the panel was reintroduced. This time the internal force measuring box of the Instron machine was used. No maximum value for the force measuring box was reached. Plastic behavior was derived from the video. Initial plastic behavior was localized failure of the threaded rod nesting against the edge element. This is essentially tension failure between the interface of rod and composite or between two composite elements. This failure mode was photographed and shown in Appendix G. After this plastic effect settled the panel regained stiffness and after a while buckling in the top element took place. Figure 54 shows the force displacement diagram of test 3.

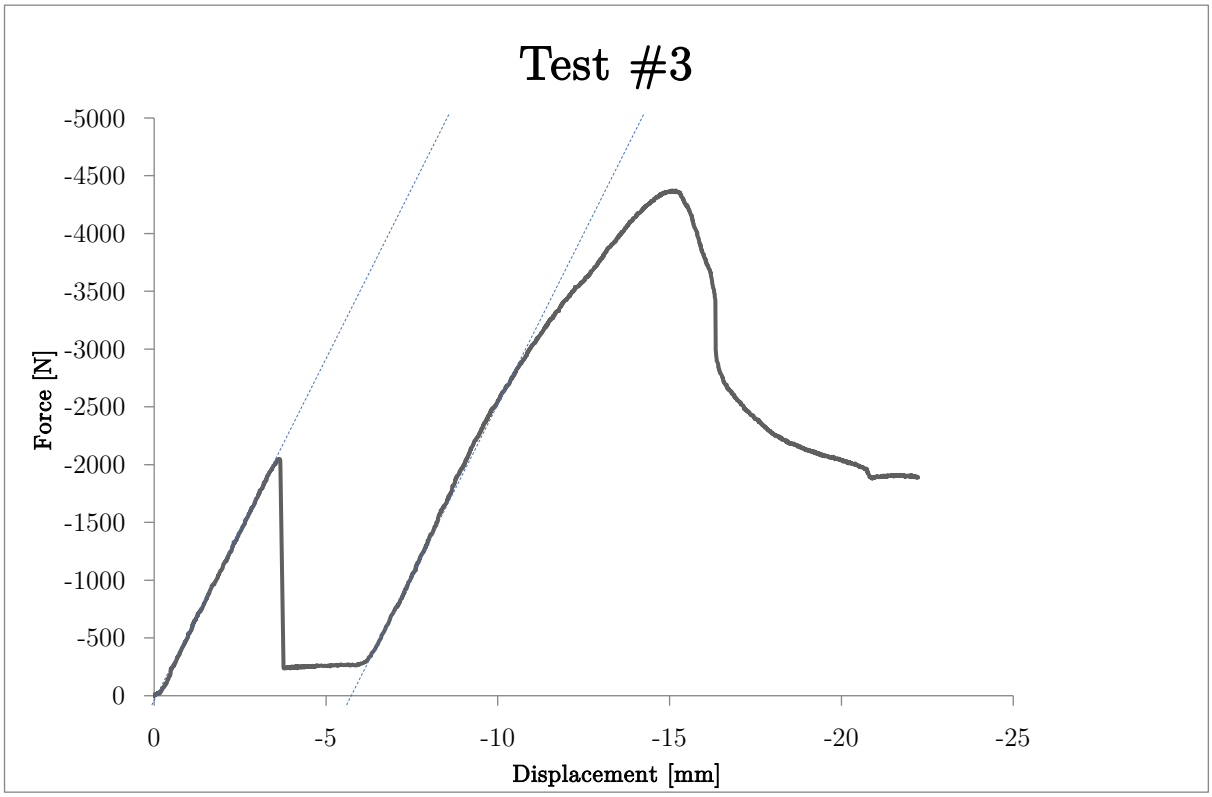

Figure 54: Force/displacement diagram of test 3

The claims stated as a result from visual cues are supported by the force displacement graph. Indeed two peaks are visible at which large plastic deformation occurs. The first smaller peak has a force value of 2026N at a displacement of 3.67mm with a negligible run-up phase. The peak coincides with an effect that can be seen in the video. An abrupt change in orientation in the panel is seen coinciding with a loud cracking sound. The top of the panel abruptly rises with the threaded rod staying in the same place. This together with the further buckling of the compression diagonals further support the theory of the threaded end being partially pushed out of the edge beam. A stiffness can be calculated from the graph leading up to this peak.

$$k_{3.1} = \frac{\Delta F}{\delta} = \frac{2026}{3.67} = 552\ N/mm$$

Afterwards the force remains at around 250N for a few mm until at around 5.60mm where the panel starts to regain stiffness. This effect could be explained by only part of the threaded end loosing connection with the edge beam. The threaded end starts to become more slanted until a point where the forces redistribute. Yet another elastic part of the structure is showing up after this redistribution of forces. This elastic part is considered between 299N at 6.18mm displacement and 3000N at 10.91mm displacement. After this the graph starts to flatten towards its peak. This implies some plastic effect occurring around the 3000N mark. Supported by the buckling deformation seen in the video from this point.

$$k_{3.2} = \frac{\Delta F}{\delta} = \frac{3000 - 299}{10.91 - 6.18} = 571 \ N/mm$$

This second elasticity seems to be around 3.3% higher again continuing the trend of raising stiffness in the cyclic loading.

The second peak takes place at 4373N with 15.09mm of displacement. The peak in the graph coincides with the start of the aggravated buckling phase as seen in the video. It is important to note the buckling does not occur in an abrupt manner but is a slow process where the panel is still able to generate stiffness. This would be seen as warning behavior in structural applications.

After the second peak some additional dip is observed at around 2000N and 20mm. This is where in the video the compressional force setup shows some sudden increase in obliquity. This could be the result of the threaded end losing its connection to the edge elements due to the increasing deformation.

9.5.3 Test 4

The fourth test was conducted with a change in setup. The previous test showed a large amount of obliquity which was of such magnitude that concerns arose about something in the setup breaking. The ball joint included in the force introduction was removed for this test. Since the threaded rod was already partially pressed out of the element it was expected it would slant again. Without the ball join the deformation will be shared by both sides of the threaded rod evenly instead of the sagging side deforming more. This could possibly put more strain on the attached side either leading to its failure or leading to a more direct force path. This test was performed at 2mm per minute.

The video of the testing shows buckling of the same element as before. It also shows tensional failure of a horizontal composite element. In the figure 55 the force displacement graph of test 4 is shown.

From the graph it can be seen that a quite a large run-up phase is present in the test on the plastically deformed panel. This phase is assumed to be a result of the detachment of the threaded end. The threaded end needs to be slanted before the forces can be transferred onto the structure. Even with the earlier buckling expected to have caused some damage to the

element the next phase is pretty much elastic. For the elastic phase the domain between 128N at 3.75mm and 1596N at 7.55mm is considered.

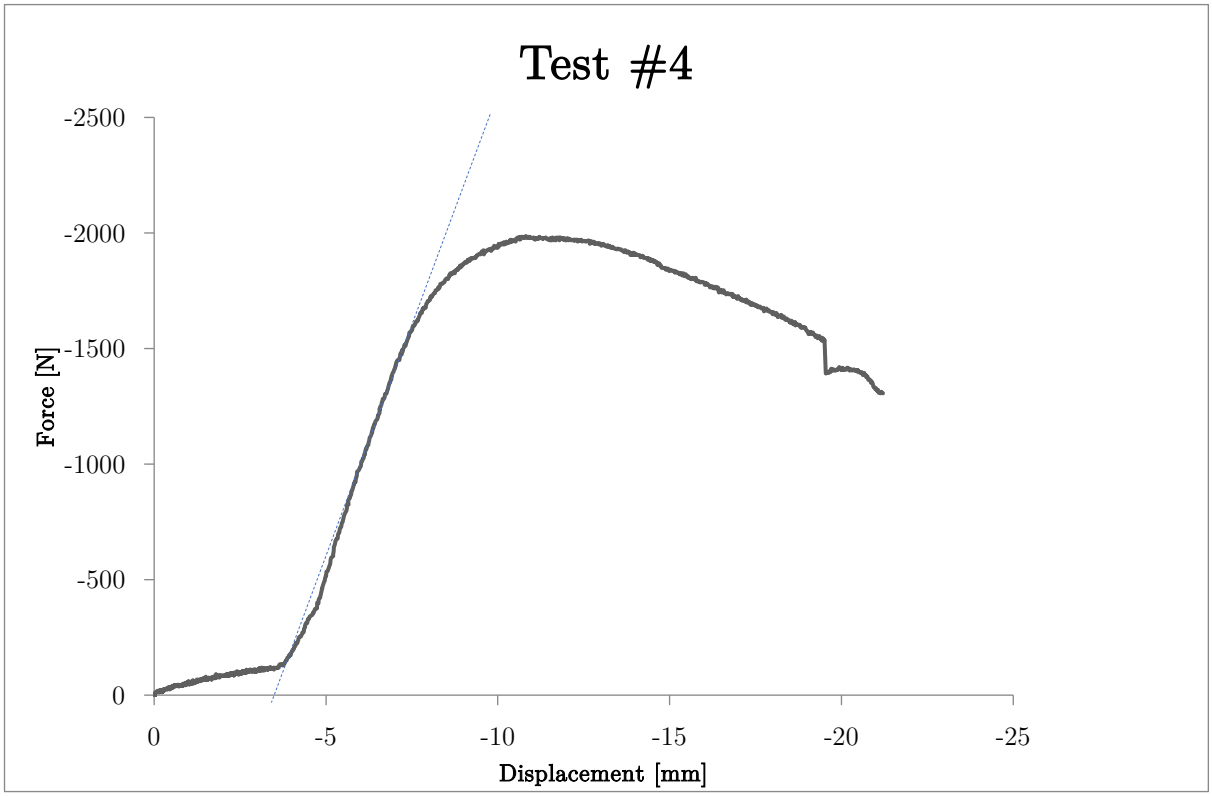

Figure 55: Force/displacement diagram of test 4

Again the same method can be used in order to derive the panels stiffness:

$$k_4 = \frac{\Delta F}{\delta} = \frac{1596 - 128}{7.55 - 3.75} = 386 \ N/mm$$

After the elastic phase buckling behavior is present which is visually almost identical to test #3. However with this time the force introduction remaining perfectly level the panel is rotating. This rotation combined with the buckling might cause some internal deformations to be bigger than at the previous test. The panel peaks at a force of 1987N at 10.82mm of displacement.

The bigger internal deformations are considered a likely cause of the next occurring failure mode. At 1538N and 19.51mm displacement a crack is heard in the recording together with a single horizontal composite element changing orientation. The force suddenly reduces from 1538N to 1392N. Redistribution of forces causes it to rise but finally dip after which the test is stopped.

9.5.4 Comparison of panels

The results of each test were composited in the graph presented in figure 56.

Figure 56: Force/displacement diagram of all tests combined

In the graph very similar stiffnesses can be seen for the elastic parts with a slight upwards trend of the cyclic loading. The following table relates the individual stiffness values to the tags in the graph.

Table 4: Comparison of elasticity observed during the different elastic phases

Test #	Stiffness tag #	Elasticity (N/mm)
1	0	493
2	1	521
3	2	552
	3	571
4	4	386

This calculation shows a trend in the applied cyclical loading where the stiffness actually increases with an average of 5% per cycle. Excluded from this average is the last test where the panel had previously buckled which explains the lower stiffness. The increase in stiffness is not very significant especially considering uncertainties in measurement. Nevertheless the effect is noteworthy, as there seems to be an actual trend. The cyclic testing should not be seen as a fatigue test in which its certain the stiffness would decrease over time. However with a small

amount of cycles the increase in stiffness is actually possible. This effect is possibly comparable to the behavior of the rope as a stand-alone material where initial load might show a smaller stiffness than a secondary load. In rope this is caused by the perpendicular compacting of individual fibers. However in composites its supposed this effect is reduced since the perpendicular compacting is prevented by the resin matrix. Before any conclusions are drawn about this effect there is more research needed.

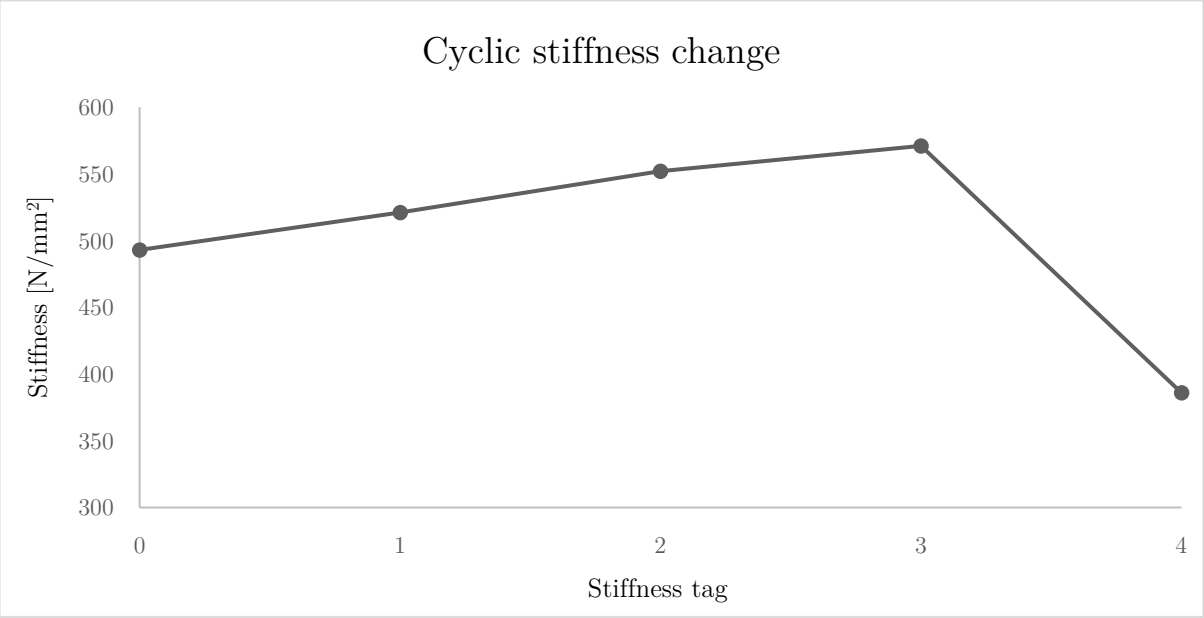

Figure 57: Comparison of elasticity with each testing cycle

9.5.5 Failure modes

In this paragraph each failure mode that was expected is compared to the observed behavior of the panel under loading. A disclaimer is that since only a single panel is tested the conclusions should not be viewed as normative. Nevertheless important effects can be identified even with just a single panel tested.

9.5.5.1 Tension

As derived during the panel's calculation the expected failure mode was tensional failure of the web in element 9. It was calculated to occur at a point load of 1.1kN. However the threshold was passed during the tests without a major sign of plastic deformation. This is partially because of the use of a design value for the tensile resistance. It could also imply that the either the tensile material properties or the composite area was underestimated. Underestimation of the composite area is unlikely since it was checked visually and no extreme differences were present. This leaves the underestimation of material properties to be the major contributor. The failure mode did however occur at test #4 with the plastically deformed panel. The failure mode is visualized in Appendix G. At this point the panels element 1 was damaged in such a way that redistribution of forces took place bringing more of the internal forces to element 9. Eventually the failure mode occurred at around 1.5kN. This value is however not to be directly compared

to the 1.1kN because of the redistribution of forces which occurred. The actual internal force in the element could be much larger. Assumptions with regard to the material properties can be made considering the second peak in test #3. Before this second peak no major redistribution of forces is assumed. Using the FEM as present in the algorithm to calculate a force of 4.4kN is applied on the panel. This leads to an internal tensional stress of 43 N/mm^2 at element 9. At this value the failure mode was still not identified so the actual value might be even higher.

9.5.5.2 Compression

The pure compressional failure would be the next failure mechanism to look for. This failure mode would according to the design occur at a point load of 3.8kN. For this failure mode the same is true, no indications of this failure mode were found at the expected mark. Aside from the underestimation from using the design value. This could also lead to the assumption that the material properties for compressional failure are underestimated. Again considering the second peak in test #3. From the updated FEM calculation it can be derived that without redistribution of forces the compressional stress in elements 1 and 5 was 12 N/mm^2 exceeding the expected critical stress of 10 N/mm^2. This would imply the compressional resistance is higher than 12 N/mm^2.

The compressional buckling in elements 1 and 5 was expected to occur at a point load of 4.2 kN. In order to find this value the upper limit was used in the form of the Euler buckling load. This value is within 5% to the peak value of 4.4kN found in the second peak of test #3. This implies that the calculation was relatively reliable on finding the Euler buckling load. This is a promising aspect implying that the geometric approximation of the edge beam was not far off. Buckling is also the only failure mode considered where the material stiffness is used in the unity check. Implying that the assumed material stiffness value is close to the actual value.

Contrary to this optimistic theory the observed buckling mode is likely aggravated by the added bending which is neglected in the finite element method as presented. This is a possible explanation as to why all material properties seem to be underestimated except in the case of buckling. In reality the effect of added bending could reduce the buckling resistance. In order to support this theory the actual bending moments that occur in the section were deduced using a commercial finite element package, something which is not possible in the axial FEM as presented in this thesis. The same panel geometry was introduced with the same boundary conditions. The single windings were omitted for sake of simplicity.

The FEA finds the values for bending as shown in figure 58. The axial forces are within 5% difference of the values calculated with the FEM as presented. In element 1 where the buckling occurred a bending moment of 3.95Nm is found together with an axial force of 950N. This moment causes an internal bending stress which can be calculated by equation 58.

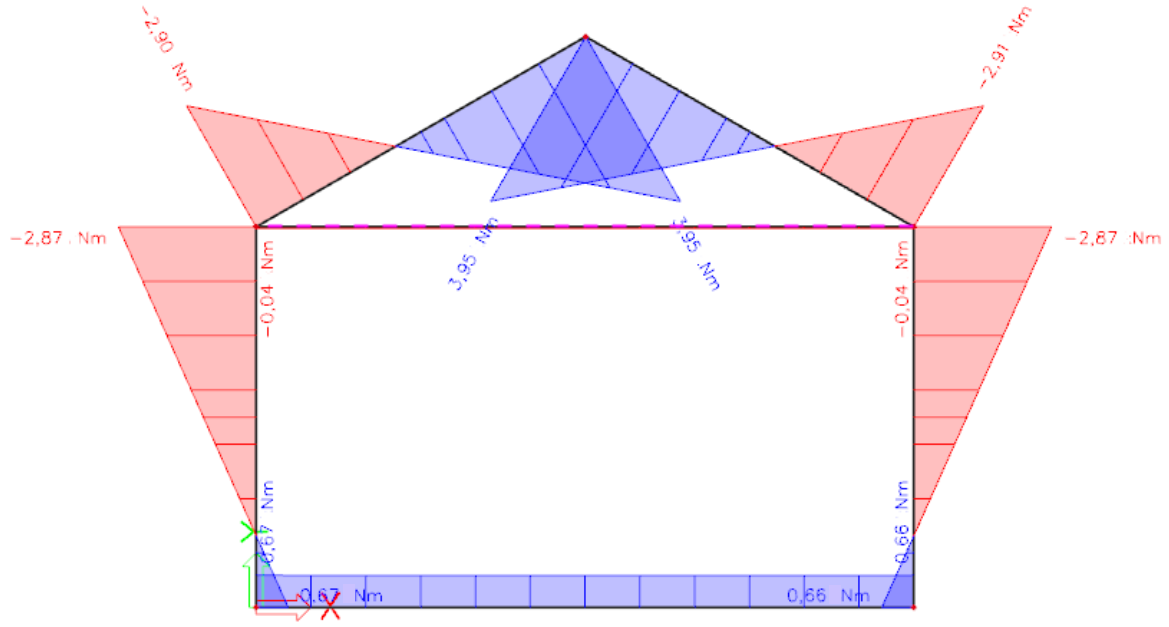

Figure 58: Bending moments at the panels edge as found by an external finite element analysis

$$\sigma_m = \frac{M * z}{I} \tag{58}$$

With
σ_M = bending stress [N/mm^2]
M = bending moment [Nmm]
z = distance from extreme fiber to neutral line [mm]
I = second area of inertia [mm^4]

As I=2747mm^4 for the composite sections with z=7.6mm, the extreme bending stress is found to be 10.9N/mm^2 which is considerable compared to the axial compression stress. Meaning buckling is likely aggravated by this additional bending stress. This does however apply at the same time as the reduction of the buckling length by using fixed connections between the elements. This reduction of buckling length in turn causes the Euler buckling force to increase because of the lower K-factor (0.5 for fixed connections instead of 1 for hinged).

There is another assumed factor in the calculation which is the stiffness used in the Euler buckling equation. If the stiffness would be higher than considered the flexural stiffness could assume a lower value. Another possible explanation could be that the material does not actually generate the amount of bending moment as the finite element model suggests. It is possible the materials area decreases slightly around the tightly wound edges of the panel. This would lead to a smaller bending arm in turn causing lower internal bending stresses to generate. These explanations are however only theories and more research on this topic is needed.

In paragraph 4.1.1. a failure mode is introduced that is expected to be negligible. The edge **torsion** was not identified during testing. While torsion could cause buckling, lateral torsional

buckling was not observed. The buckling mode that occurred was the buckling mode as expected from combined bending and axial loading.

9.5.5.3 Threaded end

Pushing out of the threaded end is the last failure mode that will be discussed but the first that was observed. The situation as manufactured is shown using the pentagonal panel as in figure 59. The failed situation can be seen in Appendix G. The designed force is introduced onto the threaded end in the peak of the panel. This is seen as the critical location of this failure mode. At the location of the supports the threaded ends are also loaded. They are essentially dividing the introduced load over two threaded ends and therefore the situation is less critical. This was underlined by the observed failure mode of the top threaded end at around 2kN.

The top threaded end is fixed in its location in several ways as can be seen in the supplied figure 59. The first way is by the wound edge elements. Two rope composites are wound around the threaded end at the top and at the bottom. The vertical force in the threaded end is to be translated to normal forces in the edge. This translation of the vertical forces likely occurs with a combination of aspects. Firstly the tension aspect will be considered and secondly the shear aspect. In reality these are two components of the actual force path. Considering these aspects separately will give insight in the failure mode.

The tension aspect consists of tension between edge windings and the edge beam, web winding and edge curve and finally threaded end and edge curve directly. A schematic of the situation is given in figure 60. The tensile strength properties that are related to this problem are the tensile strength of the resin, the resin composite interface and the tensile resistance of the resin steel interface. The value for the tensile strength of the resin can be extracted from table in Appendix B to be 68N/mm^2. The interface strength of the resin and the composite are for now assumed to be equal to the resin tensile strength, for the exact value further testing should be done. The tensile interface strength of the resin and the steel of the threaded end is deemed negligible, this value is not known. The same is to be said about the actual connection area between the edge beam and the threaded end. As shown in the top of figure 60, in the case of tension only there is no shear connection between the edge windings and the edge beam. There are however intermediate interconnections that prevent the edge windings from buckling under compression. Therefor the total tensional load from the threaded end is actually reduced by the compression in the edge windings. The web elements do not take on any compression because of elastic buckling. Assuming even distribution between the edge windings and the edge beam it can be stated that the edge windings take 1/21$^{\text{th}}$ of the compressional force in the edge each. Adjusting for the angle between the edge beams which is 120$^{\text{o}}$ it can be derived that the edge windings take on 95N each. Leaving 1.81kN to be transmitted into the edge beam. Again adjusted for the angle this leaves 1.81kN to be passed on from the edge windings to the edge beam via pure tension. The side view in figure 60 shows a marking of the approximate connection length. In order to find the connection area the section of the connection is schematized in the bottom of

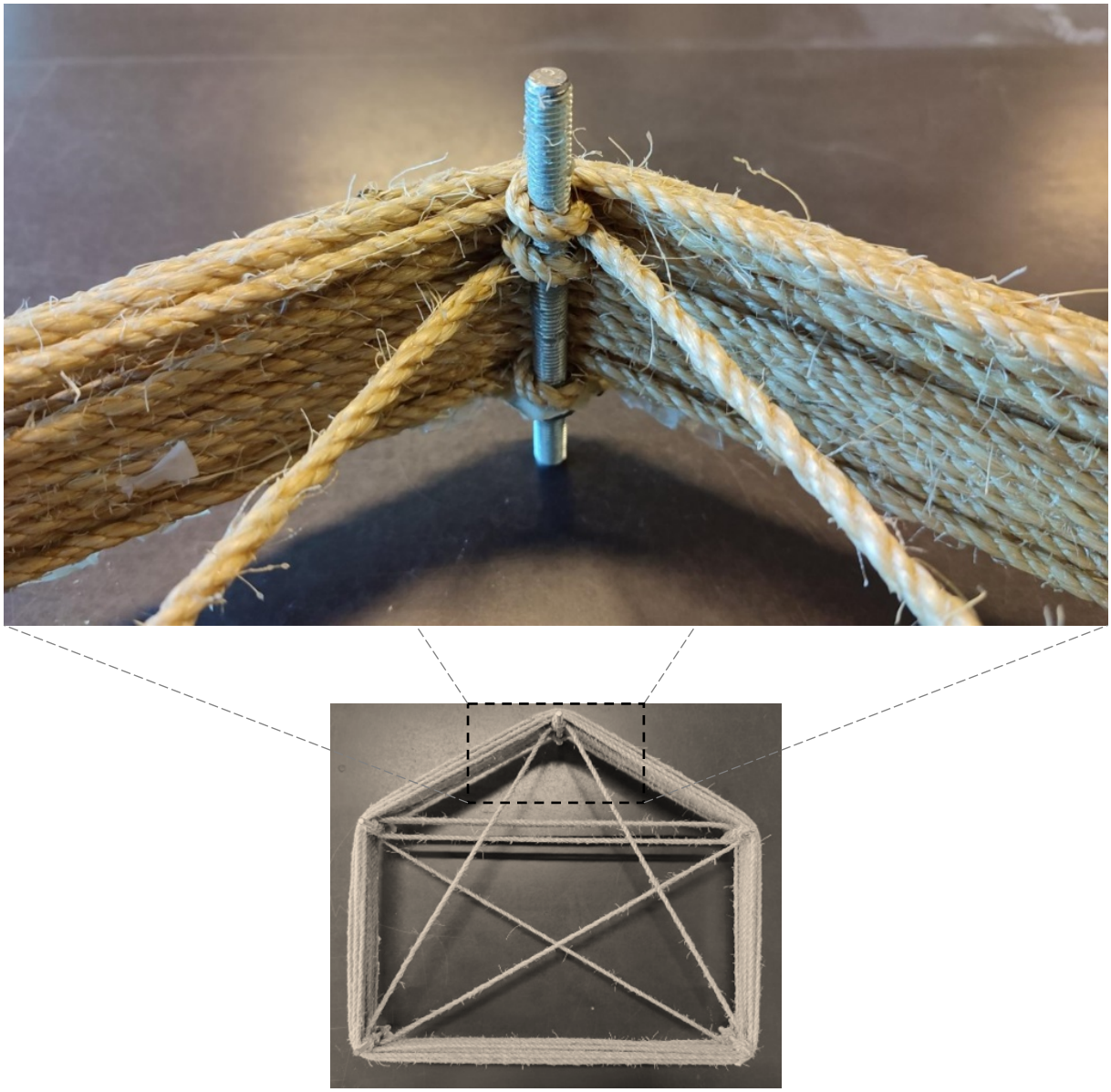

Figure 59: Location and fixation of the partially failed threaded end

the figure. Here the edge beam is shown in blue, the edge windings in red and the web winding in green. Two sections are shown for the windings as that is how the section looks at the length indicated. The grey circles are locations that are theoretically left empty, in reality these are filled with elements from the edge beam. The connection between the edge beam and the threaded end is to be neglected. The windings have ten points of interaction with the edge beam. The exact length here is not known. Theoretical area would be zero in the case of perfectly circular elements. However the composite is not fully circular because of different effects like squishing and drooping of the resin. The necessary area can be calculated using the tensional resistance of the resin and the applied force to be 27mm^2. The length in the upper part of figure 60 is assumed to be 4mm in total, which is deemed reasonable since the edge beam is wrapped around the edge winding with tension. In order to sum to a sufficient area of 27mm^2 the length of each of the 10 composite interconnections should be 0.675mm.

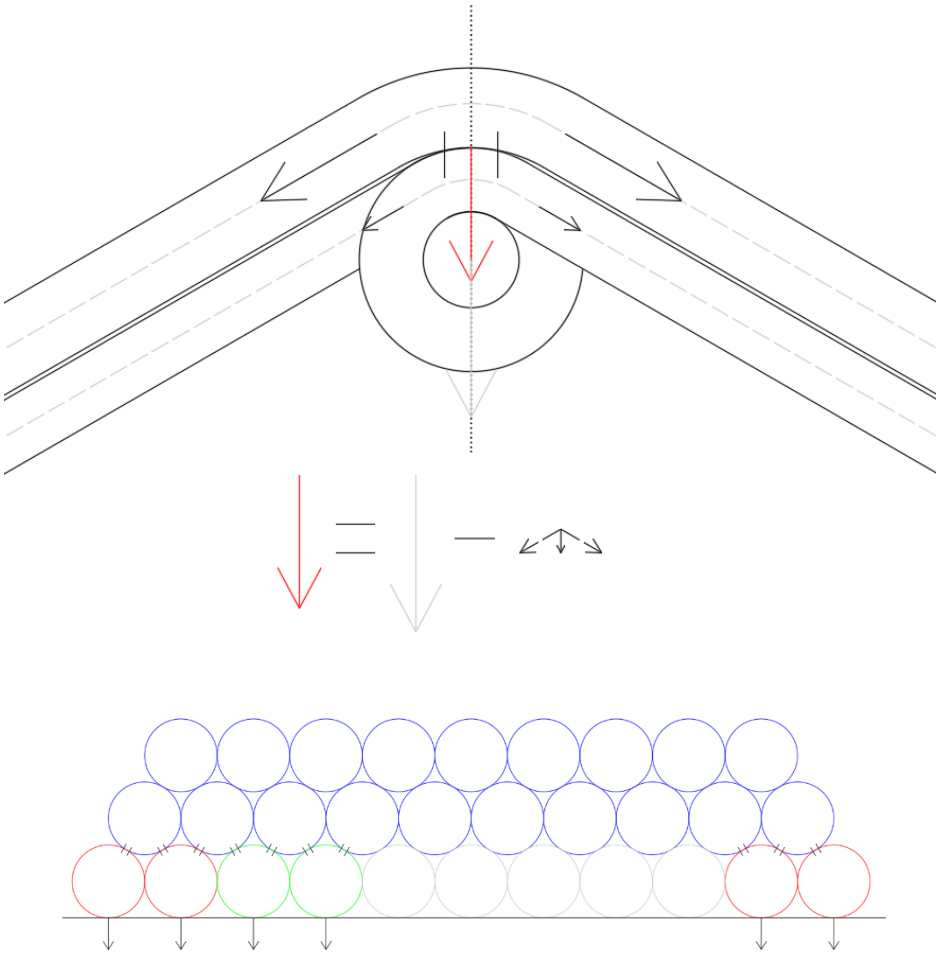

Figure 60: top: top view of connection to threaded end, bottom: section of connection to threaded end

In the case of pure shear the force calculation is a little different. From the data sheet of the resin again the maximum shear capacity within the resin itself can be known to be 43N/mm^2. The shear capacity within the composite itself might be different but is not known at this point.

At the point of force introduction the internal normal force in the edge beam is 0N while the internal normal force in each edge winding is $1.81/2 = 905$N. The width of the connection was previously stated to be 0.675mm. In figure 61 it is visualised that the edge windings have three connection areas, coming to a total width of 2.025mm. This is the case because of how the edge winding is executed. Assuming this same connection width between composites, the shear force is transmitted with 87.1N/mm of material length. Taking the force and dividing it by this value leads to a needed connected length of 10.4mm. This is the length the edge windings should be connected to the edge beam at each side of the threaded end.

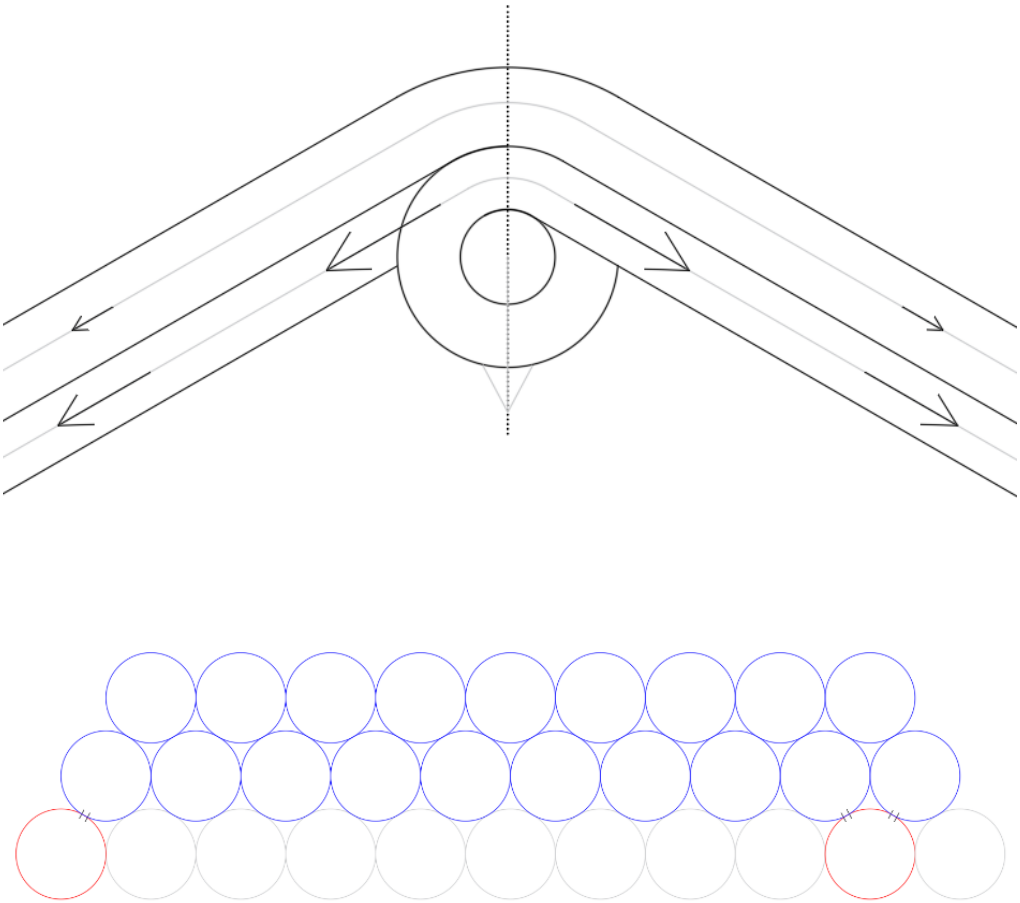

Figure 61: top: top view of connection to threaded end, bottom: section of connection to threaded end

It is not exactly known in which way the threaded end connection failed. Both the values for the tension capacity and the shear capacity seem to be realistic. However the visual check did show high variance in the placement accuracy. Due to the possible misplacement of material the theorized tension and shear areas might be less ample than expected. The accuracy of material placement could be influenced by different factors. The twist of the material could cause difference in the actual placement location. In addition the twist in combination with pulling the rope might cause the rope to rotate unexpectedly. If this rotation occurs after placement the material might rotate away from its original location. Both these effects could be prevented by using parallel strand material. Other causes for inaccuracy are misjudgement of rope diameter. This misjudgement can be very small and still have an effect because the error is summed over each layer. Another indication of inaccuracy was the change in behaviour of the rubber on the end effector tip. During the material placement it was observed the rubber started to show cracks which might change the placement location. Final cause could be the design, which keeps a gap adjacent to the threaded end as indicated by the grey circles in figure 61. The gap causes the elements building up the edge beam to move in a different location than modelled. This also could have an influence on adjacent elements. The gap is different at each threaded end and for that reason it cannot be solved by adding more encirclements for the edge beam. In order to

compose a reliable verdict about the occurred failure mode this variance should be researched. With further research into this aspect of the winding the requisite areas of shear and tension could be identified with more confidence. The connecting areas should be combined with reliable models about material behaviour. A large unknown of this research is still the material properties. Tests should establish values for the tension and shear resistance of both the composite and the composite-composite interface.

An additional effect of transmission of forces into the edge beam due to shear is the consequential bending moments that arise. The bending moment are a result of the torque originating from the difference between normal compressional forces in the edge beam and the edge winding. The bending moment is largest in the edge beam at the location of the threaded end. Figure 62 shows an isolated image of the edge beam and the edge winding in shear. The threaded end connection was cut off. At the location of the section a bending moment M1 is made visible. This bending moment is occurring due to the multiplication of the force in the edge winding F2, and eccentricity e2. Subtracted from this is the force in the edge beam F1 multiplied with its eccentricity e1. At the location of the threaded end the F1 is zero when transmission of forces due to shear only is considered. Therefor this is the location of highest bending. This bending is detrimental to the elements compressional resistance regarding the failure mode of buckling. During the panel testing the buckling that was observed did occur in the direction of bending moment M1 reinforcing the concept of the detrimental bending.

Theoretically this added moment could be avoided by decreasing the eccentricities. This is however not practically feasible with the presented winding method. Another possibility of decreasing the moment M1 would be by decreasing the need for shear force transfer between the edge winding and the edge beam. If the forces would be transferred due to tension between edge winding and edge beam the shear would not occur and therefor the bending moment would be absent.

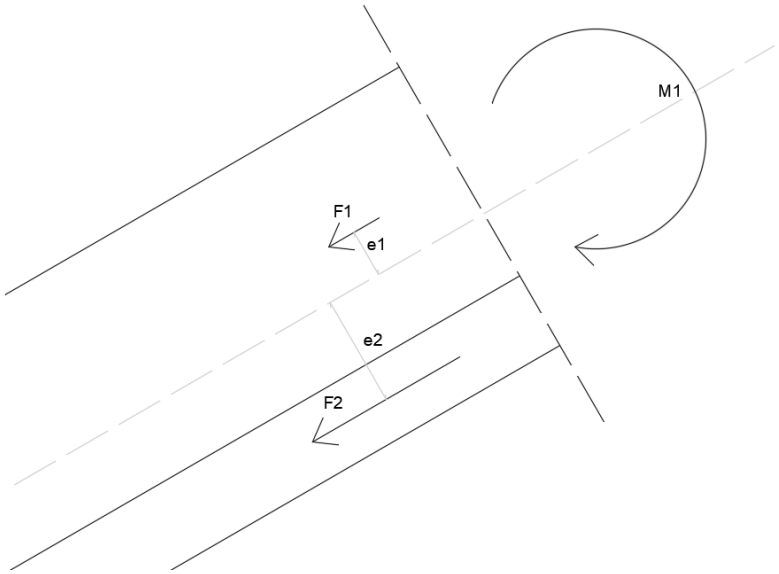

Figure 62: Isolated schematic of the edge beam and the edge winding in shear

9.5.6 Panel stiffness

With the buckling of the edge element the material stiffness seemed to be as expected. However looking at the panel deformation during testing another conclusion could be made. The assumed panel deformation at the point of introduction was 0.60mm under a 1kN load. The actual displacement at 1kN of the tip of the testing machine was measured to be 1.8mm both at test #2 and test #3. Test number 1 had an even larger displacement but there was also some initial settling phase present that is not counted. There could be several explanations for this observed discrepancy between calculation an reality. The first possibility is the overestimation of material properties. The observed buckling seems to contradict this possibility. Slight overestimation is however still possible. Another possibility is geometric effects that were not accounted for. A possible effect is slip around the threaded ends. At the locations of the supports and the load introduction the stiffness perpendicular to the composites main direction plays a role. This perpendicular stiffness could be another explanation of the underestimated panel deformation.

10. Conclusions

The goal of the research is to create an efficient, light weight building method, integrating design until assembly. In order to conclude if this goal was successfully reached all the aspects that form the building method are debated separately finishing with a general conclusion.

The concept of the design is based on integrated, high precision manufacturing. In order to achieve this, a robotic fiber winding technique is presented. Modular panels will be wound using a robotic arm placing the material at the exact locations where its structurally most needed. The forces in the panel will be separated, the tension will be taken by a thinly wound tensional web with compression being present in a thicker edge.

Firstly the materialisation is discussed. The chapter poses an introduction into mechanical properties and lists viable material options for consideration and states the importance of sustainability within the scope of this research. Feasible materials at this point are biofibers like sisal, jute, hemp or flax. It was made clear that carbon fiber is in mechanical aspects a far superior material. With future expectations of more sustainable and cheaper carbon fiber the future usage of this material will be preferable. Whichever fibrous material will be used it should be applied in a rope form, with the twist being as small as possible in order to fully utilize the strength and stiffness properties of the material. The rope will be soaked in resin in order to generate compressive capacity. Current commercially available biobased resins have an approximate biobased material percentage of 50%. In terms of mechanical material properties the research is far from finished. The thesis provides a theoretical framework based on the rule of mixtures but there are a lot of unknown factors that require more research especially on composites using biobased twisted ropes.

The design of the structure is the second thing to be discussed. The design concept is based on planar panels, with large freedom in exact shapes and boundary conditions. There are some limitations on design freedom and with that on the generality of the building method. Only convex shapes are allowed as the winding concept is not applicable to concave shapes. The designed structures are limited to a 2D workspace because of the functionality of the FEM program. And finally there is a size limit on the shape based on the robotic reach. It is clarified there are possibilities of diminishing this size limit by using an external rotational axis. Additional benefit of using an external axis would be a more constant prestress in the material during application. Since no external axis is available for experimenting this concept has not been developed further. When the panels are wound within the robotic reach the prestress is lost when the robot moves towards a vertex in the direction of the spool. It is not certain if the prestress is fully regained during the encircling of the vertex. Resulting is a panel with a possible variance in pre-stress.

The FEM program together with the proportional optimization are fully integrated within the process. These algorithms work using the boundary conditions and loads as defined in the design phase. After defining suitable parameters the designed assembly is optimized ensuring efficiency in material use. Depending on the exact geometry optimization factors of 3x are possible. An

optimization factor of 3x could mean the panel is 3x as strong with the same material or the material mass could be reduced 3x while accommodating the same load. This optimization is achieved by iteratively moving material from locations manifesting low strain energy into locations manifesting high strain energy. In the case of multiple load cases the optimization combines the strain energy ratios from each load case into an element specific The optimized panel is most effectively realized when small material diameters are used. This is mostly due to every element in the ground structure having the requirement of one winding creating stability outside of designed structural circumstances. The discretizing of element areas into material windings does not necessarily cause the optimization rate to decrease as it does add stiffness as well as material. In the FEM program the slender web elements are expected not to take on compressional forces. This was realized by iteratively reducing the stiffness modulus for the web elements in compression. The iterative processes are able to run simultaneously while still providing reliable results. A drawback of the FEM program is that it is based on axial forces only. This simplification was done in order to streamline the FEA and save time for the iterative optimization. In practice there are bending moments present in the edge beams that are not negligible as a part of edge buckling.

Structural checks are included in the algorithm. This way the applied proportional optimization can be used for specific structural causes. The structural checks can be done visually by plotting stresses and deformations on screen. Numerical checks are enclosed in the form of unity checks. The decisive unity check defines the location and type of failure mode that is expected to occur. All panel and connection elements are checked for possible failure modes. There were however some assumptions made in terms of translating the theoretic longitudinal connection elements to practical sheet elements. The structural checks form the basis of the structural design but detailed calculations are not automated. Additionally it should be mentioned the considered buckling failure method does not include the bending moments omitted from the finite element analysis. As described in chapter 9 after the panel testing it was evident these bending moments are necessary in calculating the buckling load. In order to sketch a reliable structural image of the structural panel these bending moments should be estimated or externally calculated.

In order to prepare the robotic winding a path is constructed. This path visits and encircles the vertices in the right order to form all elements as designed. The panels are divided in web windings, edge beams and additional edge windings which connect the web to the edge. The vertex order of the edge windings and edge beams are known in advance as they always follow a circular path visiting each vertex. The web winding path is deducted using an algorithm adopting graph theory. In case no Eulerian path over the web windings exist it is necessary to add elements in order to be windable. This adding of elements could decrease the optimization factor depending on the total volume and the volume of a single element. Subsequently the encircles around each visited vertex are designed for the web and edge windings. With the encirclements having some eccentricity extra bending moments could be introduced into the edge beam. These bending moments are negligible due to the symmetric windings, at the vertex of every ingoing winding there logically is an outgoing winding too. This effect largely balances

the eccentricities. Another structural consideration has to be done with regard of the web height. The height differences of the web windings cause torsion in the edge beam. This torsion manifests as shear stress in the section perpendicular to the edges direction. In order to check this shear capacity of the fiber material soaked in resin and the resin interface between elements should both be known.

From the designed path a robotic path is deduced and expressed using RAPID code. In order to limit black box processes within the research a theoretical framework is presented on the translation of a list of nodes encompassing the robotic path into robotic axis orientations. Despite this theoretical framework the RobotComponents plugin for grasshopper is responsible for the execution of the inverse kinematics.

In order to design a suitable end effector several iterations were passed. Essential takeaways from winding experiments were: the end effector should be mounted under an angle of 45° in order to avoid singularities. A rubber tip should be placed on the end effector in order to smooth material placement. Fins on the effector tip cause the rubber to let go in case it gets stuck around a vertex. Without fins the rubber tip sucks vacuum and will pull the end effector until it breaks. The end effector as designed has a tip that can wind around a threaded end with a maximum height of 80mm. This limits the panel design to 60mm in height as space has to be left for connections. The end effectors effective height could theoretically be increased by increasing the height of the nozzle. However with increased height more material stiffness is required in order to keep reliable material placement.

The peripherals are the mold, the spool fixation and resin application. The mold design is straightforward with the threaded ends being fixed using flat bolts. It is important no resin seeps between the threaded ends and the holes because of the need for removal. The threaded ends are part of the mold but remain in the panel after hardening. For the resin application the thread is ran through a resin bath using two crank arms. The resin bath could be filled using a funnel or entirely replaced by raising the crank arms. Another advantage of the crank arms is that the material could be temporarily applied dry. This could be desirable in the case of unavoidable compression/tension loading cycles in the web elements which occurs during varying multiple load cases. When no resin is applied this compression is not able to develop.

Assembly of the wound panels can be done with or without additional connecting elements. With the connecting elements the panels in the assembly are scaled down and the connections are included from the design phase. Simplified unity checks translate the modelled longitudinal elements to the implemented planar sheets. With this connection method all panels are wound around threaded ends and the connecting elements are mounted using bolts from both sides. An alternative method of assembly is presented where the connecting elements are wound panels as well. These connecting panels are calculated the same as the other panels then separated into two and wound around hollow tubes. The connecting panels are mounted again on both sides of the panels to connect.

A panel was designed and manufactured with the proposed techniques. The materials used were sisal rope and Sicomin biobased epoxy. During testing this panel achieved better mechanical strength properties than expected. This is most likely due to the use of design values for the resistance. Additionally underestimated material properties of the sisal composite could play a role. Some conclusions of the testing were: It was found that with every load cycle the stiffness of the panel increased. The overall stiffness however seemed to be overestimated as opposed to the panels strength. Several failure modes were observed. The first failure mode was pushing out of the threaded end for which an approximate calculation was made. The failure mode should be checked in future application. It could be stated that this is not a true failure mode since the panel regained strength after some force redistribution. The next failure mode was buckling. Additional FEM calculations were made to support the observation of the failure mode. These calculations found bending moments generated at the nodes are likely not to be neglected. Tensional failure did only occur after severe deformations. Because of force redistribution the exact stress at failure in the element could not be exactly derived. The different failure modes where thoroughly scrutinized and possible explanations were given. In order to validify these explanations additional material research is required.

A general conclusion can be drawn from these considered aspects. The goal of the research was partially reached and a building method was defined from start to finish. The method was developed with a few side notes presented in this chapter and further elaborated in the recommendations. The thesis should be seen as a pioneering piece. There is definitely more research needed looking into this building method. With regard to the usage of biofibers the panels seem to be underwhelming in terms of structural properties. Updating the material properties might change this. With the described prospects on carbon fiber, this material definitely seems like a future proof building material which will allow for the rise of new building methods. Robotic winding could definitely have a future on this front.

11. Recommendations

11.1 Material properties

The composite should be thoroughly tested in order to learn more about its structural properties. Possible tests include a tensile test and shear test. Calculating bending resistance could be done with a three point flexural test. The bending resistance of an edge beam should be known in order to predict the buckling behavior. For this the values for bending stiffness as well as bending strength can be extracted from such a test. A different bending resistance might be expected from an element that was angled due to winding against a threaded end. There could be due to a reduction in section shape when winding around a vertex. This would provide insight in the bending moments that exist in the wound panels. Another test providing insight in the structural properties might be a cyclical loading test on a single tensional element. This could shine light on the observed increase in stiffness with cyclical loading of the panel.

11.2 FEM

For the FEM algorithm there are several adjustments that would be beneficial to the presented building method. The first adjustment is to make the FEM based on beams which, opposite to a truss based FEM, do not necessarily include hinges at every node. This would approach the manufactured method more accurately by including bending moments in the edges. This internal bending moment could then be used to allow for more specific buckling calculation. A beam based FEM would also include possibilities of more complex ground structures. With the truss fem all the web elements have to connect to the ends of the edge. This is because an intermediate hinge in a linear element would cause instability issues. With a beam fem internal connections would also be possible the edge would have to adopt the forces from the web in bending. Using a beam based FEM would make the calculations slower as all the matrices will become larger. For instance the element stiffness matrix (k) changes from a 2x2 matrix for a truss element to a 4x4 matrix for a beam element. Additionally the force vector becomes twice as large to include moments as well, same goes for the deformation vector which now includes angular rotation.

The second beneficial adjustment to the FEM algorithm would be the expansion into three dimensions. Combined with the beam FEM this would increase the calculation time of the method drastically because of the larger matrices that are being calculated. A consequence of this would be longer optimization times. The adjustment would however be advantageous for the design freedom of the structure. In three dimensions the algorithm could be used in the development of domes.

11.3 Path definition

The varying height of the web elements could cause torsion in the edge beam. A way to control the eccentricity from the web elements could be incorporated in the algorithm. The elements which carry the largest loads should be placed close to the center of the edge beam. This way the possible torsion is optimized. This could be done by iteratively considering all the possible winding paths. This is however a very computationally heavy approach. Combined with the limited assumed effect of the torsion in most cases this was seen superfluous for the content of this thesis.

The amount of edge windings connecting the threaded end to the edge beam is a variable of forming the path. This variable has a large effect on how well the threaded end is structurally integrated in the panel. With the pushing out of the threaded end being one of the observed failure modes during the panel testing it could be beneficial to include a calculation method defining the amount of needed edge windings. The calculation method would be similar to the calculations as presented during the discussing of the failure mode. However with more material and technical winding research the exact interaction between tension and shear could be approached in a more accurate way. Including this calculation would increase the control over the observed failure modes.

11.4 Manufacturing

For winding purposes it might be useful to experiment using an external rotational axis. The same panel could be executed twice, once using the robots reach and the other time on a table controlled by the external axis. The prestress during winding could be tested by measuring the elements deformation under an out-of-plane force applied on the finished panel. The deformation of the two panels can be compared. The effect of tighter prestress during winding could also be tested in two panels where the web elements are not soaked in resin. The deformation of the two panels during loading will give insight in the tightness of the prestress.

Appendix A. Optimization table

Table 5: table showing raw data for calculation of optimization rate

		Strain energy initial [Nmm]	Strain energy opt. [Nmm]	Total volume initial [mm³]	Total volume opt. [mm³]	Vol. strain energy initial [Nmm³]	Vol. strain energy opt. [Nmm³]	Opt. Rate [x]
pentagon	∅0,36	1288,63	309,781	162969	163331	$2{,}10*10^{8}$	$5{,}06*10^{7}$	4,15
	∅1	1288,63	309,782	162969	165832	$2{,}10*10^{8}$	$5{,}14*10^{7}$	4,09
	d ∅1	1288,63	307,935	162969	166554	$2{,}10*10^{8}$	$5{,}13*10^{7}$	4,09
	∅4	1288,63	309,783	162969	208530	$2{,}10*10^{8}$	$6{,}46*10^{7}$	3,25
	d ∅4	1288,63	251,094	162969	236763	$2{,}10*10^{8}$	$5{,}94*10^{7}$	3,53
hexagon	∅0,36	1116,56	367,137	249907	250453	$2{,}79*10^{8}$	$9{,}20*10^{7}$	3,03
	∅1	1116,56	367,137	249907	254223	$2{,}79*10^{8}$	$9{,}33*10^{7}$	2,99
	d ∅1	1116,56	364,590	249907	255656	$2{,}79*10^{8}$	$9{,}32*10^{7}$	2,99
	∅4	1116,56	367,137	249907	318591	$2{,}79*10^{8}$	$1{,}17*10^{8}$	2,39
	d ∅4	1116,56	336,578	249907	338142	$2{,}79*10^{8}$	$1{,}14*10^{8}$	2,45
octagon	∅0,36	1267,80	352,523	472122	473333	$5{,}99*10^{8}$	$1{,}67*10^{8}$	3,59
	∅1	1267,80	352,364	472122	481684	$5{,}99*10^{8}$	$1{,}70*10^{8}$	3,53
	d ∅1	1267,80	350,881	472122	483356	$5{,}99*10^{8}$	$1{,}70*10^{8}$	3,53
	∅4	1267,80	349,672	472122	624270	$5{,}99*10^{8}$	$2{,}18*10^{8}$	2,74
	d ∅4	1267,80	340,213	472122	637549	$5{,}99*10^{8}$	$2{,}17*10^{8}$	2,76

Appendix B. Resin datasheet

		SR InfuGreen 810 / SD 8824		
Curing cycles →		16h @ TA + 24h @ 40°C	16h @ TA + 16h @ 60°C	16h @ TA + 8h @ 80°C
Tensile				
Modulus	N/mm^2	3 040	2 790	2 640
Maximum strength	N/mm^2	68	65	60
Breaking Strength	N/mm^2	57	57	52
Elongation at max strength	%	3,6	4,4	5
Elongation at break	%	5,3	5,9	9,5
Flexion				
Modulus	N/mm^2	3 070	2 780	2 610
Maximum strength	N/mm^2	109	107	101
Breaking Strength	N/mm^2	64	87	68
Elongation at max strength	%	4,6	5,7	6
Elongation at break	%	12,6	9,3	13,5
Shear				
Breaking Strength	N/mm^2	43	42	41
Compression				
Modulus	N/mm^2			
Yield strength	N/mm^2	91	87	82
Offset compression yield	%	12,3	11,9	14,9
Charpy impact strength				
Resilience	kJ/m^2	99	86	89
DSC glass transition				
TG1 onset	°C	71	85	82
TG1 max onset	°C			82
DTMA glass transition				
TG tan delta	°C			
TeiG onset G'	°C			
TmG midpoint G'	°C			
TefG endpoint	°C			
TG peak G ''	°C			

Figure 63: Datasheet extracted from Sicomin, 2019

Appendix C. Experiment to establish the rate of soaking

During dry winding experiments some concerns rose with regard to the rate of soaking of the fiber. If the fiber application is done with the robot the time the fiber spends in the resin bath is limited. In order to achieve reliable mechanical properties it is important that the fiber is fully soaked in resin.

RESEARCH GOAL

The goal of the experiment is to establish a reasonable time by which the sisal fiber is fully soaked in the Sicomin resin.

The method of the experiment is to prepare soaked sisal fiber samples with varying soaking times. Subsequently the rate of soaking is expressed in the resin percentage present in the material. This is done by measuring the weight of the dry fiber and comparing this with the weight of the hardened fiber composite.

Used materials:

- Sisal rope 3 strand helical wind
- Sicomin SR 8150 Epoxy Resin with corresponding SD 8824 hardener
- Aluminum container
- Wooden mixing utensil

Used measuring devices:

- Digital scale
- Stopwatch

THE EXPERIMENT

The varying soaking times are established with regard to the corresponding application. In this application the minimum soaking time will likely never exceed 5 seconds, which is set to be the maximum soaking time for this experiment. The minimum soaking time of the experiment is set to be one second. As the strands are manually inserted in and removed from the resin, a soaking time <1 second is not considered to be measurable in this method. Within the domain of 1s<t<5s three soaking times were selected: 1, 3 and 5 seconds.

In the first step the resin was mixed with the hardener. This was done in the prescribed weight ratio of 100/22 respectively. After mixing the two components thoroughly the next step is soaking the strands of sisal. Sisal strands of 200mm were used in this experiment. Timing was done using a stopwatch, the sisal was manually introduced into the container with resin. After

soaking the sisal the strand was left to harden for 16 hours at room temperature and 8 hours at 40 C. The samples were weighed before application of resin and after the hardening process. The results are shown in the following table.

Table 6: Results of soaking time experiments

Sample #	Time in resin	Dry weight sisal	Weight after hardening	Resin weight	Resin percentage	Fibre percentage		Remarks
	[s]	[g]	[g]	[g]	[%]	[%]		
1	1	2,801	5,157	2,356	45,7%	54,3%		Large drops present
2	1	2,499	4,218	1,719	40,8%	59,2%		No drops present
3	1	2,739	4,770	2,031	42,6%	57,4%		Large drops present
4	3	2,608	4,484	1,876	41,8%	58,2%		Medium drops present
5	3	2,485	4,042	1,557	38,5%	61,5%		Some drops present
6	3	2,508	4,131	1,623	39,3%	60,7%		Large drops present
7	5	2,432	3,941	1,509	38,3%	61,7%		Some drops present
8	5	2,516	4,206	1,690	40,2%	59,8%		Large drops present
9	5	2,767	4,876	2,109	43,3%	56,7%		No drops present
Time in resin		Average dry weight sisal	Average weight after hardening	Average resin weight	Average resin percentage	Average Fibre percentage		
[s]		[g]	[g]	[g]	[%]	[%]		
1		2,680	4,715	2,035	43,0%	57,0%		
3		2,534	4,219	1,685	39,9%	60,1%		
5		2,572	4,341	1,769	40,6%	59,4%		

The samples had a length of approximately 200mm. While this is a small sample size a weight of the material could be established. The sisal dry weight per length could be calculated by summation of all dry weights divided by total length. This yields a dry weight of 0.013g/mm. With the same calculation method the hardened weight can be derived to be 0.022g/mm.

Since the average resin percentages for each of the soaking times are considered to be within the margin of error there is no substantial increase in soaking rate with increasing soaking time. This leads to the conclusion that even a soaking time of 1 second would be enough to thoroughly penetrate the fiber.

Appendix D. Winding samples for material testing

In order to facilitate further research some samples were wound using the knowledge and skills attained from writing this thesis. The actual material research was done by SID-studio. This chapter only describes the experiences with the winding process.

For finding the material properties several tests are to be conducted both in compression as in tension. For this purpose a preliminary set of 2x 4 samples of 400mm length were made. Half of the samples consists of 26 strands and the other half of 52. Half of the samples were longitudinally wrapped in order to see the effect this might have on the material behavior. The following chart shows the different samples:

Table 400mm length samples:

- 2x 26 strands wrapped
- 2x 52 strands wrapped
- 2x 26 strands naked
- 2x 52 strands naked

For the samples the robot path was made in a similar fashion to the method described in chapter **4.** The comparison is mostly valid for the way the edge beams are manufactured. The winding is done around the perimeter of the shape which is in this case a special case namely a line with two hollow tubes as vertices. The section of the edge is designed as follows. In the wrapped samples the gap in-between due to the hollow tube is lost due to perpendicular compression.

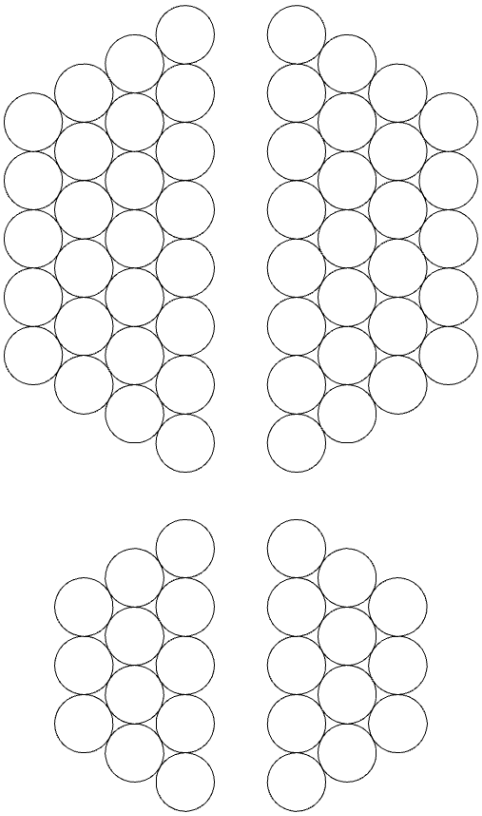

Figure 64: Geometry of wound sections, 52 and 26 strands

The same materials, end effector and peripheral equipment is used. The same mold is also applied but the threaded ends were covered in hollow tubes as to remove the samples from the mold.

Figure 65: Photograph of initial winding session

After winding it was noticed a lot of spillage was present. This made it difficult to remove the samples from the mold after hardening. The resin had seeped between the hollow tubes and the threaded ends. The next iteration the hollow tubes are to be completely covered in Teflon tape. The hole in the rubber piece through which the material was led was made smaller in order to lessen the dripping of the material during placement.

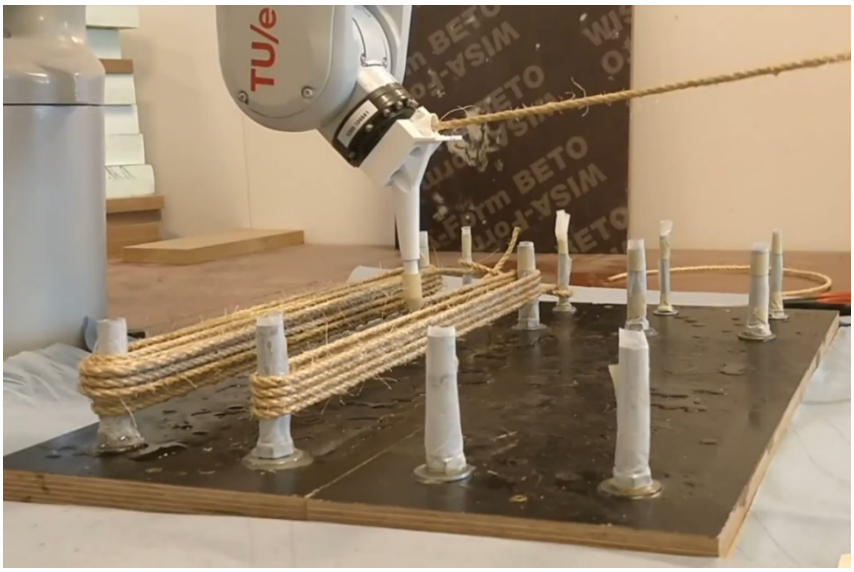

Figure 66: Photograph showing teflon covering

During the winding of the second batch of elements the end effector failed. This was the case because some rope got stuck on the crank. This location was smoothened so this situation cannot occur again. Also reinforcements were made in the end effector. The shaft broke very easily so extra material is added there. Three sessions were required in order to successfully wind all the required samples. Approximately 500mL of resin was used with every 4 samples.

Appendix E. Winding of panel initial experiment

In order to test the manufacturing part of the research a hexagonal panel was planned to be wound. After winding this panel would be subject to loading in order to learn more about its failure modes and structural capacity. Since the panel was never completed the exact design data is deemed superfluous and is therefore omitted. Only concise design data is included. The hexagonal panel was first designed to be able to withstand a 1kN point load while being simply supported on two points.

This yielded a panel with a thickness of 70mm. With the end effector used at the time the maximum safe reach was set to be 80mm. Therefor it was expected the threaded end would have 10mm to spare at the top in order to create a connection point for testing.

The mold was constructed from 700x700mm plywood. With holes drilled in it in order to form a regular hexagon with a diameter of 500mm. This is to be the distance between the hearts of the threaded ends. The final panel has a slightly larger outer diameter of approximately 518mm because of the width of its edge elements adding 4 times the strand diameter of 4.45mm.

THE WINDING PROCESS

Preparations

The path was completely prepared in advance. The mold was simulated at a certain distance from the robot (67mm). The complete robot path was simulated in robot studio 2020 in order to find potential errors in the rapid code. No errors were found.

Set up

The threaded ends of 110mm were used. They were connected to the base plate using a flat nut at either side. Every threaded end was measured to stick out of the base plate 85mm in order to accommodate the panel winding which takes place right above the nut. Consequently the bottom of the threaded ends sticking out were covered in tape in order to make sure no resin would get into the holes and complicate the removal of the panel in a later stage. Two extra threaded ends are installed in order to serve as connection for the start and the end of the winding pattern. However during weaving it was found that the connection for the start of the fiber should be on the inside of the panel, otherwise it would clash with the formation of the edge windings.

The mold was placed at 67mm from the robot edge in a parallel manner to the robot. While this can be measured with a tape measure the precision of the placement is not sufficient. The next step is therefor to calibrate the robot to the threaded ends. This is done by first getting the end effector in the right orientation. The end effector is manually jogged to hover exactly over two opposing threaded ends. Coordinates are extracted from the robots user interface. The x and y coordinates are used to position and rotate the polyline that forms the basis for the RAPID-

code in such a way to fit the two points. The height is decided by averaging the measurements and manually adjusting the z location of the polyline to fit the threaded ends.

In order to ensure no errors in the RAPID-code the entire code is checked again using robot studio. With the RAPID-code checked the next step is to prepare the resin. The infugreen 810 is mixed with hardener SD8824 in a ratio of 100/22, creating 200ml of mixed resin. The biofiber is led trough the peripherals and the end effector and connected to the threaded end serving as starting point.

Winding

In order to start the winding the RAPID-code for both the robot path and the end effector geometry is uploaded to the controller. The controller is used to control the speed of the robot which for this winding process is set at 50% of the 40mm/s defined in the code. The robot path starts with the robot going to its home position. However the threaded end forming the start of the biofiber collided with the path of the end effector going from the home position to the first target. For that reason the robot was not allowed to simply follow the programmed path, instead a small deviation was made by jogging the robot around the threaded end. This was thought to avoid the problem however this brought with it its own problem. As the rapid code is restarted from an intermediate point the code does not pass the commands for turning off linear configuration control and joint configuration control. The robot starts calculating its new axis rotations from the edited starting point instead of the home location. This causes problems in the path further on. As a result the end effector started spinning around since some axis reached its rotation limit and had to be reset. In order to troubleshoot the problem the end effector was removed and the robot path was finished. It was found that this unexpected rotation of the end effector was something that occurred several times in the path. With the solution not known at the time the winding session was prematurely terminated. In future executions the robot should always start from the home position.

Additional to this mistake some more problems were identified. With increasing height the windings became more and more tight. At some points the end effector clashed with previously laid cable. This clash wasn't enough to cause damage as the existing cable slipped out of the way and the end effector was able to continue its path. Would the path have been completed however the clash might have become an actual problem. This occurrence was caused by the cable diameter. Until now the diameter was assumed to be 4.45mm. This value was measured by using a digital caliper at several locations of the cable. Since the cable consists of biofiber the variance in its thickness is large, this variance was underestimated with the previous measurements. Resulting in a diameter that was too small. This wasn't noticed in the earlier completed test samples since their height is smaller. The effect of a underestimated diameter adds up with every winding height thus reaching a point where it becomes problematic. In order to solve this a new measurement of the cable is done. For this purpose the cable was led trough the caliper, fixing the caliper in place the smallest width where the cable doesn't hit the edges

of the caliper was found to be 5mm. An important footnote is that this was done with a finite amount of cable, its possible different parts of cable have different diameters. In order to be on the safe side 5.1mm was assumed for all following applications. Where underestimating the cable diameter can cause clashes overestimating the diameter has less severe effects.

Another observation that was tied to the underestimated material diameter is the underestimation of the height of the panel. With the calculated height being around 70mm the actual height was larger. After finishing the web windings by hand it was found that in fact there was no more buffer at the end of the threaded end and the winding actually exceeded the height of the threaded end. This was even after an overlooked algorithm failure caused some windings to be omitted from the panel which would've otherwise added another two times the diameter in height. Solutions for this problem can be found in two directions. The first solution is to design an end effector with a larger reach. This way the threaded ends can be made longer in order to accommodate both the windings for the panel as well as some empty space for the connection. The reach of the end effector could also be increased by a limited amount by increasing the encircling radius this method ensures the end effector base will stay clear of the top of the threaded end. The other directions where can be looked is not that of the winding method itself but that of the design. The design could be changed to accommodate smaller forces in the final panel. With a lower order polygon, for instance pentagon, there is also substantial lower height. Encircling the threaded ends now requires a full encircle, this can be adjusted to be just a wrap around. Finally the material can be changed to a material with a smaller diameter. The height automatically will decrease as the web elements that are nonstructural but executed for stability in transport will have a smaller diameter. The structural elements will need the same diameter and are therefore executed in higher number. Considering all options it was

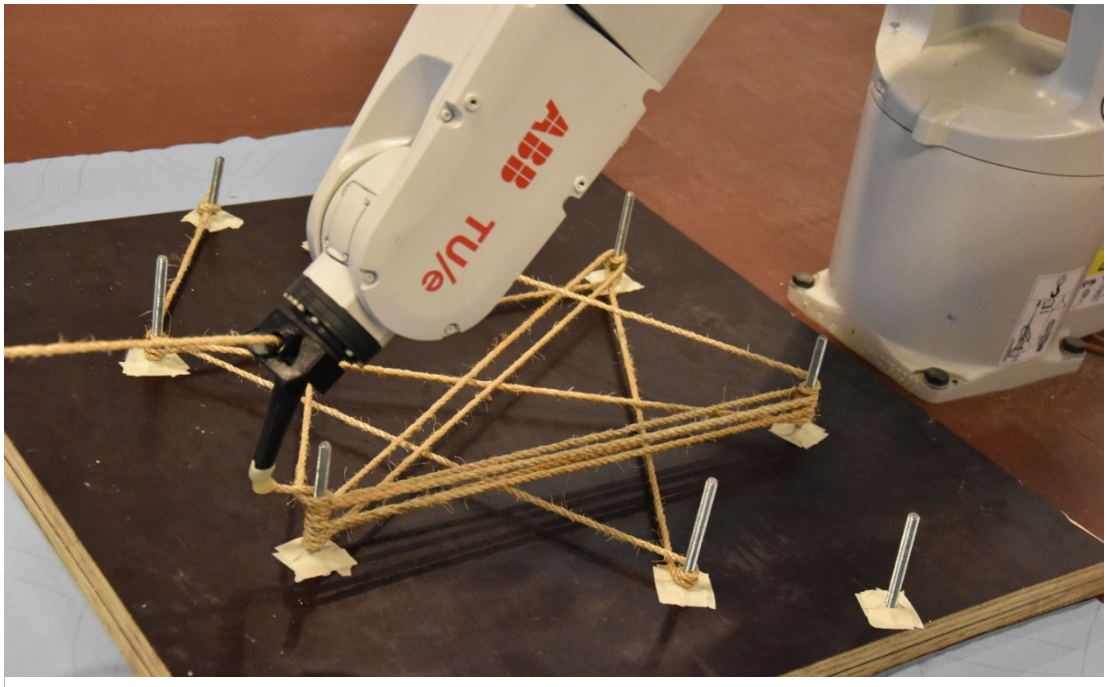

Figure 67: Error in the winding method is foreshadowed by the logo being upside down

decided to create a pentagon as this is the least experimental method. The other options would all need either additional research about feasibility or major changes in the script or setup.

Appendix F. Usecase bridge edge

In order to prove the construction method that was developed in this thesis a usecase is introduced. A bridge railing will be designed as a finishing element of a biobased bridge. The bridge had dimensions as shown in the figure below. The bridge decking is getting thinner towards the edges.

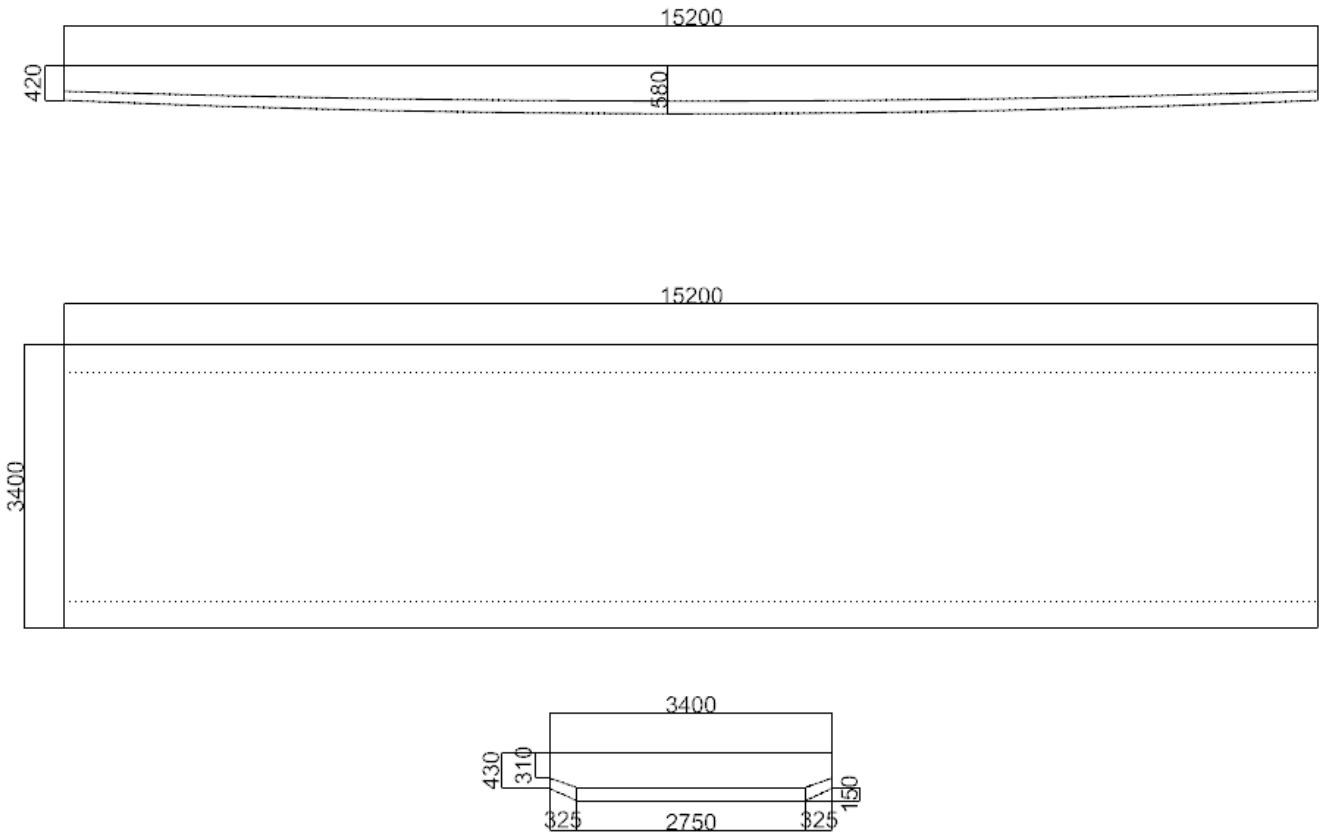

Figure 68: technical specifications of the bridge on which the railing will be designed

DESIGN

The design of the bridge railing was loosely based on a turtle shell. The shell of the turtle consists of tessellated hexagons forming an overall curved appearance. The height of the railing is designed to be approximately 1000mm. In order to provide a wide feeling the railing is slightly slanted outwards with an angle of 5°. This angle is kept small in order to avoid climbing.

The outline of the four panels was manually defined. Subsequently the location of the two internal nodes was decided using a Galapagos based solving method giving the same area of $2.41*10^5$mm to each panel. Galapagos is an evolutionary solver running within grasshopper.

In order to form the structure the connections between the panels are modeled by offsetting the panels by 15mm. Because the panels are expected to have two windings forming the edge beams the width around the vertices will likely not exceed 10mm. If this value is found to be wrong

later in the process the offset should be defined with a larger value. The ground structure containing all the possible diagonals is subsequently formed by the algorithm.

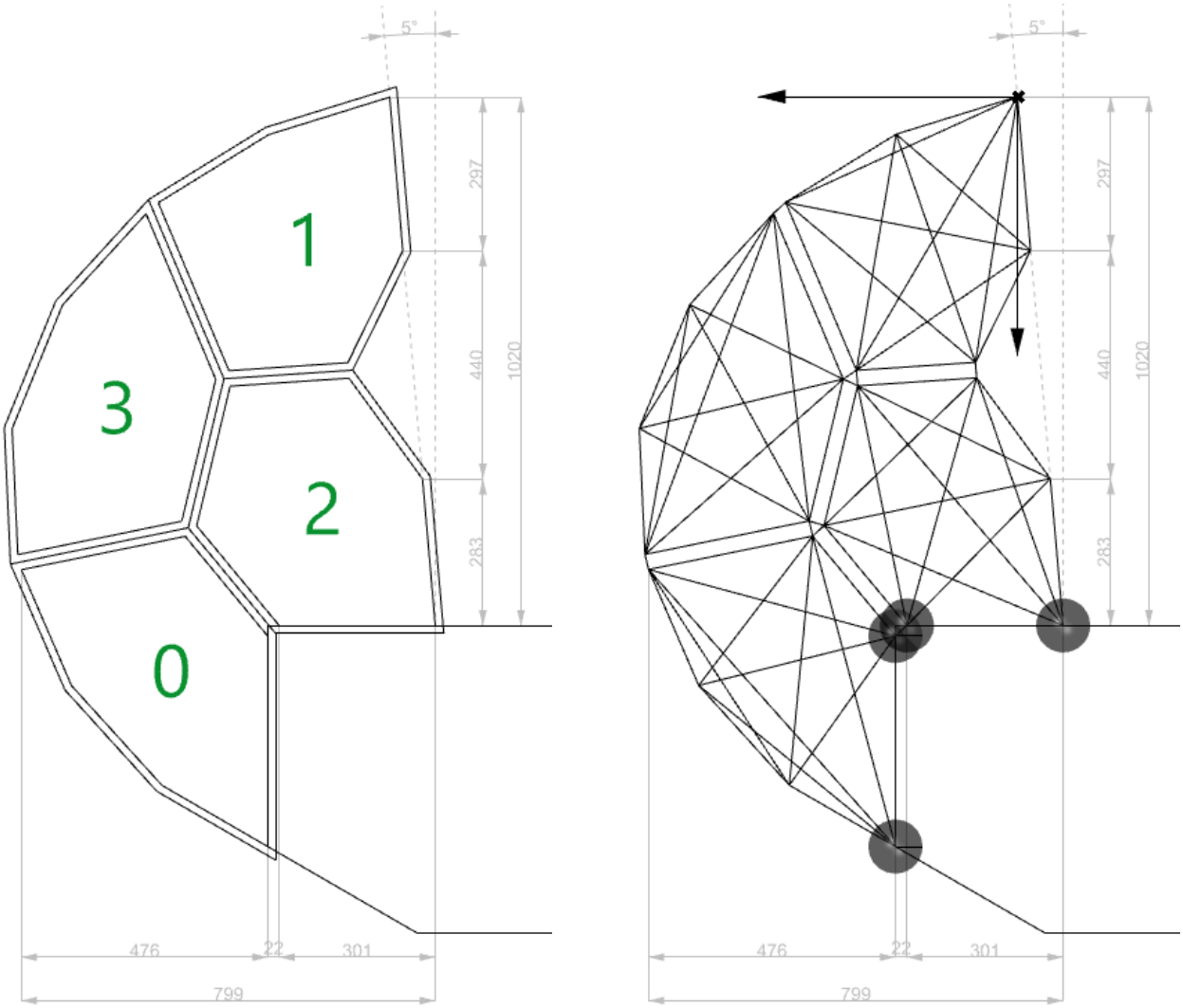

Figure 69: Assembly design and boundary conditions

BOUNDARY CONDITIONS

Loads

Regarding loads on the bridge edge EC1 part 2, section 4.8 gives us the rated values. Considering a public accessible bridge, both a horizontal as well as a vertical line load of 3.0 kN/m should be applied to the bridge railing. Since the railing consists of elements that are placed intermittently the center to center distance has influence on the point load on the railing. Using a center to center distance of 0.5m would lead to a horizontal and vertical point load of 1.5kN on the structure.

With its experimental and temporary character in mind the construction was placed in CC1 following EC0 table NB1 2.1. This means the construction has a maximum lifespan of 5 years.

From EC0 table NB.5 the load combinations can be acquired for CC1. The permanent load on the railing can be neglected. The only things forming permanent load is the wooden railing (diameter of 60mm) and steel ropes (diameter 20mm) interconnecting the panels. Also the self-weight of the panel could be defined as permanent load. Approximate calculation of permanent load is shown in table 7.

Table 7: Permanent loads

	Weight	Load (for 0.5m c.t.c.)
Wooden railing	1.98 kg/m	9.9 N
2x Steel Rope	2x 1.26 kg/m	12.6 N
Self-weight	13.2kg	132 N

The self-weight is calculated in retrospect. Knowing the used material length will be $5.73*10^5$mm the weight of the total structure from resin and sisal can be calculated to be $5.73*10^5$mm* 0.022g/mm = 12.6kg. Added to this self-weight should be the threaded ends. A total of 24 threaded ends are used of approximately 150mm each. With a weight of approximately 0.177kg/m the total weight comes down to 0.64kg. The weight of the connections is neglected.

Adding the permanent loads from table 7 it can be found that the total comes to 155N which is approximately 10% of the considered variable load (1.5kN for panels with 0.5m centre to centre). For this reason and the high complexity of properly defining the self-weight the permanent loads are neglected.

The load combination becomes simply:

LC.1: 1.35 * 3.0 kN/m Yielding a horizontal point load of 2.0 kN on the railing

LC.2: 1.35 * 3.0 kN/m Yielding a vertical point load of 2.0 kN on the railing

Supports

In order to properly support the structure as designed the following supports are schematized. There are hinged supports at three points, one hinged support is shared by two panels. Since the exact connection with the bridge deck has yet to be discussed with external parties at this point the calculations will be of the railing itself. The connection is expected to be similar to the internal connections within the panel assembly.

MATERIAL

For the material again the same material was considered as described in the section for **panel winding.**

Material properties for the composite material is assumed to be:

- Resistance: 10 N/mm2
- Modulus of elasticity: 9000 N/mm2

These are design values for both compression and tension.

Additionally material for the connections has to be selected. The material that is chosen for the connections has to be easily shaped to fit the connections. It has to be resistant to outside use and stiff and strong enough to form reliable connection elements. With these considerations in mind carbon fiber reinforced polymers were considered.

The anisotropic from is chosen as shown in table 8. The stiffness is considered to be 50.4GPa and the maximum stress 481MPa

Table 8: Material properties of CFRP

Series	Laminate code	t/mm	E_x/GPa	E_y/GPa	ν_{xy}	G_{xy}/GPa	σ_o/MPa	G_c/kJ m^{-2}
Plain weave cross-ply (PX)	PX2	0·51	50·4	50·4	0·103	4·42	481	26·0
	PX4	1·03	51·4	51·4	0·092	4·42	527	27·7
	PX8	2·03	53·1	53·1	0·083	4·42	538	22·7
Plain weave quasi-isotropic (PQ)	PQ4	1·02	37·2	37·2	0·353	13·8	390	21·6
	PQ8	2·03	36·8	36·8	0·328	13·9	428	17·9
	PQ12	3·17	35·2	35·2	0·297	13·6	372	18·3
Five harness satin cross-ply (5X)	5X2	0·81	45·1	45·1	0·077	3·78	419	28·8
	5X4	1·60	47·0	47·0	0·062	3·78	535	20·0
	5X8	3·15	47·4	47·4	0·053	3·78	456	17·6
Plain weave quasi-isotropic (5Q)	5Q4	1·53	34·1	34·1	0·296	13·2	375	19·2
	5Q8	3·17	33·5	33·5	0·320	12·7	347	16·8
	5Q12	4·59	34·8	34·8	0·322	13·2	370	12·9

OPTIMIZATION

For the structure the minimum winding area was defined as the area of a single rope which is 15.9mm for the rope with a diameter of 4.5mm.

The area of the web and the connections is the same over the entire structure and is 45mm^2 and 20mm^2 respectively. The area for the edge beams is different for each panel and is shown in **table x.**

Both the optimization and the tension only algorithm took place in the same iteration cycle. For the optimization an area dampening factor of η= 0.900 was used. The tension only algorithm was executed with a modulus reduction factor of p=0.900. The maximum amount of iterations was set to be 100 but at 74 iterations convergence was reached.

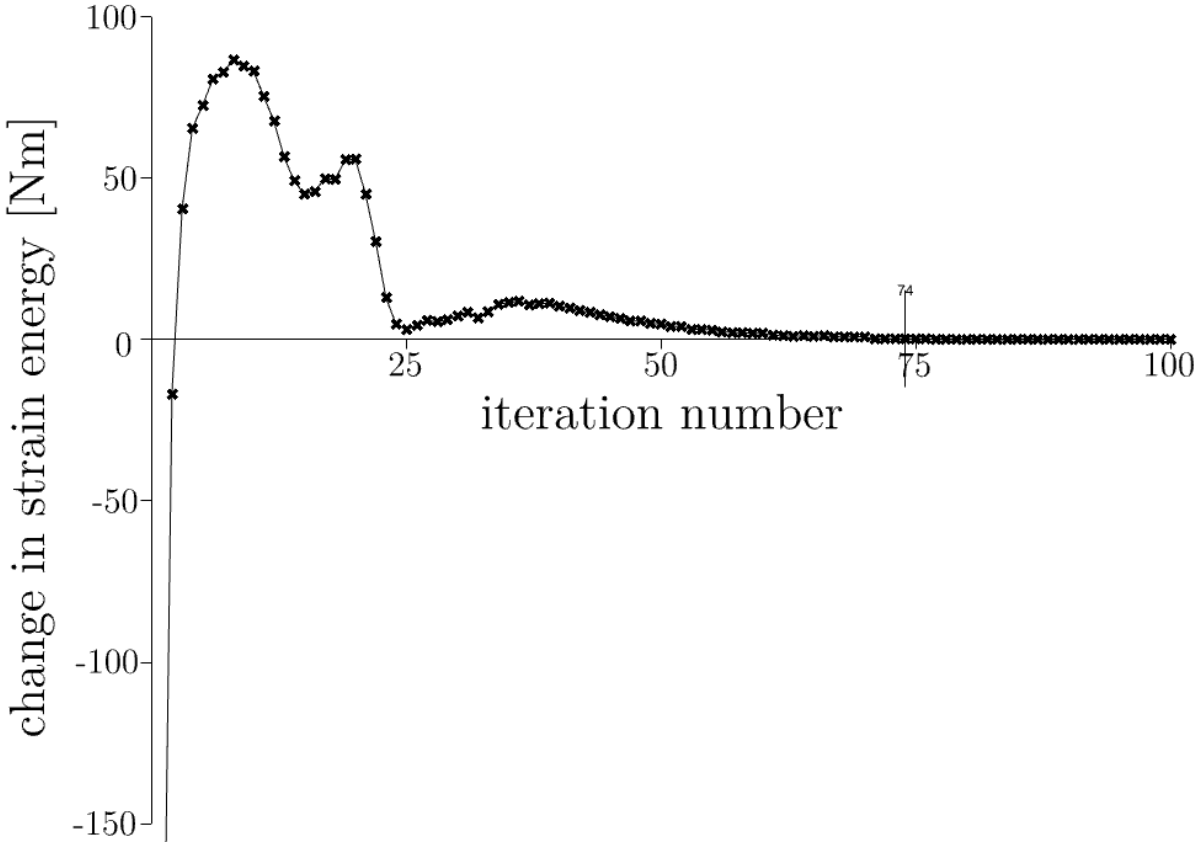

Figure 70: Convergence graph of the considered panel assembly

The first two iterations have a change in strain energy of -1441Nm and -257Nm respectively. For visualization purposes they are not included in the figure.

After the optimization the further steps for winding of the panel are conducted as described in this research. In order to visualize the results all panels are examined separately.

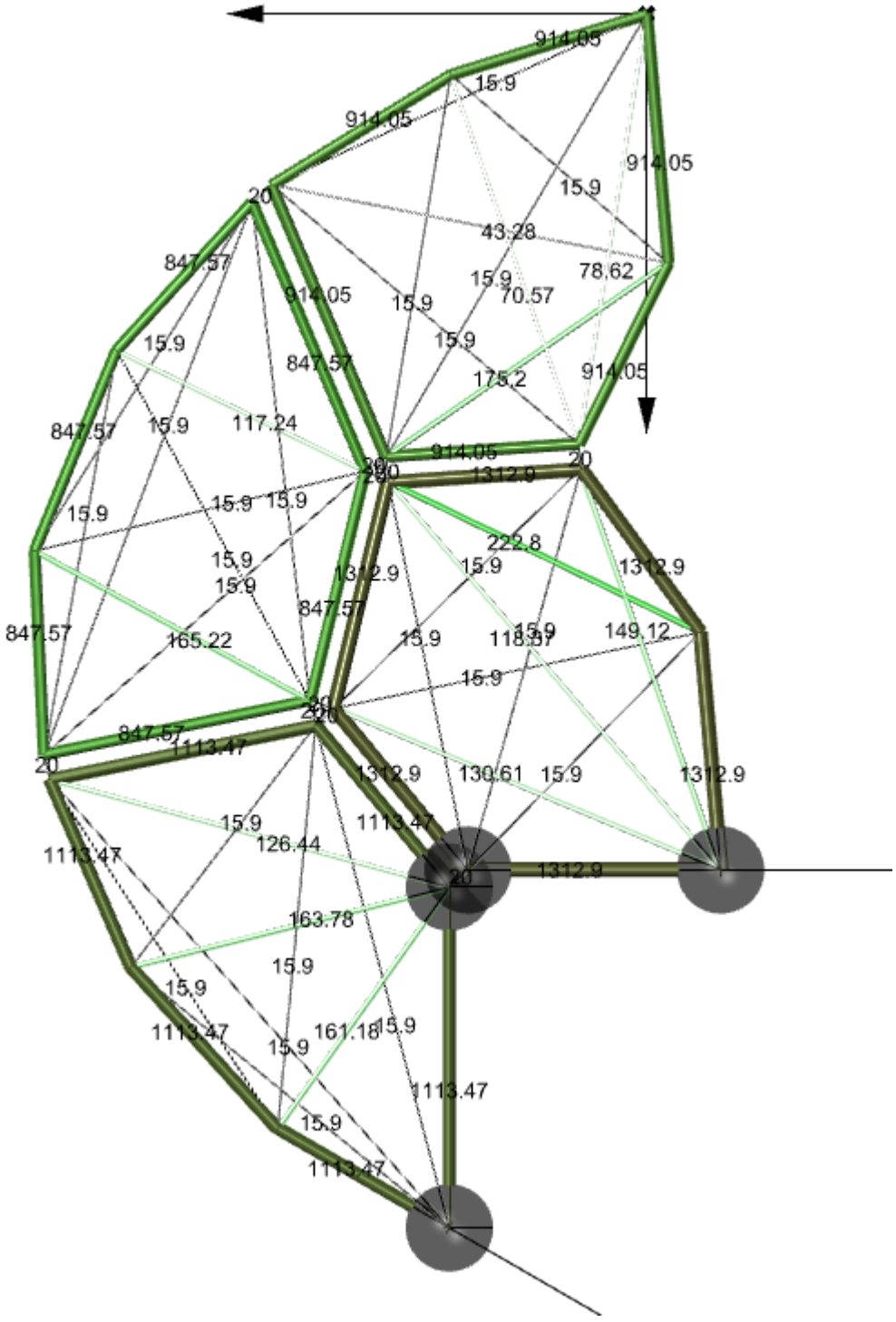

Figure 71: Optimized form of the bridge railing showing area for every element

Table 9: Amount of windings and elemental properties shown for each panel

Panel	Web elements [#]	Web height [#]	Edge elements [#]	Height [mm]	Edge area [mm²]
0	33	34	69	161	1113
1	28	28	56	133	914
2	44	40	81	189	1312
3	24	26	53	124	847

A difference can be observed between the amount of web elements and the web height. During the test for the existence of an Eulerian path some elements could be added in order to make the collection of elements windable. Afterwards during the iterative height increase of the windings the path is checked for clashes. This part of the winding path generation could decrease the total height of the web. Another more obvious factor is the amount of windings around each vertex as with each winding the height increases by the diameter of a single element.

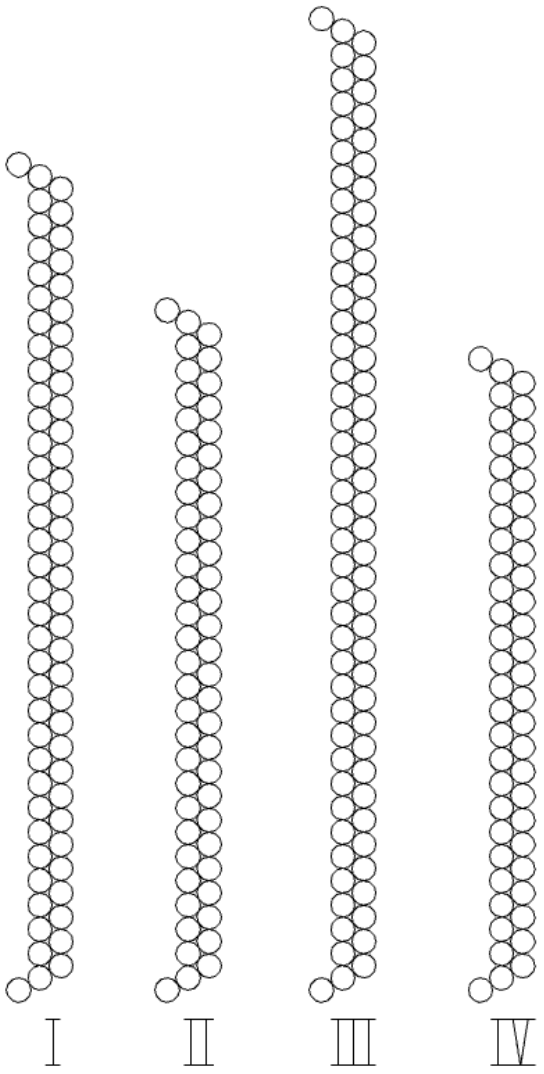

Figure 72: Geometric layout of every edge beam

In order to construct the sections as shown in the figure 72 there are several factors to consider. For each different edge beam the corresponding web height of the panel influences the edge beam height. In the sections also the two edge windings are visualized. In order to yield to buckling constraints but also to construct an integral whole, every edge beam has a minimum thickness of two elements.

In order to find a suitable geometry for the edge beam the winding of the web has to be completed first in order to know the height. The buckling is then considered using unity checks for each panel. First step is to check the tensional properties of the edge beam. There can be tension present in the panel edges, this tension is however generally small of magnitude. This concept is supported by the unity checks as presented in the next table.

Table 10: Unity checks for the edge of each panel in the assembly

Panel	Edge tension	Edge compression	Edge Buckling
0	0.002	0.325	0.388
1	0.047	0.241	0.259
2	0.074	0.116	0.122
3	0.129	0.325	0.325

These relatively low unity checks is resulting from the minimum of two layers for the edge beam as required for general integrity. Using two layers decreases the effect of errors in material placement. Since the edge beams can be separately designed also separate unity checks are presented. The unity checks for the web tension and the connection elements only one unity check is shown for the entire structure. For the connection only simple failure is considered, because of the small dimensions geometric instability is not checked. With CFRP both compression and tension capacity is the same. All unity checks presented are the governing checks over both load cases.

Table 11: Unity checks for web tension and connection failure overall

Web tension	Connection
0.895	0.499

With the unity checks being confirmed the panels winding patterns will be finalized. The encircling radius is set to be 3mm in order to accommodate m6 threaded rods. The resolution of encircles is set to be 8mm and every vertex is encircled one time. As shown in the edge beam sections the edge windings are executed twice, once above and once below the web windings. All these inputs lead to the winding paths as shown in figure x.

RESULTS

From the design of the bridge railing it can be concluded that the algorithms as described in this thesis work as expected. The actual design of the bridge could however be seen as partially unfulfilling. the railing elements were designed with a center to center distance of 500mm. However with the thickness of the railing elements exceeding 190mm the actual side to side distance of the panels comes to approximately 310mm. Resulting from this it could be concluded that while the process runs smoothly the material is less suitable for this application. Using a material with higher strength would lead to drastically thinner panels. The applied sisal material has a tensile resistance of 10N/mm2 as designed. Sisal fiber itself has a theoretic tensile strength of 500N/mm2 as presented in figure 8. Using a rope with a better morphology could possibly increase the tensile strength together with a better definition of the design resistance. If the tensile strength would be increased by a factor 2 the panels would halve in thickness. This theory however has a limit as the minimum amount of winding still exists. Another albeit less effective method for reducing panel thickness would be by using a smaller rope diameter. This would decrease the minimum winding thickness and in that effect reduce panel thickness.

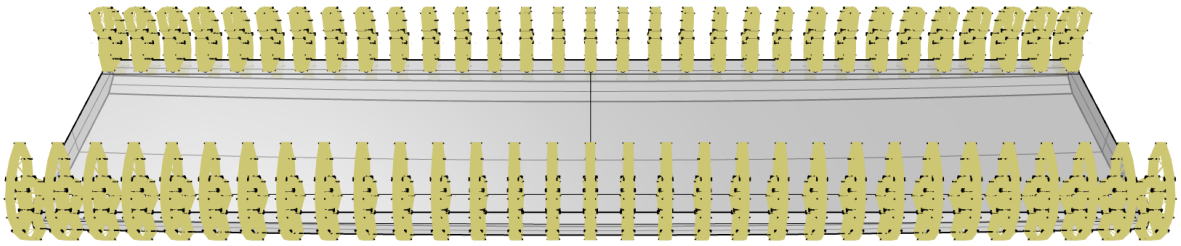

Figure 73: View of the array of panel assemblies forming the bridge railing

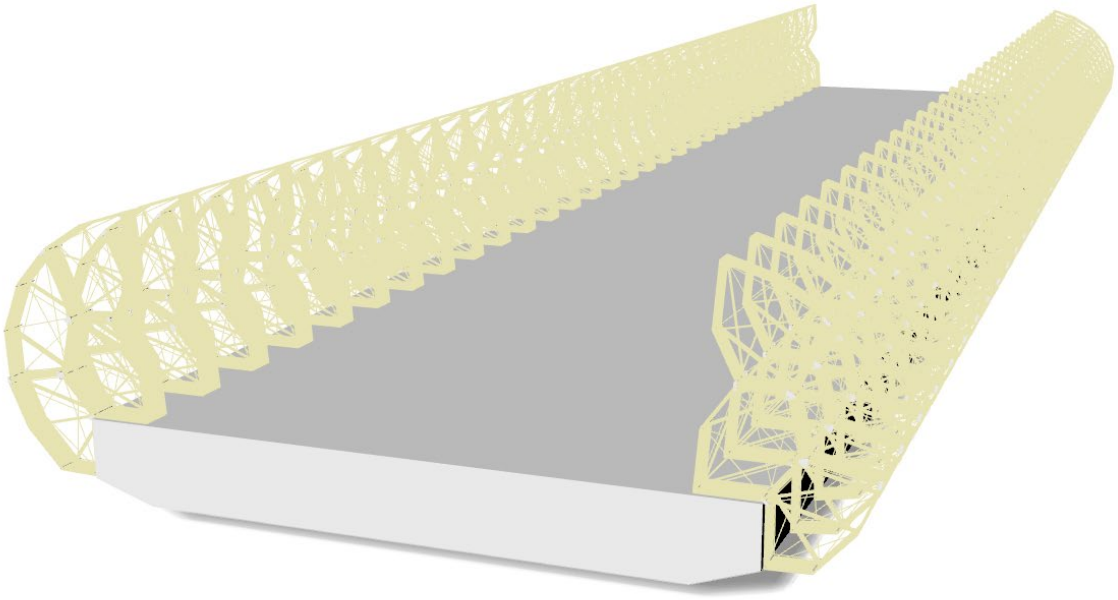

Figure 74: Render of bridge railing

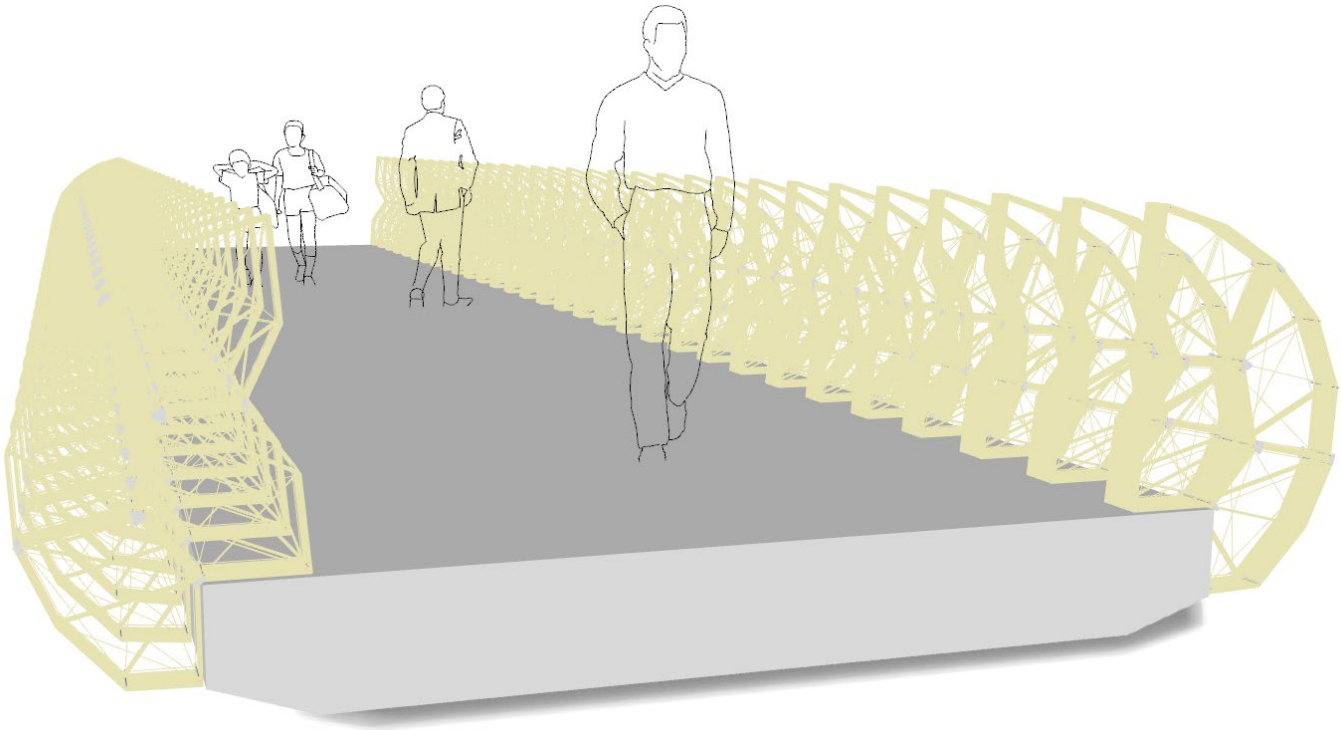

Figure 75: Render of bridge railing

Appendix G. Images of failure modes

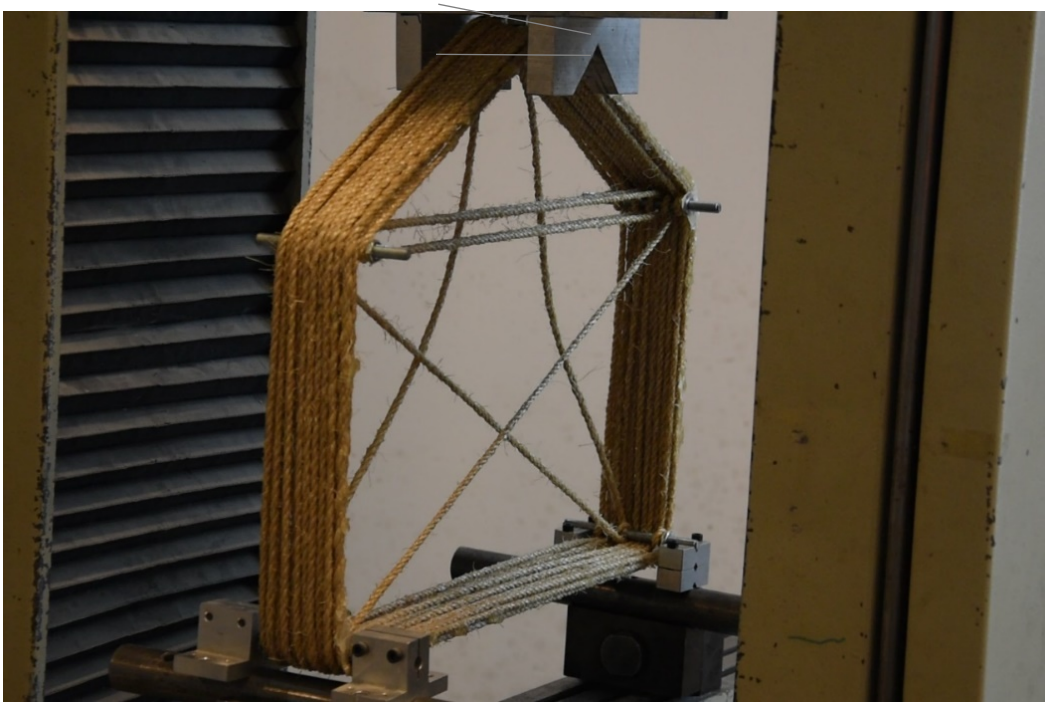

Figure 74: Threaded end slip

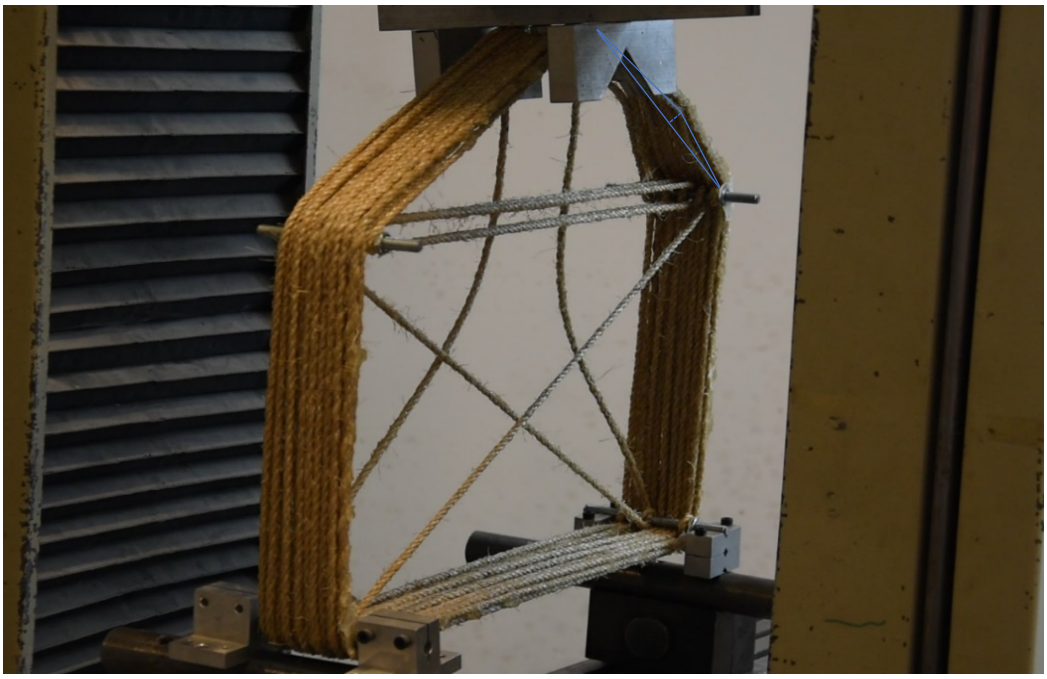

Figure 75: Buckling of edge beam

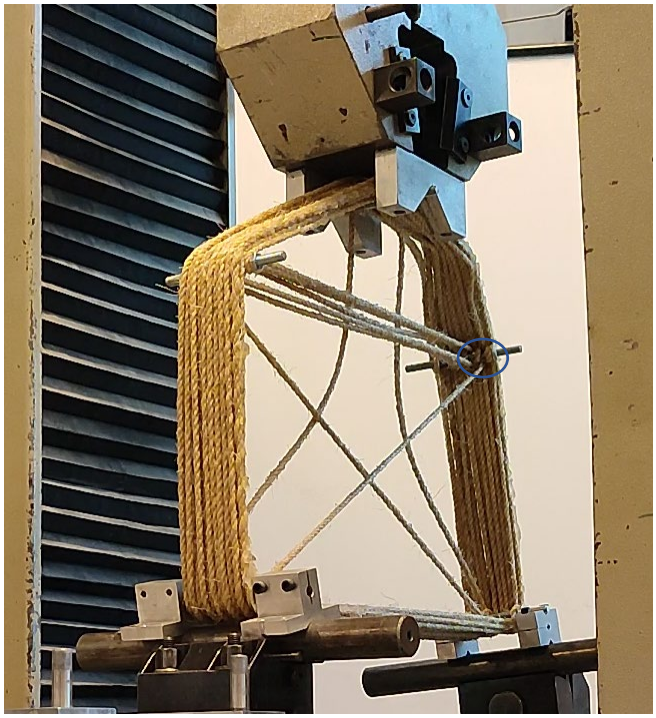

Figure 76: Tensional failure in web

Appendix H. Grasshopper script

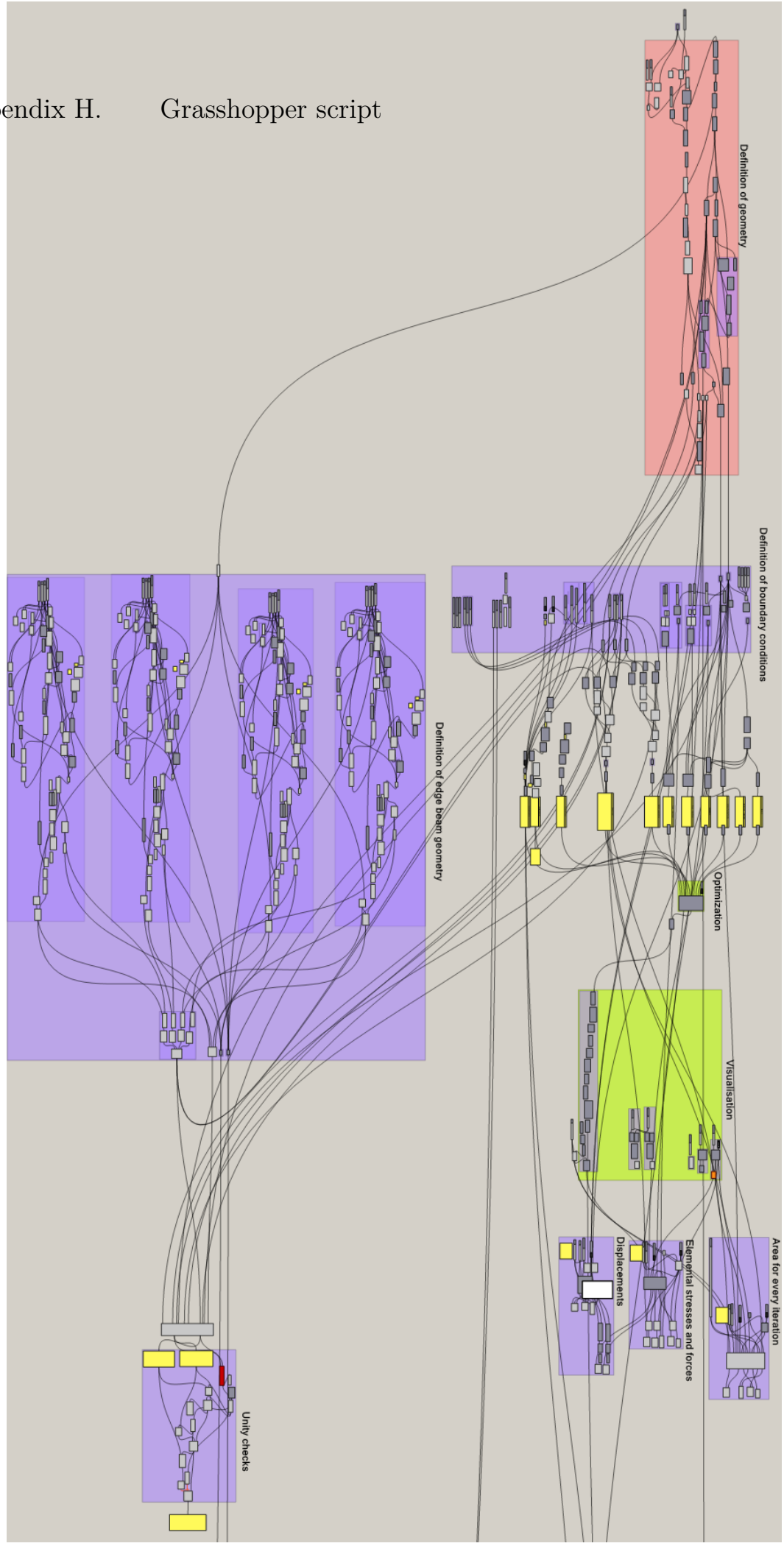

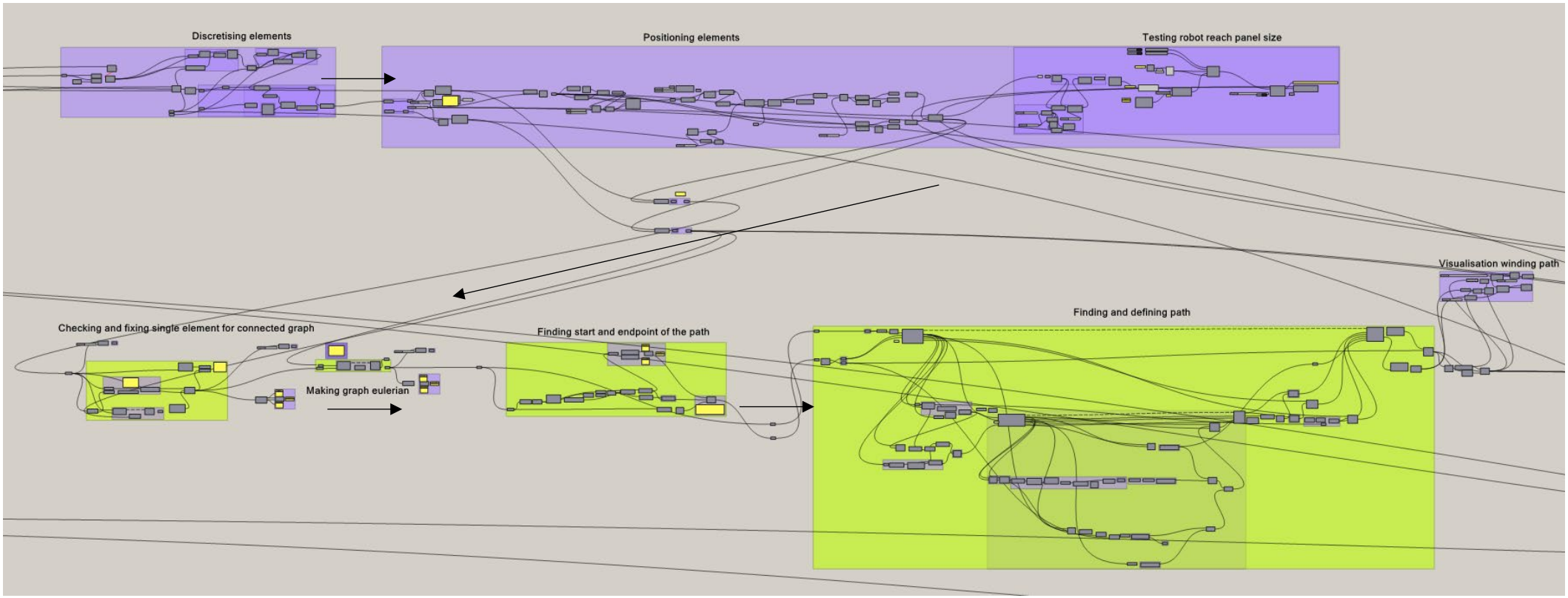
Discretising elements
Positioning elements
Testing robot reach panel size
Visualisation winding path
Finding and defining path
Checking and fixing single element for connected graph
Finding start and endpoint of the path
Making graph eulerian

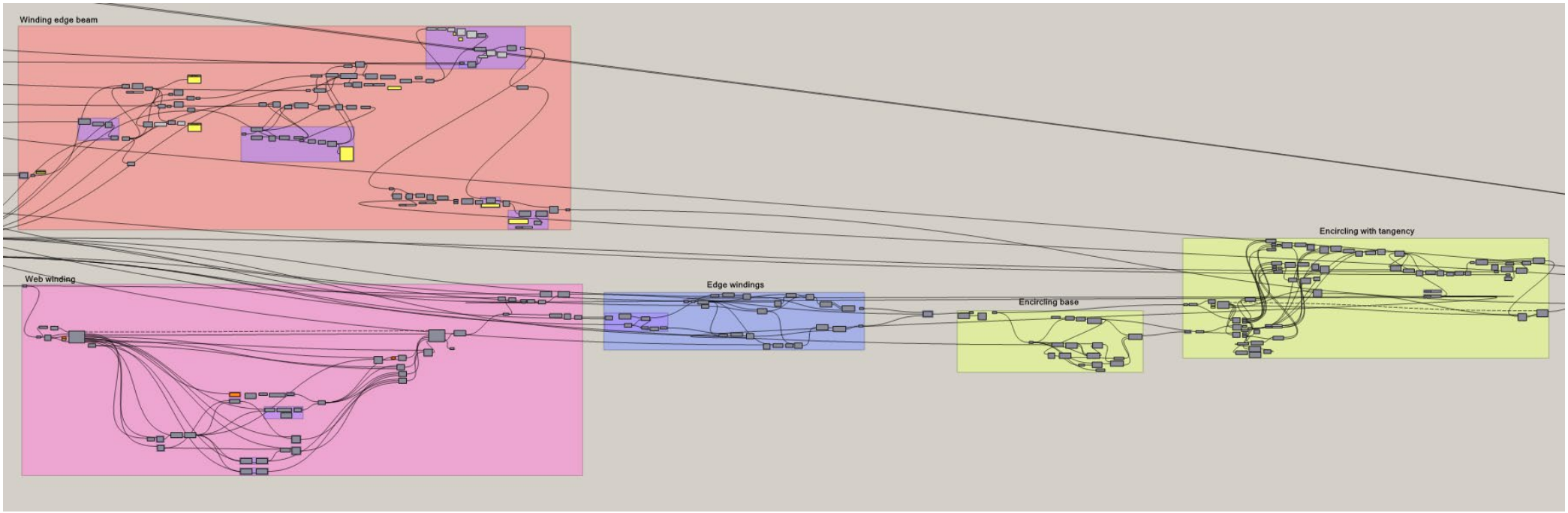
Winding edge beam
Web winding
Edge windings
Encircling base
Encircling with tangency

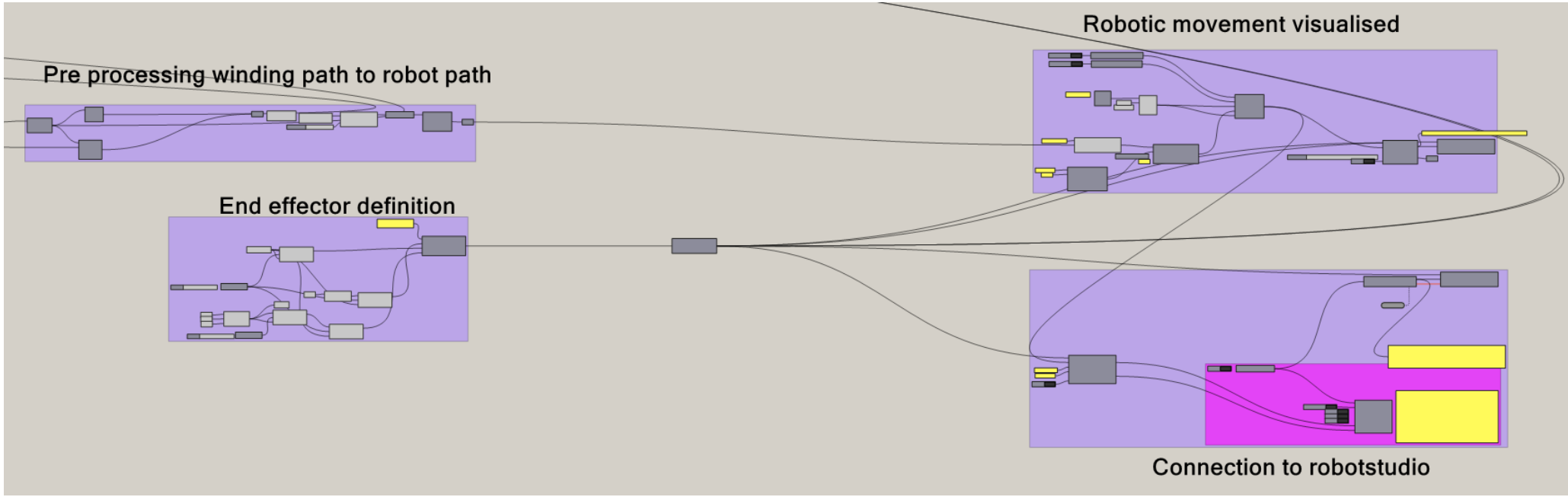
Robotic movement visualised
Pre processing winding path to robot path
End effector definition
Connection to robotstudio

Appendix I. Python script

The python script is ran within the 'optimization' part of the grasshopper script. In order to avoid the limitations of the rhino python solver the python installed on the pc is used with popen pipe calling a new process for running the python script.

The script that is run within grasshopper in order to call the pipe is supplied:

```
import rhinoscriptsyntax as rs
from subprocess import Popen, PIPE
import json

# json.loads(text) -> returns a dictionary
# json.dumps(dictionary) -> returns text

# i.e.:
# json.loads("{ 'x': [0, 5] }") = dict({ x: [0, 5] })
# json.dumps(dict({ x: [0, 5] })) = "{ 'x': [0, 5] }"

if toggle:

    # What file to run
    scriptToRun = "C:\Users\s132953\PycharmProjects/bar_fem22.py"

    # What python to use
    pythonToUse = "C:\Users\s132953\AppData\Local\Programs\Python\Python38\python.exe"

    # Start python script
    p = Popen([pythonToUse, scriptToRun], stdin=PIPE, stdout=PIPE, stderr=PIPE)

    # Convert data from Rhino to a string for python
    nodes               = nodes
    degrees_of_freedom  = dof
    elements            = elements
    restrained_dofs     = restrained
    forces              = forces
    stiffnessess        = Y_modulus
    areas               = areas
    ind_comp            = ind_comp
    conv_options        = conv_options
    forces2             = forces2
    ind_con             = ind_con

    allVars = [
        nodes,
        degrees_of_freedom,
       elements,
       restrained_dofs,
       forces,
       stiffnessess,
       areas,
       ind_comp,
       conv_options,
       forces2,
       ind_con
    ]

    # Pass string or binary data using communicate()
    output, err = p.communicate(json.dumps(allVars))
    #rc = p.returncode

    # If there is an error, throw it
    if err:
       raise Exception(err)
```

```
    # Otherwise, print our output.
    if output:
        print(output)
```

Additionally the python script that is ran is added on the following pages.

Appendix J. Utilized software

RobotStudio 2020

Pycharm with Python 3.8

Rhino 6 with Grasshopper:

Kangaroo

https://www.food4rhino.com/en/app/kangaroo-physics
From the Kangaroo plugin the components for interconnect points and remove duplicate lines/ points were used. These components were used in a variety of situations. The components could also be constructed from native grasshopper components but this would require a lot of components for the same task.

Anemone

https://www.food4rhino.com/en/app/anemone
From the anemone plugin the loops were used. These loops are essential for iterative programming in grasshopper. The fast loop function was used

RobotComponents

https://www.food4rhino.com/en/app/robot-components
Robot components is a plugin forming the connection with the robot. It was used for performing inverse kinematics and other simulations within grasshopper. Another big usage is the connection to the robot studio software which in turn connects to the robot. The 3D model of the ABB IRB 1200-5 used in several images was extracted from this plugin.

```
import numpy as np
from numpy.linalg import norm #length of a vector
import sys
import json
import ast

#connection to grasshopper
entireInput = sys.stdin.readlines()
allVars = json.loads(entireInput[0])

#define coordinate system
x_axis = np.array([1,0])
y_axis = np.array([0,1])

#define model (dictionary)
nodes              = ast.literal_eval(allVars[0])
degrees_of_freedom  = ast.literal_eval(allVars[1])
elements           = ast.literal_eval(allVars[2])
restrained_dofs    = ast.literal_eval(allVars[3])
forces1            = ast.literal_eval(allVars[4])
forces2            = ast.literal_eval(allVars[9])
conv_options       = ast.literal_eval(allVars[8])

it_no = conv_options[0]
comp_penal = conv_options[1]
cutoff  = conv_options[2]
switch_cutoff = conv_options[3]
dampening_factor = conv_options[4]
dampening_factor_edge = dampening_factor
dampening_factor_web = dampening_factor
web_opt = conv_options[5]
edge_opt = conv_options[6]

properties = {'x_axis':x_axis, 'y_axis':y_axis, 'nodes':nodes, 'degrees_of_freedom'
: degrees_of_freedom, 'elements':elements, 'restrained_dofs':restrained_dofs, 'ndofs':
ndofs}

ndofs = 2 * len(nodes)
areas              = ast.literal_eval(allVars[6])
initialareas       = ast.literal_eval(allVars[6])
stiffnesess_f1 = ast.literal_eval(allVars[5])
stiffnesess_f2 = ast.literal_eval(allVars[5])
initialstiffnesess = stiffnesess_f1

assert len(restrained_dofs) < ndofs
```

```
44 assert len(forces1) == len(nodes) == len(forces2)
45 assert len(elements) == len(stiffnesess_f1) == len(stiffnesess_f2) == len(areas)
46
47 elements_all = np.arange(start=1, stop=(len(elements)+1), step= 1)
48 elements_compressive = ast.literal_eval(allVars[7])
49 elements_connection = ast.literal_eval(allVars[10])
50 el_nontensile = elements_connection + elements_compressive
51 elements_tensile = np.setdiff1d(elements_all, el_nontensile)
52
53
54 #finding the indices of the compressive elements to exempt them from area iteration
55 index = np.argsort(elements_all)
56 sorted_x = elements_all[index]
57 sorted_index = np.searchsorted(sorted_x, elements_compressive)
58 yindex = np.take(index, sorted_index, mode='clip')
59 mask =elements_all[yindex] != elements_compressive
60 indices_compressive = np.ma.array(yindex, mask=mask)
61 #print('element indices compressive', indices_compressive)
62
63 #finding indices of tensile elements
64 index = np.argsort(elements_all)
65 sorted_x = elements_all[index]
66 sorted_index = np.searchsorted(sorted_x, elements_tensile)
67 yindex = np.take(index, sorted_index, mode='clip')
68 mask =elements_all[yindex] != elements_tensile
69 indices_tensile = np.ma.array(yindex, mask=mask)
70
71 #finding indices of connecting elements
72 index = np.argsort(elements_all)
73 sorted_x = elements_all[index]
74 sorted_index = np.searchsorted(sorted_x, elements_connection)
75 yindex = np.take(index, sorted_index, mode='clip')
76 mask =elements_all[yindex] != elements_connection
77 indices_connection = np.ma.array(yindex, mask=mask)
78
79
80 def points(element, properties):
81     elements = properties['elements']
82     nodes = properties['nodes']
83     degrees_of_freedom = properties['degrees_of_freedom']
84
85     #find the nodes one element connects to
86     fromNode = elements[element][0]
87     toNode = elements[element][1]
88
```

```
89      #find coordinates for those nodes
90      fromPoint = np.array(nodes[fromNode])
91      toPoint = np.array(nodes[toNode])
92
93      #find the degrees of freedom for each node
94      dofsfrom = degrees_of_freedom[fromNode]
95      dofsto = degrees_of_freedom[toNode]     #extend flattens the list
96      dofs = np.array(dofsfrom + dofsto)
97      return fromPoint, toPoint, dofs
98
99  def unit_vector(vector):
100     return vector / np.linalg.norm(vector)
101
102 def direction_cosine(vec1, vec2):
103     v1_u = unit_vector(vec1)
104     v2_u = unit_vector(vec2)
105     return np.clip(np.dot(v1_u, v2_u), -1.0, 1.0)
106
107 def rotation_matrix(el_vector, x_axis, y_axis):
108     # find the direction cosines
109     x_proj = direction_cosine(el_vector, x_axis)
110     y_proj = direction_cosine(el_vector, y_axis)
111     return np.array([[x_proj, y_proj,0,0],[0,0,x_proj,y_proj]])
112
113 def get_matrices(properties, areas, forces, stiffnesess):
114     #construct global stiffness matrices
115     x_axis      = properties['x_axis']
116     y_axis      = properties['y_axis']
117     ndofs       = properties['ndofs']
118     elements    = properties['elements']
119     restrained_dofs = properties['restrained_dofs']
120
121     K = np.zeros((ndofs, ndofs))
122     Cj = []
123     kj = []
124     Lj = []
125     Ckg = []
126     dofsj = []
127     el_vectorg = []
128
129     for element in elements:
130         #find element geometry
131         fromPoint, toPoint, dofs = points(element, properties)
132         el_vector = toPoint - fromPoint
133         #find elemental and stiffness matrices
```

```
134         length  = np.linalg.norm(el_vector)
135         area    = areas[element-1]
136         E       = stiffnesess[element-1]
137 
138         Ck = E * area / length
139         k = np.array(([1, -1],[-1, 1]))
140 
141         #find rotated mass and stiffness matrices
142         tau     = rotation_matrix(el_vector, x_axis, y_axis)
143         tauT    = np.transpose(tau)
144         k_r     = np.linalg.multi_dot([tauT, k, tau])
145 
146         #changing from element to global coordinates
147         index = dofs-1
148         B = np.zeros((4,ndofs))
149         for i in range(4):    #since each element has 4 degrees of freedom
150             B[i,index[i]] = 1.0
151         BT = np.transpose(B)
152         K_rG = np.linalg.multi_dot([BT, k_r, B])
153 
154         K += Ck * K_rG
155         Cj.append(B)
156         kj.append(k_r * Ck)
157         Lj.append(length)
158         Ckg.append(Ck)
159         dofsj.append(dofs)
160         el_vectorg.append(el_vector)
161 
162     #find the force vector
163     F = []
164     for f in forces.values():
165         F.extend(f)
166     F = np.array(F)
167 
168     #remove the restraind degrees of freedom
169     remove_indices = np.array(properties['restrained_dofs']) -1 #subtraction element
    by element
170     for i in [0,1]:
171         K = np.delete(K, remove_indices, axis=i)
172     F = np.delete(F, remove_indices)
173 
174     #solve for displacements (X)
175     X = np.linalg.solve(K, F)
176 
177     #disp = global displacement matrix (put back removed dof)
```

```
178     a = np.array(restrained_dofs) - 1
179     b = np.arange(start=0, stop=ndofs, step=1)
180     c = np.setdiff1d(b, a)
181     disp = np.zeros(ndofs)
182     np.put(disp, list(c), list(X))
183 
184     #global strain energy
185     XT = np.transpose(X)
186     Utot= 0.5 * np.linalg.multi_dot([XT, K, X])
187 
188     Ugdensity = []
189     Vg = []
190     stress = []
191     force_int = []
192     Fcr_int = []
193     compressionindexg = []
194     Vgnew = []
195 
196     for i in elements:
197         Celem = Cj[i-1]                                  #elemental [B] matrix (global
    placement matrix)
198         uj = np.dot(Celem, disp)                         #elemental displacement matrix  [
    uj]
199         fromPoint, toPoint, dofs = points(i, properties)
200         el_vector = toPoint - fromPoint
201         length = np.linalg.norm(el_vector)
202 
203         di1 = [uj[0],uj[1]]
204         i1new = fromPoint + di1
205 
206         di2 = [uj[2],uj[3]]
207         i2new = toPoint + di2
208 
209         el_vectornew = i2new - i1new
210         lengthnew = np.linalg.norm(el_vectornew)
211         dl = lengthnew - length
212 
213         strain = dl/length
214         stressjactual = strain * initialstiffnesess[i-1]
215         stressj = strain * stiffnesess[i-1]
216         force = stressj * areas[i-1]
217         stress.append(stressj)
218         compressionindex = length / lengthnew
219 
220         Uj = 0.5 * force * dl
```

```
221
222         Vj = Lj[i-1] * initialareas[i-1]
223         Vjnew = Lj[i-1] * areas[i-1]
224
225         inertia_area = 0.25 * np.pi * (areas[i - 1] // np.pi) ** 2
226         Fcr = ((np.pi) * (np.pi) * stiffnesess[i - 1] * inertia_area) / (length ** 2)
227
228         Ujdensity = Uj/Vj                       #Uj density is Uj/L
229         Ugdensity.append(Ujdensity)
230         Vg.append(Vj)
231         Vgnew.append(Vjnew)
232         compressionindexg.append(compressionindex)
233         stress.append(stressjactual)
234         force_int.append(force)
235         Fcr_int.append(Fcr)
236
237     Vg = np.array(Vg)
238     Ugdensity = np.array(Ugdensity)
239     stress = np.array(stress)
240     force_int = np.array(force_int)
241     Fcr_int = np.array(Fcr_int)
242
243     return Ugdensity, Vg, Lj, Utot, compressionindexg, stress, force_int, Fcr_int, disp
244
245
246 def modifygeom(Ugdensity1, Ugdensity2, Vg, Lj):
247     x = np.zeros_like(areas)
248     Ugdensity1web = np.array(Ugdensity1)
249     Ugdensity2web = np.array(Ugdensity2)
250     Vg_web        = np.array(Vg)
251     Vg_edge       = np.array(Vg)
252
253
254     ####web optimization####
255     for i in indices_connection:
256         np.put(Ugdensity1web, i, 0)
257         np.put(Ugdensity2web, i, 0)
258         np.put(Vg_web, i, 0)
259
260     for i in indices_compressive:
261         np.put(Ugdensity1web, i, 0)
262         np.put(Ugdensity2web, i, 0)
263         np.put(Vg_web, i, 0)
264     Ugdensityweb = Ugdensity1web + Ugdensity2web
265     Ugdensitytotweb = sum(Ugdensity1web) + sum(Ugdensity2web)
```

```
266     Vg_web = sum(Vg_web)                                    #Ugdensitytot is sum of
    strain energy density in system
267
268     Ratios = []
269
270     for i in indices_tensile:
271         initialarea = initialareas[i]
272         Ratio = Ugdensityweb[i] / Ugdensitytotweb            # ratio of strain
    energydensity part to strain energy density total (is equal to ratio of material)
273         Ratios.append(Ratio)
274         Vj_new = Ratio * Vg_web                              #new element volume
    decided by multiplying total volume with ratio
275         xj = Vj_new / Lj[i]                                  #new element area decided by
    dividing volume by length
276         xj = ((xj - initialareas[i]) * dampening_factor_web) + initialareas[i]
277
278         if web_opt > 0:                                      #only activate when web_opt is
    on
279             np.put(x, i, xj)                                 #new element area put in list, area
    list completed
280         if web_opt < 1:
281             np.put(x, i, initialarea)
282
283
284     #### edge optimization####
285     Ugdensity1edge = np.array(Ugdensity1)
286     Ugdensity2edge = np.array(Ugdensity2)
287
288     for i in indices_connection:
289         np.put(Ugdensity1edge, i, 0)
290         np.put(Ugdensity2edge, i, 0)
291         np.put(Vg_edge, i, 0)
292         np.put(x, i, areas[i])
293
294     for i in indices_tensile:
295         np.put(Ugdensity1edge, i, 0)
296         np.put(Ugdensity2edge, i, 0)
297         np.put(Vg_edge, i, 0)
298
299     Ugdensityedge = Ugdensity1edge + Ugdensity2edge
300     Ugdensitytotedge = sum(Ugdensity1edge) + sum(Ugdensity2edge)
301     Vg_edge = sum(Vg_edge)
302
303     Ratios = []
304     for i in indices_compressive:
```

```
305         initialarea = initialareas[i]
306         Ratio = Ugdensityedge[i] / Ugdensitytotedge                # ratio of strain
    energydensity part to strain energy density total (is equal to ratio of material)
307         Ratios.append(Ratio)
308         Vj_new = Ratio * Vg_edge                                   #new element volume
    decided by multiplying total volume with ratio
309         xj = Vj_new / Lj[i]                                        #new element area decided
    by dividing volume by length
310         xj = ((xj - initialareas[i])* dampening_factor_edge) + initialareas[i]
311         if edge_opt > 0:                                           #only activate when edge_opt
     is on
312             np.put(x, i, xj)                                       #new element area put in list,
    area list completed
313         if edge_opt < 1:
314             np.put(x,i,initialarea)
315     return x
316
317
318 #applying reduced Youngs modulus only to cables in compression
319 def modifystiffness(compressionindexg):
320     stiffnesess_adj = np.zeros_like(stiffnesess)
321     for i in indices_compressive:
322         if force_int[i] < -Fcr_int[i]:
323             np.put(stiffnesess_adj, i, stiffnesess[i])
324         if force_int[i] > -Fcr_int[i]:
325             reduced_stiffness = stiffnesess[i] * 1
326             if reduced_stiffness < 10:
327                 reduced_stiffness = 10
328             np.put(stiffnesess_adj, i, reduced_stiffness)
329     for i in indices_connection:
330         np.put(stiffnesess_adj, i, stiffnesess[i])
331     for i in indices_tensile:
332         if compressionindexg[i] > 1:
333             reduced_stiffness = stiffnesess[i] * comp_penal
334             np.put(stiffnesess_adj, i, reduced_stiffness)
335         else:
336             np.put(stiffnesess_adj, i, stiffnesess[i])
337     return stiffnesess_adj
338
339 ##calling and combining the functions##
340 minimumarea = 0.1
341 areas_it = []
342 Utot_it = []
343 stress1 = []
344 stress2 = []
```

```
disp_it1 = []
disp_it2 = []

for i in range(it_no):
    #first load case
    forces = forces1
    stiffnesess = stiffnesess_f1
    Ugdensity, Vg, Lj, Utot, compressionindexg,stress, force_int, Fcr_int, disp = get_matrices(properties, areas, forces, stiffnesess)
    stiffnesess_adj = modifystiffness(compressionindexg)
    stiffnesess_f1 = stiffnesess_adj
    Ugdensity1 = Ugdensity
    Utot1 = Utot
    stress1 = list(stress)
    del stress1[1::2]
    stress1 = np.array(stress1)
    force_int1 = force_int
    disp_it1.append(disp)

    #second load case
    forces = forces2
    stiffnesess = stiffnesess_f2
    Ugdensity, Vg, Lj, Utot, compressionindexg,stress, force_int, Fcr_int, disp = get_matrices(properties, areas, forces, stiffnesess)
    stiffnesess_adj = modifystiffness(compressionindexg)
    stiffnesess_f2 = stiffnesess_adj
    Ugdensity2 = Ugdensity

    #combining load cases and optimizing
    Utot2 = Utot
    stress2 = list(stress)
    del stress2[1::2]
    stress2 = np.array(stress2)
    force_int2 = force_int
    disp_it2.append(disp)
    Utot = Utot1 + Utot2
    x = modifygeom(Ugdensity1, Ugdensity2, Vg, Lj)
    areas = x

    #enforcing minimum area
    for (i, area) in enumerate(areas):
        if area < minimumarea:
            areas[i] = minimumarea

    radius = []
```

```
388     for i in range (3):
389         radius = np.sqrt(areas[i] / np.pi)
390 
391     areas_it.append(areas)
392     Utot_it.append(Utot)
393 
394     ##cutoff when not improving##
395     if len(Utot_it) > 2 and (abs(Utot - Utot_it[-2]) / Utot) * 100 < cutoff:
396         break
397     ##cutoff when switching between two values and not improving##
398     elif len(Utot_it) > 3 and (abs(Utot - Utot_it[-3]) / Utot) * 100 < switch_cutoff:
399         break
400     else:
401         continue
402 
403 #deciding optimum in case of state switching
404 if Utot_it[-1] > Utot_it[-2]:
405     optimized_index = int(-2)
406 else:
407     optimized_index = int(-1)
408 optareas = list(areas_it[optimized_index])
409 
410 
411 #communicating back to grasshopper
412 print(list(areas))
413 print('#')
414 for i in Utot_it:
415     print(i)
416     print('/')
417 print('#')
418 print(force_int1.tolist())
419 print('#')
420 print(force_int2.tolist())
421 print('#')
422 print(list(disp_it1[-1]))
423 print('#')
424 print(list(disp_it2[-1]))
425 print('#')
426 for areas in areas_it:
427     print(list(areas),'/')
428 print('#')
429 disp_tot = disp_it1 + disp_it2
430 for i in disp_tot:
431     print(i)
432     print('/')
```

```
433  print('#')
434  print(len(Utot_it))
435  print('#')
436  print(Utot_it[optimized_index])
```

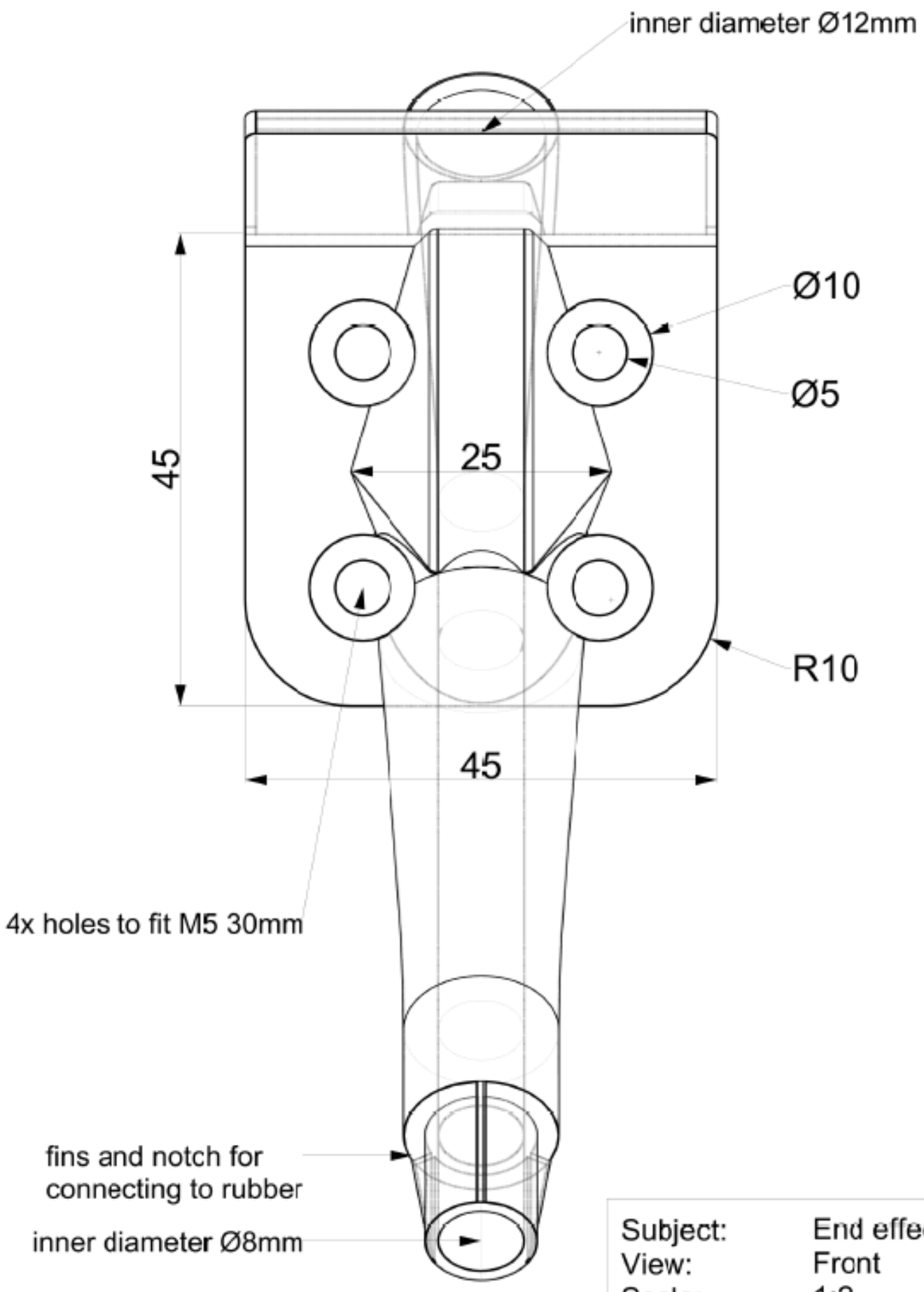

Subject:	End effector
View:	Front
Scale:	1:2
Drawing:	1/2
Author:	D. Jansen

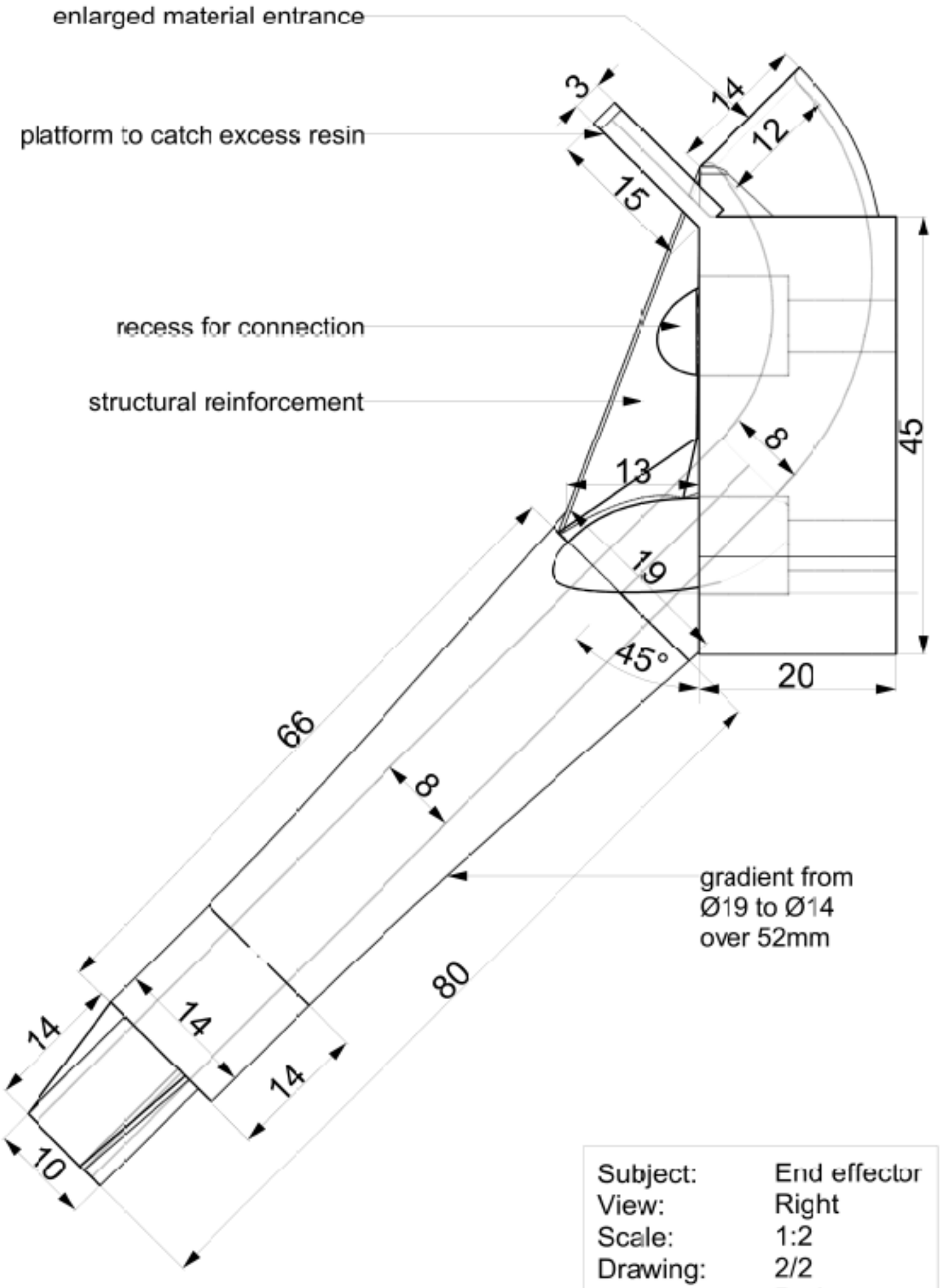

Subject:	End effector
View:	Right
Scale:	1:2
Drawing:	2/2
Author:	D. Jansen

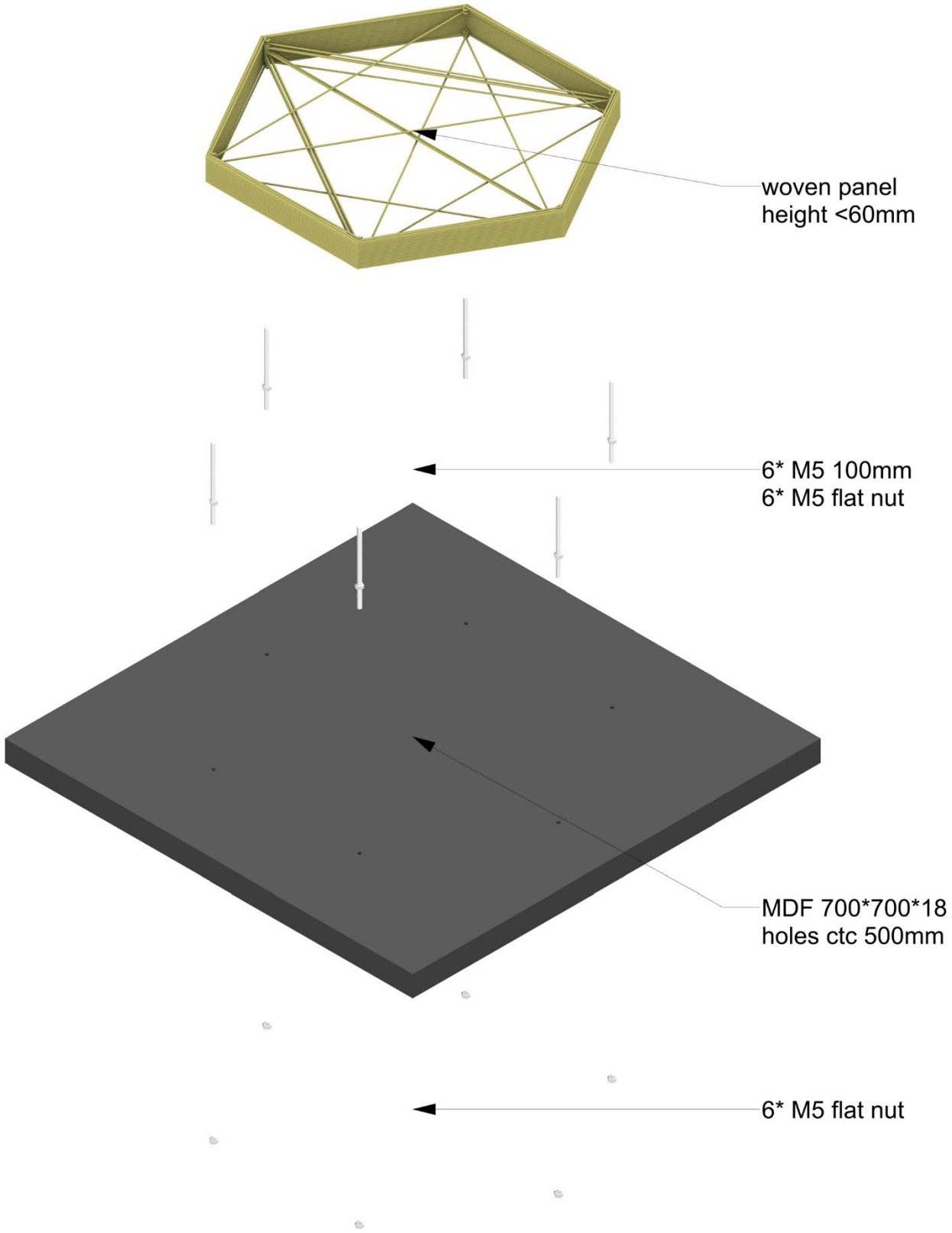

Subject:	Mold
View:	Isometric
Scale:	1:7
Drawing:	1/1
Author:	D. Jansen

Bibliography

ABB. (2021). *IRB 1200*. ABB Global. https://new.abb.com/products/robotics/industrial-robots/irb-1200

Ahmad, H., Crocombe, A. D., & Smith, P. A. (2013). Physically based finite element strength prediction in notched woven laminates under quasi-static loading. *Plastics, Rubber and Composites*, *42*(3), 93–100. https://doi.org/10.1179/1743289812y.0000000038

Ariail, K. D. (2010, 1 december). *Model of cable net structure (Dorton arena)* [Image]. https://indyweek.com/culture/art/gregg-show-demonstrates-modernism-s-surprising-raleigh-history/

Ashby, M. F. (2013). Strength and modulus of fibers [Graph]. In *Materials and the Environment* (Second Edition, p. 337).

Baker, D. A., & Rials, T. G. (2013). Recent advances in low-cost carbon fiber manufacture from lignin. *Journal of Applied Polymer Science*, *130*(2), 713–728. https://doi.org/10.1002/app.39273

Bendsoe, M. P., & Sigmund, O. (2011). *Topology Optimization*. Springer Publishing.

Elmogahzy, Y. E. (2020). General rope construction [Image]. In *Engineering Textiles* (Second edition, p. 235).

Khaled, S. (2020, maart). *Sets intersection*. Rhinoceros forum. https://discourse.mcneel.com/t/sets-question/98381/14

Kumar, S., Samal, S. K., Mohanty, S., & Nayak, S. K. (2016). Recent Development of Biobased Epoxy Resins: A Review. *Polymer-Plastics Technology and Engineering*, *57*(3), 133–155. https://doi.org/10.1080/03602559.2016.1253742

Mallick, P. (2018). 2.18 Particulate Filled and Short Fiber Reinforced Polymer Composites. *Comprehensive Composite Materials II*, 360–400. https://doi.org/10.1016/b978-0-12-803581-8.03837-6

McKenna, H. A., Hearle, J. W. S., O'Hear, N., & Textile Institute. (2004). *Handbook of Fiber Rope Technology*. Elsevier.

Mittelman, A., & Roman, I. (1990). Tensile properties of real unidirectional Kevlar/epoxy composites. *Composites*, *21*(1), 63–69. https://doi.org/10.1016/0010-4361(90)90099-i

Sicomin. (2019, februari). *SR InfuGreen 810 / SD 882X*. http://sicomin.com/datasheets/product-pdf1243.pdf

Stevens, P. S. (1974). *Patterns in Nature*. Little, Brown.

University of Cambridge. (z.d.). *The concept of the rule of mixtures* [Image]. https://www.doitpoms.ac.uk/tlplib/bones/derivation_mixture_rules.php

Wilson, R. J. (1996). *Introduction to Graph Theory*. Longman.